EVALUATION OF CONCRETE-FILLED GFRP DOWELS FOR JOINTED CONCRETE PAVEMENTS

By

Scott Murison

A Thesis Presented
to the University of Manitoba for

Degree of Master of Science

Department of Civil Engineering
University of Manitoba
Winnipeg, Manitoba
May 2004

THE UNIVERSITY OF MANITOBA

FACULTY OF GRADUATE STUDIES
*****
COPYRIGHT PERMISSION

Evaluation of Concrete-Filled GFRP Dowels For Jointed Concrete Pavements

BY

Scott Murison

A Thesis/Practicum submitted to the Faculty of Graduate Studies of The University of Manitoba in partial fulfillment of the requirement of the degree

Of

MASTER OF SCIENCE

Scott Murison © 2004

Permission has been granted to the Library of the University of Manitoba to lend or sell copies of this thesis/practicum, to the National Library of Canada to microfilm this thesis and to lend or sell copies of the film, and to University Microfilms Inc. to publish an abstract of this thesis/practicum.

This reproduction or copy of this thesis has been made available by authority of the copyright owner solely for the purpose of private study and research, and may only be reproduced and copied as permitted by copyright laws or with express written authorization from the copyright owner.

ABSTRACT

For decades, smooth, round, steel dowels have been used to transfer traffic wheel loads across the joints of concrete pavements. These dowels are subjected to shear and bending stresses due to thermal gradients in the pavement slabs in addition to the traffic loads. Over time, the concrete pavement joints become damaged due to the corrosion of the steel dowels as a result of the use of de-icing salts. As well, the small diameter, high strength, steel dowels create high bearing stresses in the concrete surrounding the dowels which causes the concrete to crush and spall locally. This eventually causes the dowels to become loose which is the major cause of pavement joint faulting. Dowel materials such as stainless steel, stainless clad, and glass-fibre reinforced polymer (GFRP) have been introduced in recent years as possible solutions to the corrosion problem. The size of the dowels has remained the same, typically 38 mm (1.5") in diameter for high traffic roads, which does not solve the bearing stress problem and costs can be very high for stainless steel.

In order to solve both the corrosion and bearing stress problems, large-diameter concrete-filled GFRP tube dowels have been introduced. This study at the University of Manitoba examined and compared the performance of four dowel types using analytical, finite element and experimental methods. The dowel types included 38 mm epoxy coated steel, 38 mm solid, pultruded GFRP dowels, and two sizes of concrete-filled GFRP tube dowels having diameters of 50.8 mm and 63.5 mm each. The dowels, which were cast in full-scale depth concrete slabs in the experimental program, were instrumented with strain gauges and small LVDTs attached to the dowel by small steel rods extending down through a small slot in the

concrete slab. Behaviour of the dowels was evaluated based on measured displacements, bending strains, and performance over one million load cycles.

Laboratory tests and finite element analysis results showed that the concrete-filled GFRP tube dowels exhibited considerably lower displacements and therefore, lower bearing stresses than the smaller 38 mm steel and pultruded GFRP dowels. After one million load cycles in the laboratory, the concrete-filled dowels and the concrete slab showed no signs of fatigue damage and exhibited great potential for use in jointed concrete pavements.

ACKNOWLEDGEMENTS

There are a number of individuals I would like to thank for their contributions to this project. I would like to thank Dr. Ahmed Shalaby, Department of Civil Engineering at the University of Manitoba, for proposing the project and for providing his direction and assistance throughout the course of the study. I would also like to thank Dr. Aftab Mufti, Department of Civil Engineering at the University of Manitoba and President of ISIS Canada, for his direction and support.

I would like to thank Mr. Moray McVey, ISIS Canada Technician, and Mr. Scott Sparrow, Structural Engineering Lab Technician, and Mr. Grant Whiteside, Lab Assistant, for their time and assistance. Finally, I would like to thank the following Graduate Students, Carlos Mota and Andi Bogdanovic for their help as well.

TABLE OF CONTENTS

CHAPTER 3: FINITE ELEMENT ANALYSIS

CHAPTER 4: EXPERIMENTAL PROGRAM

CHAPTER 6: ANALYSIS AND DISCUSSION

LIST OF TABLES

Chapter 2

Chapter 3

Chapter 4

Chapter 5

Chapter 6

LIST OF FIGURES

Chapter 2

Chapter 3

Chapter 4

Chapter 5

Chapter 6

Chapter 1

Introduction

1.1 Problem Statement

There is a great demand for better designed, longer lasting jointed concrete pavements. For almost a century, smooth, round, steel dowels have been used to transfer vehicle loads across concrete pavement joints. These dowels are subjected to shear and bending stresses due to thermal gradients in the pavement slabs in addition to the traffic loads. The dowels are also subjected to harsh corrosive environments due to de-icing salts used in colder climate regions. The corrosion problem of steel has led to the need to find alternative dowel materials.

The pavement joints are created to allow the slabs to expand and contract under changes in temperature requiring the dowels to move within the concrete slab. The volume change associated with corrosion of steel causes the joints to lock up and the concrete surrounding the dowels to crack. The epoxy coatings placed on steel dowels for the purpose of preventing corrosion are easily damaged allowing for the intrusion of corrosive agents. Stainless steel dowels have been used to prevent the corrosion problem, however, the cost of one of these bars can be as much as six times the cost of an epoxy-coated steel dowel. The lower-cost alternative, stainless steel-clad dowels, does not provide a great improvement because the cladding can chip or experience wearing over time.

In recent years glass fibre-reinforced polymers (GFRP) have been introduced as a promising alternative material to steel. GFRP are not affected by de-icing salts, provides good strength, and do not require surface de-bonding agents like its steel counterpart. Use of 38-mm diameter pultruded GFRP dowels, similar in size to the epoxy-coated steel dowels, has been increasing and tests have shown them to perform comparably to steel in the field [Eddie et al. 2001]. FRP has a higher tensile strength than steel, however, it has a significantly lower elastic modulus. The problem with the lower elastic modulus is that the dowel bar will bend and deflect more easily than steel under load causing higher concrete bearing stress in the critical region that is closest to the joint face. Damage to the concrete surrounding the dowels due to high bearing stress is already common with steel dowels. High bearing stresses produced by the dowel cause the surrounding concrete to crush and spall off, thereby causing the dowel to become loose. 'Dowel looseness' is a common cause of joint faulting which occurs when one slab deflects more than its adjacent slab under traffic loads.

It is known that bearing stress can be reduced by increasing the size of the dowel bar [Friberg 1938]. Using larger solid steel or GFRP dowels will increase costs and therefore may be less feasible for use in concrete pavements. Large-diameter concrete-filled GFRP tube dowels have recently been suggested as a possible solution to this problem. There is no available information on the performance of this type of dowel, however, tests at the University of Manitoba [Eddie 1999, Murison 2000] have shown them to exhibit good potential for use in concrete pavement joints. The required strength for shear and bending of the dowel is provided mainly by the FRP tube alone as the concrete core becomes cracked under load. The concrete or grout core of the dowel provides internal support to the shell

preventing the tube from collapsing under traffic loads. The concrete-filled GFRP dowels combine bearing stress-reducing size with non-corrosive material properties and are less expensive than solid GFRP dowels of the same size.

1.2 Objectives

The main objective of this study is to examine and compare the behaviour of various dowel types embedded in concrete pavement slabs under static and cyclic loads. The effect of diameter and stiffness on the behaviour of a dowel bar will be examined through the use of theoretical, finite element, and experimental methods. Characterization of the behaviour of each dowel type will encompass the following:

1. Displacements of each dowel type in the concrete under service loads.
2. Load-deflection behaviour of dowels loaded up to failure.
3. Longitudinal flexural strains in the dowel bars.
4. Vertical compressive strain in the concrete below the dowels.
5. Performance of dowels over one millions loads cycles.

The types of dowels examined include 38-mm diameter epoxy-coated steel dowels, 38-mm solid, pultruded GFRP dowels, and 50.8-mm and 63.5-mm diameter concrete-filled GFRP tube dowels.

1.3 Scope and Contents

The study comprises a finite element analysis (FEA) and an experimental investigation. The finite element study utilizes a three-dimensional model of a portion of a pavement slab to predict the effect of dowel diameter and stiffness on the deflected shape of the dowel bar and

the bearing stress produced in the concrete. Results of the preliminary finite element analysis were compared with linear-elastic solutions for a beam on an elastic mass. The experimental work was used to test the predictions made with the FE model and to examine the performance of concrete-filled GFRP dowels along with two other common dowel types, 38-mm epoxy-coated steel and 38-mm solid pultruded GFRP. The finite element model was later adjusted using the same material properties obtained from the laboratory tests and used to compare with experimental results.

The experimental program comprised two phases. The first phase, Phase I, was focused on examining the performance of the dowels and concrete slabs over the course of receiving one million load repetitions. The full-scale depth (250 mm) slabs contained two embedded dowel bars spaced 305 mm (12") on center. Four slabs, each containing one of the four dowel types, were tested in this phase. The second phase, (Phase II) using four similar pavement slab specimens, was conducted to examine the behaviour of the dowels loaded up to failure. The GFRP dowels were loaded up to failure and the steel dowels, which had a significantly higher stiffness, were loaded until yielding of the extreme fibers was observed. Both phases of tests were conducted with an identical test apparatus that comprised a rigid beam as the base support and a steel loading device to simulate a force caused by an applied vehicle axle-weight.

The contents of this thesis are briefly listed below:

Chapter 1 - Introduction, Objective, Scope

Chapter 2 provides literature review on jointed concrete pavements and includes a description of closed-form linear-elastic solutions for a beam on an elastic foundation that are commonly used in the design of doweled pavement joints. Information on previous experimental work is also provided.

Chapter 3 discusses the preliminary finite element analysis conducted to investigate the effect of dowel bar size and stiffness on deflections and concrete pavement slab stresses in the vicinity of the dowel bar. This part of the study involves a comparison to the closed-form linear-elastic solutions provided in the previous chapter.

Chapter 4 describes the experimental program conducted at the University of Manitoba including materials, instrumentation, fabrication of the test specimens, and details of the test set-up.

Chapter 5 presents the results of the experimental program including measured dowel bar deflections, load-deflection and load-strain behaviour of the dowels, and vertical strains in the concrete below the dowels.

Chapter 6 provides discussion of the results provided in Chapter 5 combined with comparisons to the finite element analysis as well as theoretical solutions. Discussion on the use of analytical equations for design with GFRP dowels is also provided.

Chapter 7 provides the summary and conclusion for this study. Recommendations for future work are also given.

Chapter 2

Literature Review

2.1 Jointed Plain Concrete Pavements

The most common type of concrete pavement is jointed plain concrete pavement (JPCP). JPCP incorporates longitudinal joints, parallel to traffic flow, and transverse joints, perpendicular to traffic flow, to control thermal cracking of the concrete slab. The transverse joints or controlled cracks create discontinuities in the concrete slab that affect the ability of the slab to carry vehicle loads. In most cases, smooth, round dowels are placed in the concrete to assist in the transfer of vehicle loads across the joints. The dowels also help to prevent faulting of the slabs that causes the thumping noise experienced by drivers on some concrete roads.

2.1.1 Pavement Joints

Joints are created by sawing through a small depth in the concrete slab, usually 1/3 of slab thickness or less, to initiate a crack location and allowing the shrinkage and thermal stresses to propagate cracking down through the remaining depth of the slab. Dowels are used to ensure effective load transfer across the joints. The dowels are placed at mid-depth of the slab and run parallel with the direction of traffic. Figure 2.1 shows a diagram of a typical doweled concrete pavement joint.

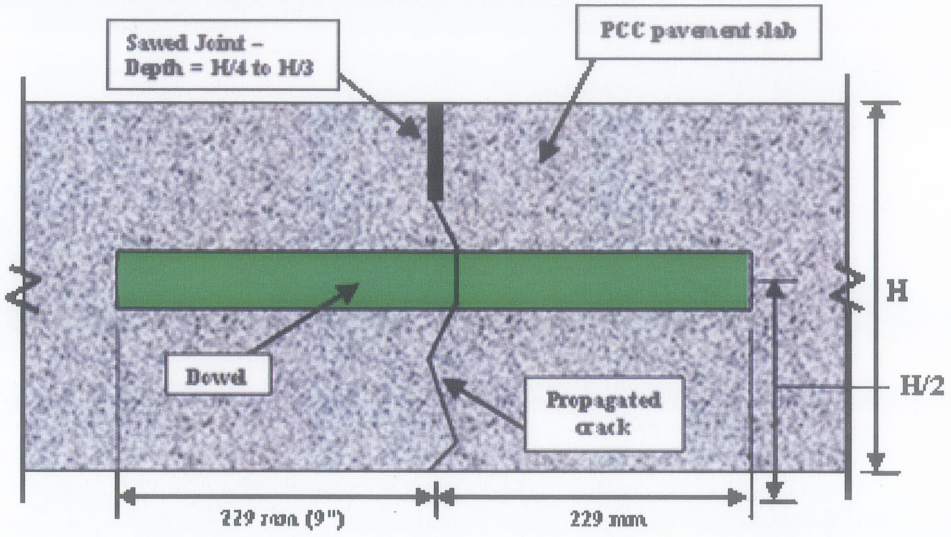

Figure 2.1: Typical Doweled Pavement Joint

2.1.1.1 Joint Spacing

Spacing of transverse joints in concrete pavements is typically between 4 and 5½ meters (13 and 18 ft) [ERES 1998]. The length of each concrete slab affects the amount of contraction and expansion that occurs due to temperature changes. Increased joint spacing will result in larger changes in length of the slab as shown by the equation below.

[1] $$\Delta L = CL(\alpha\Delta T + \varepsilon)$$

where C is the frictional restraint, L is the length of the slab, α is the thermal expansion coefficient for Portland Cement Concrete, ΔT is the change in temperature, and ε is the strain due to shrinkage of the slab. The amount of shrinkage of the slabs will affect the width of the joint opening between them. Larger joint openings will cause greater bending moments in the dowels under traffic loads and can increase stress on the jointed pavement system.

2.1.1.2 Load Transfer Efficiency

The measure of the effectiveness of the joint in transferring load from the loaded slab to the unloaded slab is called Load Transfer Efficiency (LTE). LTE is expressed as a percent as given in Equation 2.

[2] $$LTE_{\delta} = (\delta_{unloaded} / \delta_{loaded}) \times 100$$

where, LTE_{δ} = Deflection load transfer efficiency, percent
δ Unloaded = Deflection of the unloaded slab
δ Loaded = Deflection of loaded slab (adjacent to unloaded slab)

If a joint has 100 percent efficiency both adjacent slabs will deflect equally under load. If the efficiency is zero percent, the unloaded slab will not deflect at all. Figure 2.2 illustrates this concept. Desirable deflection load transfer efficiencies are generally greater than 70 percent to prevent pavement distresses such as pumping, faulting, and cracking [ERES 1998].

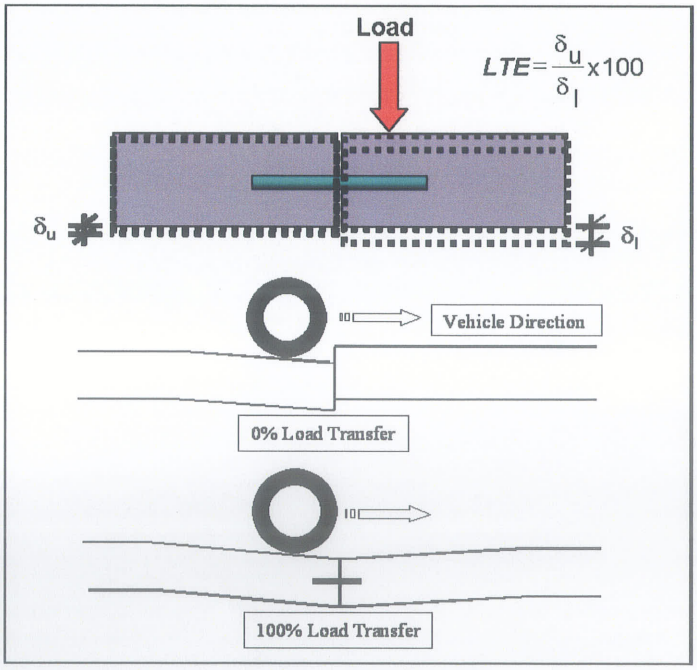

Figure 2.2: Load Transfer Efficiency (LTE)

2.1.1.3 Pavement Joint Load Transfer

The ability of a joint to transfer load efficiently and effectively is affected by several conditions. Conditions such as the support provided by the base material beneath the pavement slab, width of joint opening, and dowel looseness can affect the amount of load transferred across the joint. Ideally, the maximum amount of load that can be transferred across a joint is 50 percent of the applied load. The other 50 percent is transferred directly to the base material below. There are two mechanisms for which load transfer at a joint is accomplished. These mechanisms are aggregate interlock and dowel action.

Aggregate interlock is the mechanism where the aggregates in the concrete on both sides of the crack transfer load through bearing and friction. The shear force transfer provided by aggregate interlock can become ineffective when gaps form at the joints due to temperature effects and excessive deflections under load. Therefore, the most important and reliable mechanism of load transfer is dowel action.

The mechanism by which dowels transfer shear forces across a joint is commonly referred to as dowel action. These shear forces are induced in the dowels due to the movement of the concrete slabs relative to one another. The dowels are subjected to shear and bending stresses due to vehicle loads as well as curling of the concrete slabs due to temperature changes.

2.2 Design of Concrete Pavement Joints

Pavement joint design methods were first developed by B.F. Friberg [Friberg, 1938] and were based on closed-form linear-elastic solutions for an infinitely long beam

in an elastic mass solved by Professors S. Timoshenko and J.M. Lessels [Timoshenko and Lessels, 1925]. According to Timoshenko, the deflection of a beam in an elastic mass is determined using the following differential equation:

[3] $$EI\frac{d^4y}{dx^4} = -ky$$

where k is a constant called the modulus of foundation and y is the deflection. The modulus of foundation, represents a force per unit length to produce a unit deflection in the elastic mass. The solution to this equation is:

[4] $$y = e^{\beta x}(A\cos\beta x + B\sin\beta x) + e^{-\beta x}(C\cos\beta x + D\sin\beta x)$$

where,

$\beta = \sqrt[4]{k/4EI}$ = relative stiffness of the beam on an elastic foundation
k = modulus of foundation
E = modulus of elasticity of the dowel (beam)
I = moment of inertia of the dowel (beam)

Applying the appropriate boundary conditions to solve for A, B, C, and D, for a semi-infinite beam with a bending moment, M_o, and a point load P_t, Equation [4] becomes the following:

[5] $$y = \frac{e^{-\beta x}}{2\beta^3 E_d I_d}\{P_t\cos\beta x - \beta M_o(\cos\beta x - \sin\beta x)\}$$

Friberg applied Timoshenko's elastic solution to a dowel bar of semi-infinite length embedded in concrete. The peak deflection measured at the joint face of the slab is determined by setting x = 0 in Equation [5] and obtaining the following equation:

[6] $$y_o = \frac{P_t}{4\beta^3 E_d I_d}(2 + \beta z)$$

where β, the relative stiffness of the dowel embedded in a concrete mass, is given by:

[7] $$\beta = \sqrt[4]{\frac{Kb}{4E_d I_d}}$$

K = modulus of dowel support (K-value)
b = diameter of the dowel (width of beam)
E_d, I_d = elastic modulus and moment of inertia of the dowel
P_t = load transferred by the dowel
z = the width of the gap between the two slabs.

Figure 2.3 shows the deflected shape of the dowel bar calculated by Equation [5].

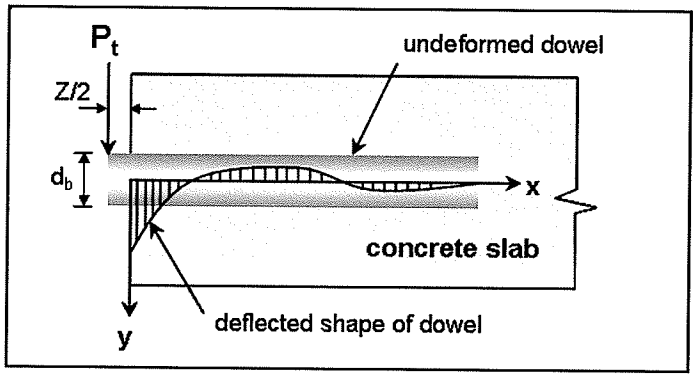

Figure 2.3: Deflected shape of dowel bar

Friberg used the expression Kb in place of Timoshenko's modulus of foundation, k. Friberg used the modulus of dowel support, K, which is a constant representing a force per unit area that would cause a unit deflection.

In Equation [5], the bending moment in the dowel, M_o, is caused by the eccentricity of the applied load, Pt, which would result from the adjacent slab being loaded, and is calculated from the following equation:

[8] $$M_o = P_t \frac{z}{2} = \text{bending moment at the face of the surrounding mass}$$

The bearing stress along the dowel/concrete interface, σ_b is obtained by multiplying the deflections calculated from Equation [5] by the modulus of dowel support or 'K-value' as shown in the equation below.

[9] $$\sigma_b = Ky$$

Figure 2.4 shows the distribution of stress in an elastic mass (concrete) under the dowel bar, as described by Timoshenko, where the concrete above the dowel is neglected. The stress in the concrete is greatest directly beneath the bottom of the dowel bar. In the analytical solution, the maximum bearing stress computed by Equation [9] above is located just below the dowel surface at the joint face of the pavement slab where the dowel deflection is greatest.

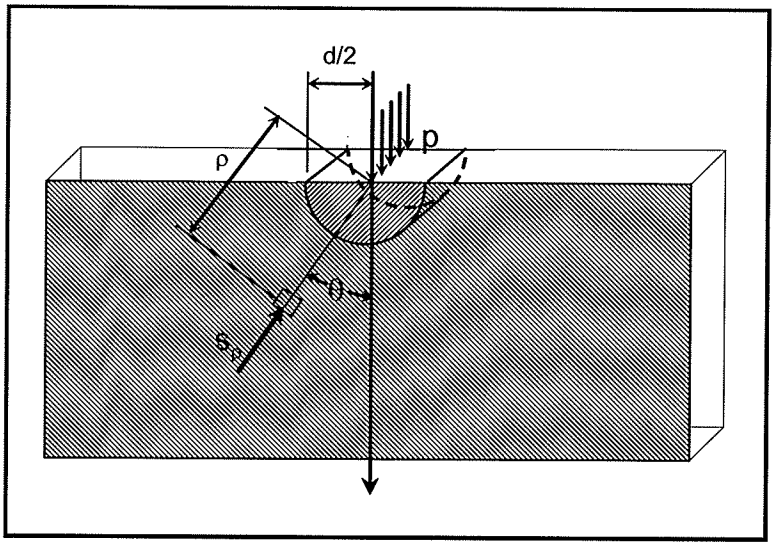

Figure 2.4: Distribution of stress in concrete below dowel bar

The maximum load transferred by a dowel, P_t, across the pavement joint is determined by a concept known as 'dowel group action' [Huang, 1993]. Dowels that cross the joint within a specified spacing act as a system to share the loads applied to the pavement. It is

estimated that the load sharing contribution of each dowel decreases linearly with distance away from the dowel directly under or closest to the location of the wheel load. The number of adjacent dowels that experience load is determined by the relative radius of stiffness of the slab-subgrade system [Westergaard, 1925] as:

$$[10] \qquad \ell = \sqrt[4]{\frac{E_c h^3}{12(1-\nu^2)k}}$$

where, h = thickness of concrete slab
E_c = modulus of elasticity of concrete slab
ν = Poisson's ratio of concrete
k = modulus of subgrade

The modulus of dowel support, K, is a parameter that incorporates the elastic properties of the surrounding mass which is the concrete in this case. The K-value expresses the bearing stress in the concrete developed under a unit deflection of the dowel bar. The Timoshenko-Lessels analytical expressions adopted by Friberg for calculating the deflections of the dowel and the bearing stress in the concrete are highly dependant upon this elastic parameter. The selection of a K-value in design can greatly affect the predicted deflections and bearing stresses. Determination of the correct K-value has been shown to be practically impossible as it can vary with load level, concrete strength, dowel diameter and several other factors [Mannava 1999, Ioannides 1992]. Early theoretical approaches by Friberg estimated the K-value to range from 82 to 409 GN/m^3 depending on the properties of the dowel-slab system.

2.3 Research on Dowels for Concrete Pavements

A recent study at the University of Oklahoma [Mannava et al. 1999] investigated the load-deflection behaviour of a dowel bar embedded in concrete using an experimental approach. This study measured the deflected shape of the dowel bar under load using a set of LVDTs (linear variable displacement transducers) through small vertical shafts leading up through the top of the concrete slab. The test set-up that they used is shown in Figure 2.5. The test specimens incorporated three different dowel bar sizes, three concrete strengths, and two sizes of joint openings. Each specimen comprised a dowel bar with each end embedded in a small concrete slab. Bar deflections were measured in the unloaded slab which rested on a rigid support while the loaded slab was free to displace downward. The concept was very similar to the analytical approach shown in Figure 2.3.

The measured dowel deflections were compared with predicted calculations using the elastic theory. An example of the results is also shown in Figure 2.5. Correlation between the two methods was found to be highly dependant upon the value of the modulus of dowel support. It was found that the back calculated K-value was considerably larger than the early estimates of 82 to 409 GN/m^3 provided by Friberg. K-values required to match experimental results ranged from 240 to 1250 GN/m^3 depending on the load level, concrete strength, and other characteristics of the test specimens.

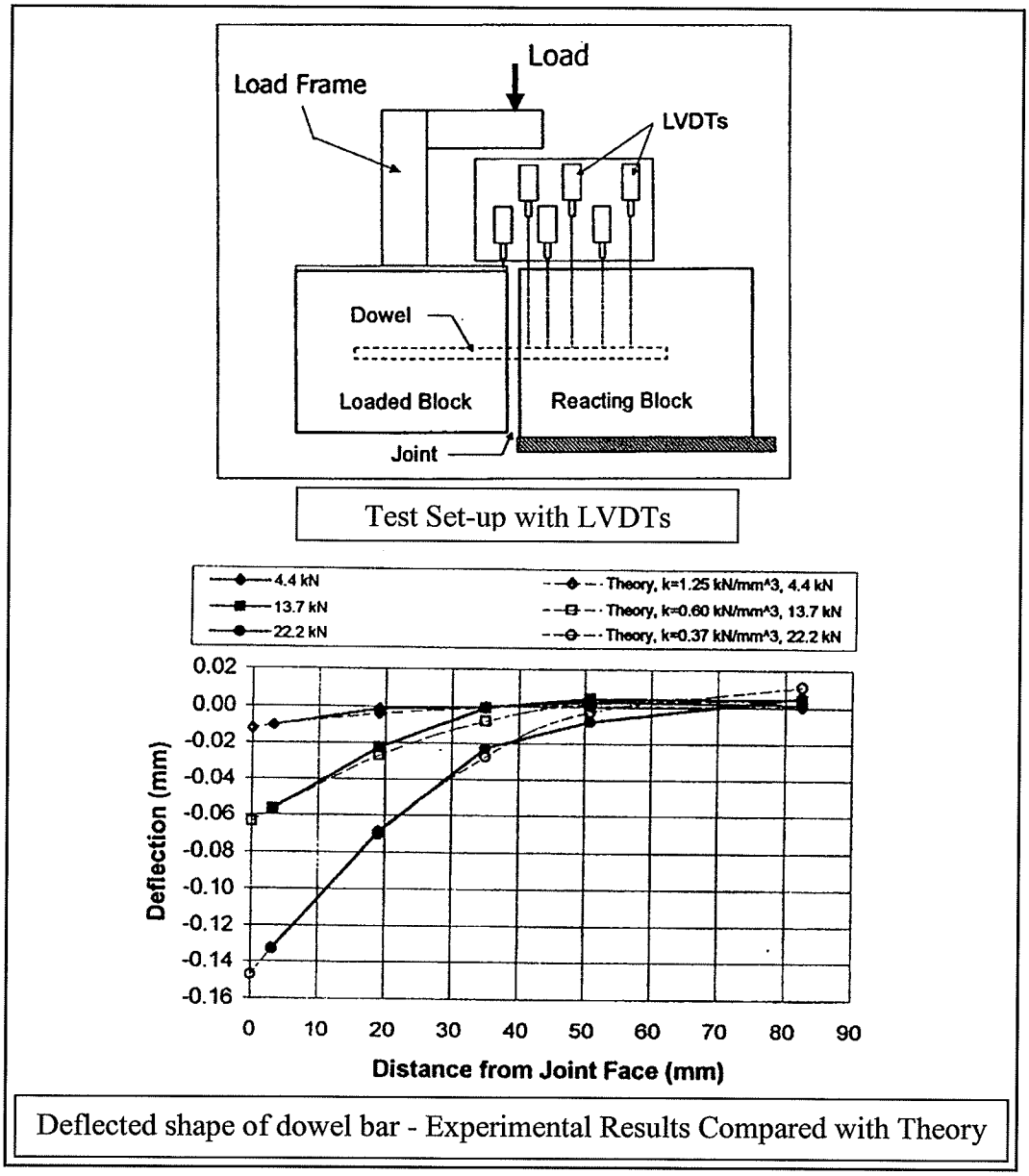

Figure 2.5: Experimental Work by Mannava et. al.

2.4 FRP Dowel Research

Glass fibre-reinforced polymer (GFRP) dowels have been recently introduced as a possible solution to the corrosion problem posed by steel dowels. In addition to their non-corrosive properties, GFRP dowels have a low pull-out force, thereby eliminating the need to grease the dowels before paving the concrete. Glass fibre-reinforced polymer has

a higher strength than steel as seen in Figure 2.6, however, the modulus of elasticity is lower.

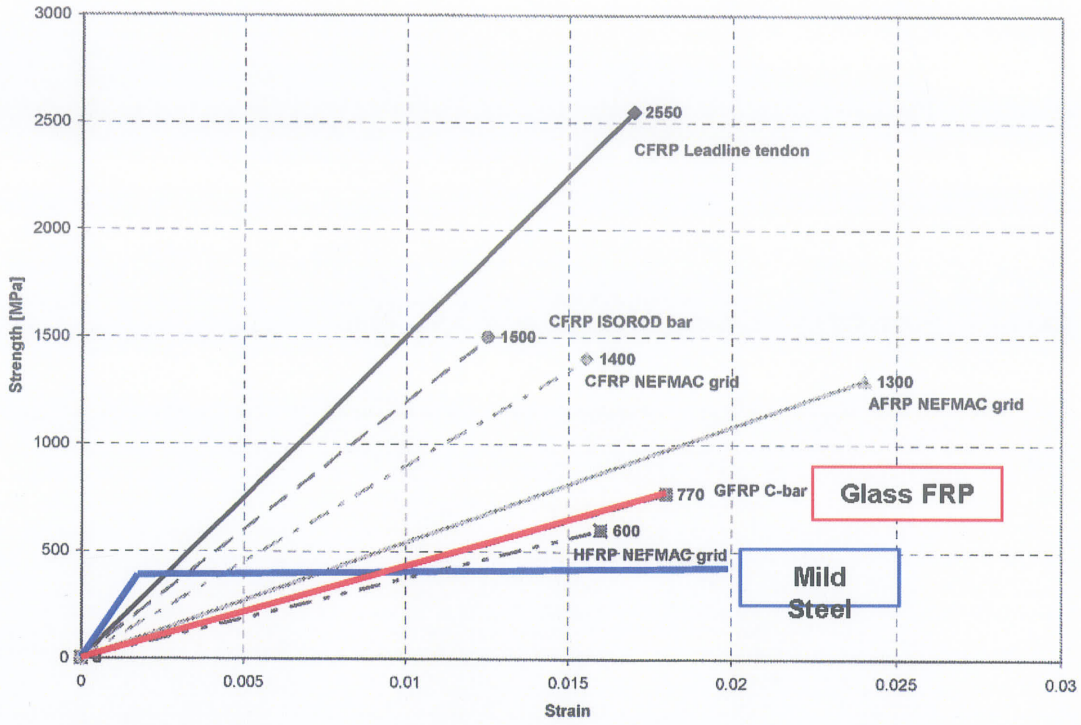

Figure 2.6: Stress-strain relationships for various FRP materials
Source: ISIS Canada Design Manual No. 3 – Reinforced Concrete Structures

The lower modulus results in a lower flexural stiffness for the FRP dowel compared to the steel. As seen in Equations [5] and [7], the magnitude of displacement of the dowel in the concrete slab is dependent upon the flexural stiffness (E_dI_d) of the dowel. A lower stiffness will result in higher dowel displacements which will in turn result in a greater bearing stress at the joint face of the slab. The bearing stress in the concrete can be reduced, however, by increasing the size of the dowel.

There were two studies conducted at the University of Manitoba on the use of glass fibre-reinforced polymer dowels in jointed concrete pavements. The first study [Eddie 1999]

investigated the use of 38-mm (1.5") diameter pultruded GFRP dowels for concrete pavement. This study involved extensive laboratory tests of full scale concrete slabs and resulted in a field application for GFRP dowels. The second study [Murison 2000] investigated the use of large-diameter (60 mm) dowels comprising pultruded and filament wound GFRP tubes filled with concrete. The latter study involved strength testing of the dowels to determine if a concrete-filled GFRP dowel was suitable for use in concrete pavements. The larger dowel was selected as a possible solution to the bearing stress problem outlined earlier. Figure 2.7 shows examples of the dowel specimens tested.

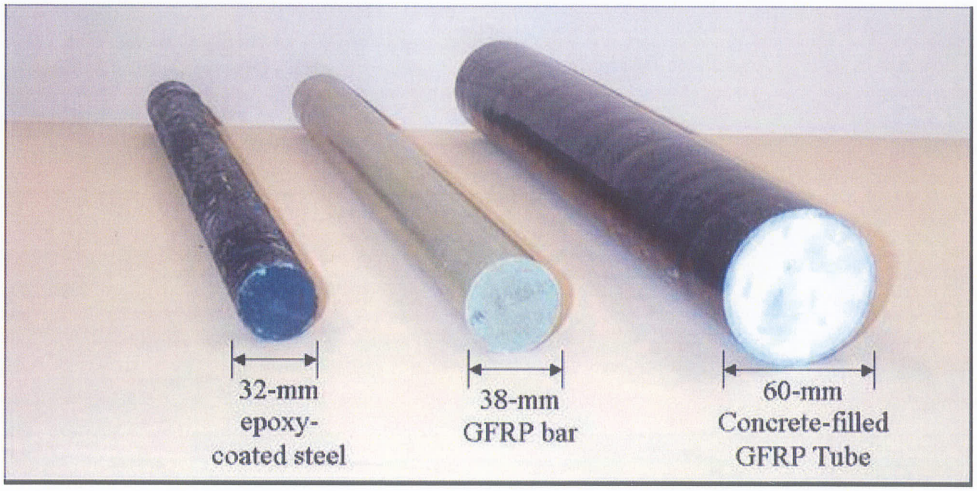

Figure 2.7: Samples of dowels tested at the University of Manitoba

The first study compared two brands of 38-mm FRP dowels to 32-mm epoxy-coated steel dowels that were commonly used by the local transportation department. The dowels were cast in full-scale depth concrete slabs, 254 mm (10") thick and 610 mm (24") wide, which were placed on a compacted subgrade material. The dowels were placed at mid-depth of the slab and a small joint opening was cast between the adjacent slabs. The slab

on one side of the joint was loaded and the load transfer efficiencies were computed. It was found that the GFRP dowels had comparable load transfer efficiencies to the steel dowels. Figure 2.8 shows photos of the experimental work.

Results of this study led to the construction of a field test section on a busy arterial street in Winnipeg, Manitoba. A section of the east-bound lanes of Bishop Grandin Boulevard was used for the field application where three brands of the 38-mm diameter pultruded GFRP dowels were placed along with the 32-mm epoxy-coated steel dowels for control specimens. Figure 2.9 shows photos of the field application.

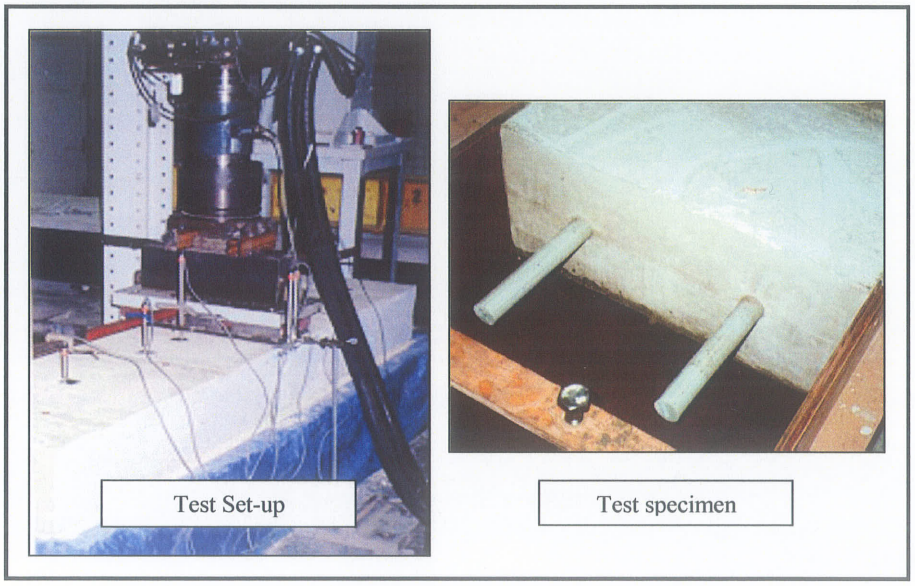

Figure 2.8: Experimental Test Set-up (Eddie 1999)

Figure 2.9: Bishop Grandin Field Application with GFRP dowels

Falling Weight Deflectometer (FWD) Tests were conducted on the field test section after one year of being open to traffic. The results of this test conducted by a geotechnical consulting company showed that two of the three GFRP dowel types tested were performing as well or better than the steel dowels. One of the GFRP products, which had not been tested in the laboratory, exhibited lower LTE values than the other two products that were tested, however, the values were still quite good. The FWD tests were conducted after two years of traffic and similar results were found. The results for all dowel types are quite good thus far, however, two years of traffic will not cause significant changes in performance. Testing of the field application will continue in the future to obtain longer-term performance data. FWD results for the first year are shown in Figure 2.10.

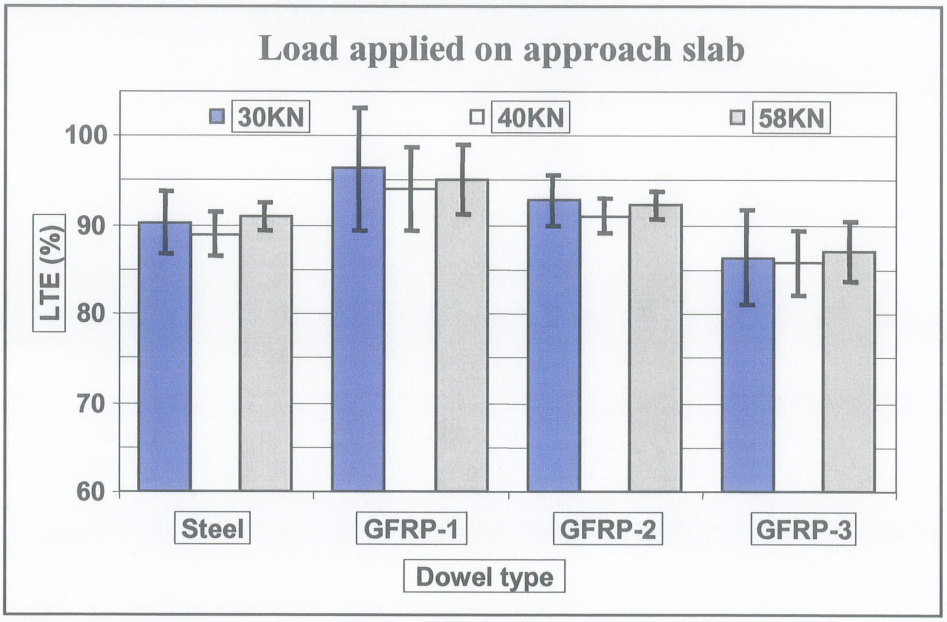

Figure 2.10: Falling Weight Deflectometer Test Results after 1 year of traffic on the Bishop Grandin Boulevard field application.

The second study conducted at the University of Manitoba investigated the possible use of concrete-filled GFRP tube dowels. This study involved tests of the dowel properties including shear and flexural strength tests of various dowel configurations. Shear and flexural strengths were determined from double shear and four-point bending tests which are shown in Figure 2.11.

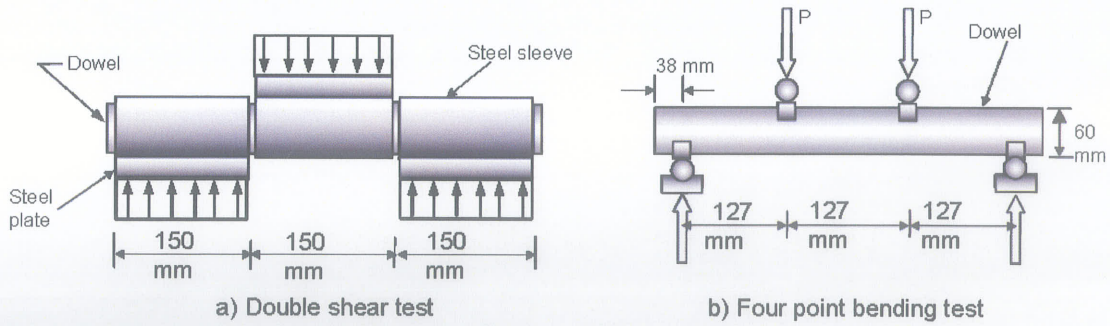

Figure 2.11: Double Shear and Four-Point Bending Test Apparatus

The four types of 60-mm diameter GFRP tubes tested comprised different wind angles and numbers of layers of glass as shown in Figure 2.12. The first dowel type, designated as CF-1, comprised seven glass layers with a 2:1 wind angle and had a wall thickness of 3 mm. Dowel CF-2 comprised only pultruded glass fibres and had a wall thickness of 3 mm. Dowel CF-3 had a similar construction to the CF-1 GFRP tube, however, the wall thickness was only 2 mm. Dowel CF-4 contained six thin glass layers with reversing wind angles of +/- 45 degrees and a wall thickness of 1.6 mm.

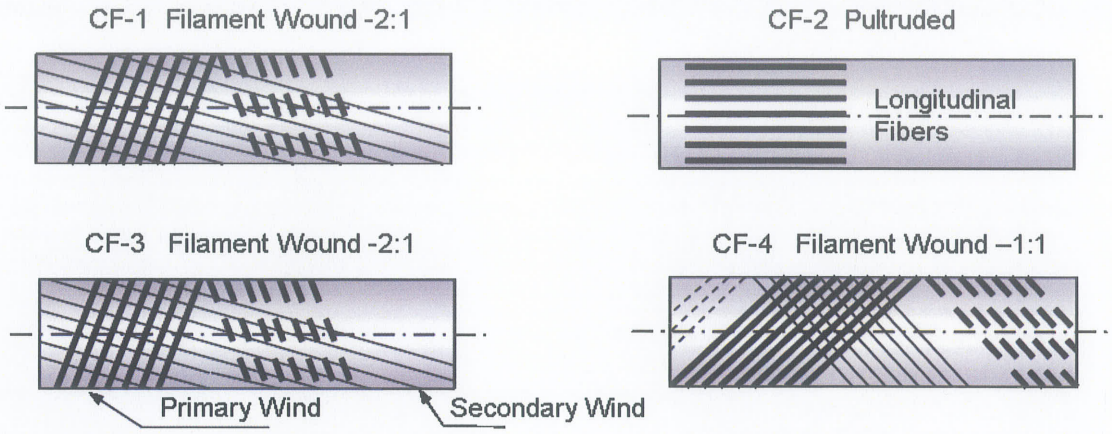

Figure 2.12: Glass fibre orientations for concrete-filled GFRP tube dowels

The concrete core of each dowel comprised Type I (10) cement with the addition of a expansive cement component. It is critical that the concrete core does not shrink because it provides internal strength for the surrounding GFRP tube. Two strengths of concrete were tested in the dowels. The 28-day compressive strengths of the concrete cores were 40MPa and 70MPa.

The results of the dowel strength tests, provided in Table 2.1, showed that concrete-filled GFRP tube dowels exhibited lower shear strengths and lower flexural moduli than the 38-

mm GFRP dowels, however, the strengths were well in excess of the stresses that would be applied to the dowels under traffic loads. For example, the minimum shear load resisted by the concrete-filled dowels was 53 kN which is substantially higher than the expected applied load of 12 kN. This table also includes results of strength tests on the 38-mm GFRP dowels and 32-mm epoxy-coated steel dowels conducted in the first study (Eddie).

Table 2.1: Results of double shear and 4-point bending tests on dowels

Dowel Type	Dowel Diam. mm	No. of samples	Ultimate Shear Load (kN)		Shear Strength (MPa)		4-Pt bending Load (kN)		Max Moment Mr (N.m)	Elastic Modulus (MPa)
			Mean	Std. Dev.	Mean	Std. Dev.	Mean	Std. Dev.		
Steel	31.75	3	450.5	7.0	570.0	8.8	N/A	N/A	-	200,000
GFRP-1	38.10	3	122.0	4.3	107.0	3.8	N/A	N/A	-	41,300*
GFRP-2	38.10	3	171.5	3.7	150.0	3.2	N/A	N/A	-	
GFRP-3	38.10	3	115.5	3.5	101.3	3.1	N/A	N/A	-	
CF-1	62.00	4	85.1	1.1	28.2	0.4	27.4	2.2	3840	30,000
CF-2	60.00	4	53.0	3.5	18.7	1.2	11.3	1.0	1435	31,500
CF-3	60.00	4	55.1	4.0	19.5	1.4	11.9	0.6	1511	25,300
CF-4	60.00	4	66.6	5.4	23.6	1.9	9.4	0.3	1194	20,000

* Estimated from mechanical properties

Figures 2.13(a) and 2.13(b) show graphs that compare the double-shear and 4-pt bending test results for the four concrete-filled GFRP tube dowels tested (Single shear loads are plotted for the double shear test results). The graphs show how diffenences in the properties of each GFRP tube type affect their strength and stiffness. For example, the CF-4 tube, that was filament wound with a 1:1 wind angle, exhibited the greatest shear strength, while the pultruded CF-2 tube had the greatest stiffness (bending test).

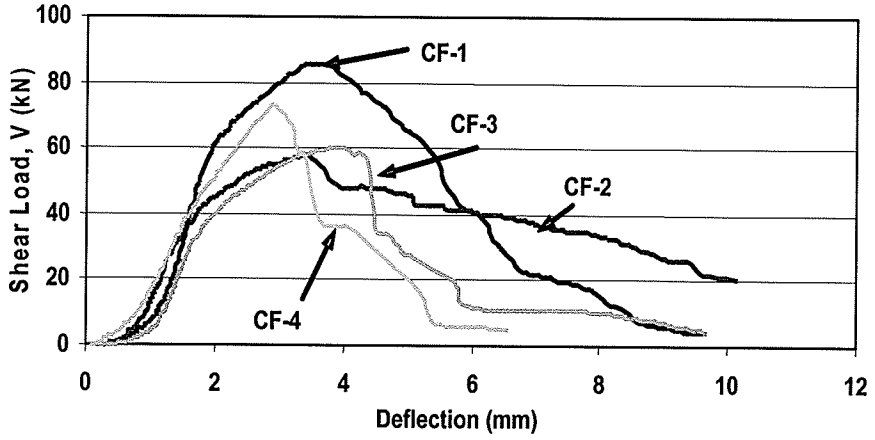

Figure 2.13(a): Load-deflection – Double shear tests on concrete-filled GFRP dowels

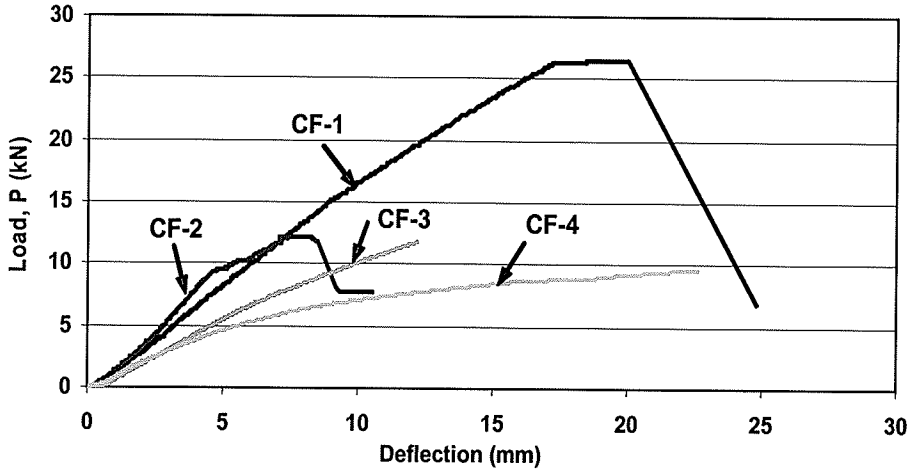

Figure 2.13(b): Load deflection – 4-Point bending tests on concrete-filled dowels

The studies conducted at the University of Manitoba concluded that GFRP dowels, both the solid pultruded dowels, and concrete-filled tube dowels, are suitable for use in jointed concrete pavements, however, the GFRP tubes would need to be altered to provide a greater wall thickness for increased strength and provide a smooth, resin-rich outer surface to allow the dowel to slide without a de-bonding agent.

2.5 Cost of Dowel Materials

The following table provides examples of approximate costs of various dowels or dowel components (Prices listed as of April 2002). It can be seen that the 38-mm solid pultruded GFRP dowels cost approximately 50% more than the epoxy-coated steel dowels of the same size. This may seem large, however, the cost for dowels is a relatively small part of the total cost of new pavement construction. In addition, the long-term cost benefits due to eliminated maintenance for corroded dowels will greatly offset the added capital cost for the dowels. For larger diameter dowels, the GFRP tubes are lower in cost compared with the larger solid pultruded dowels. The prices listed in the table for the GFRP tubes do not include the cost of grout or concrete filling, however, the prices listed would be lower if purchased in mass quantities. The 50.8-mm concrete-filled GFRP tube dowel is estimated to cost approximately $6-$7 US ($9-$10 CDN) when manufactured in mass quantities. It is clear though, that all types of GFRP dowels are lower in cost compared with the stainless steel dowels.

Table 2.3: Approximate Cost Data for Dowel Products

Product Description	Size/Diameter	Price (US)	Price (CDN)
Epoxy-coated Steel	38 mm (1.5")	$4.00	$6.00
Fiberdowel Solid Pultruded GFRP Bars Product of RJD Industries (Contractors Price)	38 mm (1.5")	$6.50	$9.25
	44.4 mm (1.75")	$9.20	$13.75
	50.8 mm (2.0")	$12.00	$18.00
Extren Series 625 GFRP Tubes Product of Strongwell Inc. (GFRP tubes only – No concrete core) (Price per 20 foot minimum purchase)	50.8 mm x 6.35 (2.0" x ¼")	$7.10	$10.65
	63.5 mm x 6.35 (2.5" x ¼")	$9.10	$13.65
Solid Stainless Steel	38-mm (1.5")	$18.00	$27.00

All prices listed for 456 mm (18") dowel lengths.

Chapter 3

Finite Element Analysis

3.1 General

Finite element modeling has become a very powerful and useful tool for predicting and describing the behaviour of many different entities. It can be especially useful for the analysis of three-dimensional models and non-linear materials. A dowel bar embedded in a concrete slab is a good example. The analytical solution for calculating the bearing stress in the concrete around the dowel bar [Friberg 1938] is based on closed-form linear-elastic theory for a beam on an elastic foundation [Timoshenko-Lessels 1925]. Recent experimental work has shown the dowel-concrete system to exhibit non-linear behaviour [Mannava et. al., 1999], however, the linear-elastic solution is still widely used for the design of concrete pavement joints.

As part of this study, a linear finite element analysis was conducted to model the behaviour of a dowel bar embedded in a concrete pavement slab. The analysis was used to predict the behavioural differences between different sizes of steel and GFRP dowels. The material properties of the model represented a worst-case scenario that included a large joint opening of 25 mm and a low concrete compressive strength of 30 MPa. The results of the FE analysis are compared with the linear-elastic analytical solutions.

3.2 The Model

The model was created using ADINA release 7.4 finite element analysis software. Unlike other finite element analyses of jointed concrete pavement systems, this analysis takes a much closer look at the dowel-concrete interface. The mesh in this model is very fine in the critical region around the bar near the joint face of the pavement slab. This was necessary because the deflections and bearing stresses dissipate rapidly with distance from the joint face and more elements were required to achieve greater accuracy.

3.2.1 Geometry

Consistent with the analytical model by Timoshenko and the experiment by Mannava, the finite element models in this investigation comprise a single concrete slab with a dowel bar protruding from one end where the load, P_t is applied. In addition, the model incorporates a linear-elastic base material under the slab. This model attempts to investigate the deflected shape of a dowel bar under load and determine the level of bearing stress produced at the dowel-concrete interface. Four models were analyzed using different types of dowel bars. The dowels modelled were two steel bars with 38-mm and 60-mm diameters and two GFRP bars with the same two diameter sizes. The slab was 300 mm wide and 1000 mm long. The dowel bar extended the full 1000 mm in length as well. This was obviously not an infinite length as used in the analytical approach by Timoshenko, however, it was assumed that the slab was sufficiently long to behave in such a way. The selected slab thickness was 250 mm, however, the top half was removed in the model for simplification and to reduce the number of elements. The base material beneath the slab was 200 mm thick. The base material was incorporated into the model to allow the slab to experience some deflection as it would in the

field, however, the magnitude of displacement of the slab was not important in this study. In theory, the amount of deformation of the dowel bar in the concrete is independent of the slab deflection. Therefore, using a deeper base for the pavement slab was unnecessary.

The location where deflections and bearing stresses are most critical is the region of the bar near the joint face of the slab. Therefore, the mesh was designed to be much smaller in this region and larger with distance away from the joint face and distance away from the dowel bar itself. Figure 3.1 shows the model mesh for both the 38-mm and 60-mm diameter dowels.

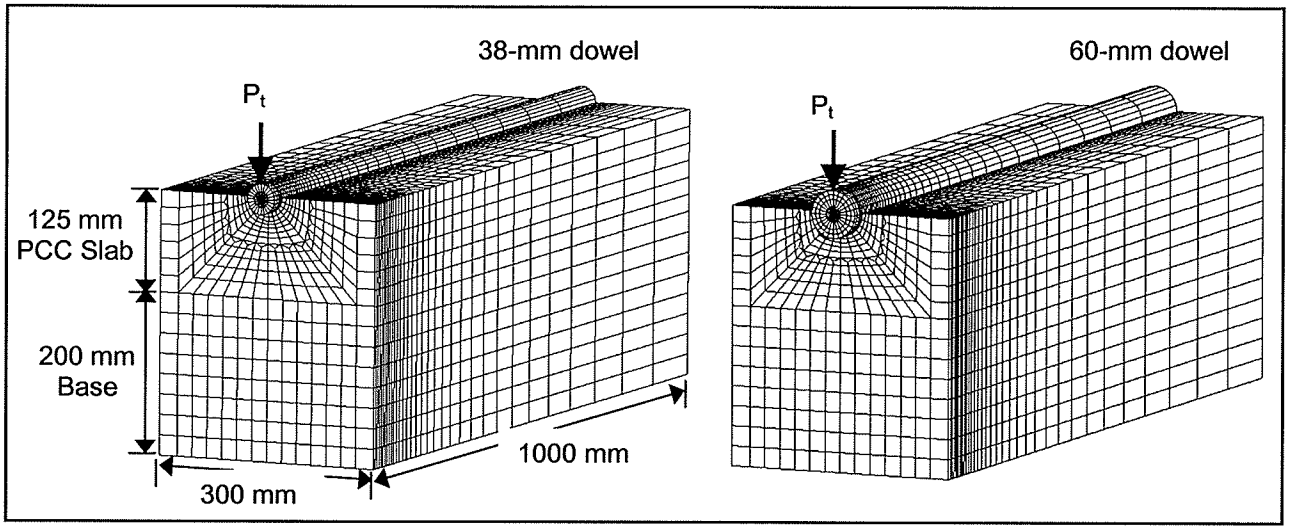

Figure 3.1: Mesh plots for the 38-mm and 60-mm dowels

The models consisted of 8-noded hexagonal (brick) elements. The aspect ratio of the elements was kept under a value of two for elements in the critical region where higher accuracy was required. The aspect ratio of elements at large distances to the side of the dowel and away from the joint face exceeded a value of two, however, deflections and bearing stresses in these regions were of no concern.

3.2.2 Material Properties

The steel bar has an elastic modulus of 200,000 MPa and a poisson's ratio of 0.3. The GFRP was modelled using an elastic isotropic material similar to steel for simplicity, but given a significantly reduced stiffness. The GFRP dowels were given an elastic modulus of 40,000 MPa and a poisson's ratio of 0.3. The concrete had an elastic modulus of 24,600 MPa with a poisson's ratio of 0.2. The concrete compressive and tensile strengths selected were 30 MPa and 5 MPa respectively. The base material was modelled using an elastic isotropic material with a modulus of 1400 MPa and a poisson's ratio of 0.3.

3.2.3 Load

The selection of the load, P_t, to be applied to the end of the protruded dowel bar was determined using the pavement design formulas developed by Friberg. Equation 6, given in the previous chapter, was used to determine the number of dowels that would 'share' the load applied to the surface of the pavement. The largest dowel load was computed and selected for use in the model. A half-axle truck load of 40 kN was used in the calculation which gave a maximum dowel load of 12 kN. In theory, the load is applied to the protruded end of the dowel bar as a point load at a position located at half the width of the joint opening. The joint opening modeled in this study was 25 mm wide so, in theory, a point-load of 12 kN would be applied at 12.5 mm out from the joint face of the slab.

In the finite element model the load was placed quite differently. Instead of a point-load, the load was applied as a vertical pressure acting on the top surface of the protruded portion of

the dowel bar. This was considered more accurate because the load on the dowel would be applied by an adjacent concrete slab which would act as a constant pressure. This would also prevent a high concentration of stress where the load is applied to the dowel. The joint opening or extension of the applied load affects the bending moment produced in the dowel bar, therefore, it was important to ensure that the loading condition in the model produced the same moment as in the theoretical approach. The load in the model was applied to the entire 25-mm extension of the bar, therefore, the resultant of the load would act at the centre, or 12.5 mm out from the face of the concrete slab, producing the same moment as in the theoretical analysis.

3.3 Validation Of The Model

Dowel bar deflections and concrete bearing stresses were obtained from the FEM results and plotted for each of the four dowel bar types. The values were obtained for each of the nodes along the bottom centreline of the dowel-concrete interface. The FEM deflection curves were compared with calculated deflection curves obtained using the analytical expressions based on linear-elastic theory [Timoshenko] that incorporated the same dowel and pavement slab properties. The peak dowel deflections, which occur at the joint-face of the slab, were matched for the two curves by adjusting the modulus of dowel support, or K-value, in the analytical expression. The K-value, which is a linear-elastic property of the concrete surrounding the dowel, represents a bearing pressure caused by a unit deflection of the dowel. The K-value required to match the peak deflections for the FEM and analytical solution was recorded and then multiplied by the deflections calculated with the analytical solution. This produced a curve showing the bearing stress under a dowel bar which was

then plotted against the bearing stress curve obtained from the FEM result. The curves for the FEM and linear-elastic analytical solutions were then compared.

3.3.1 Dowel Deflection

Deflections obtained from the FE models are plotted along with the analytical results in Figure 3.2. It can be seen that the deflections are greatest at the joint face and dissipate rapidly with distance away from the face.

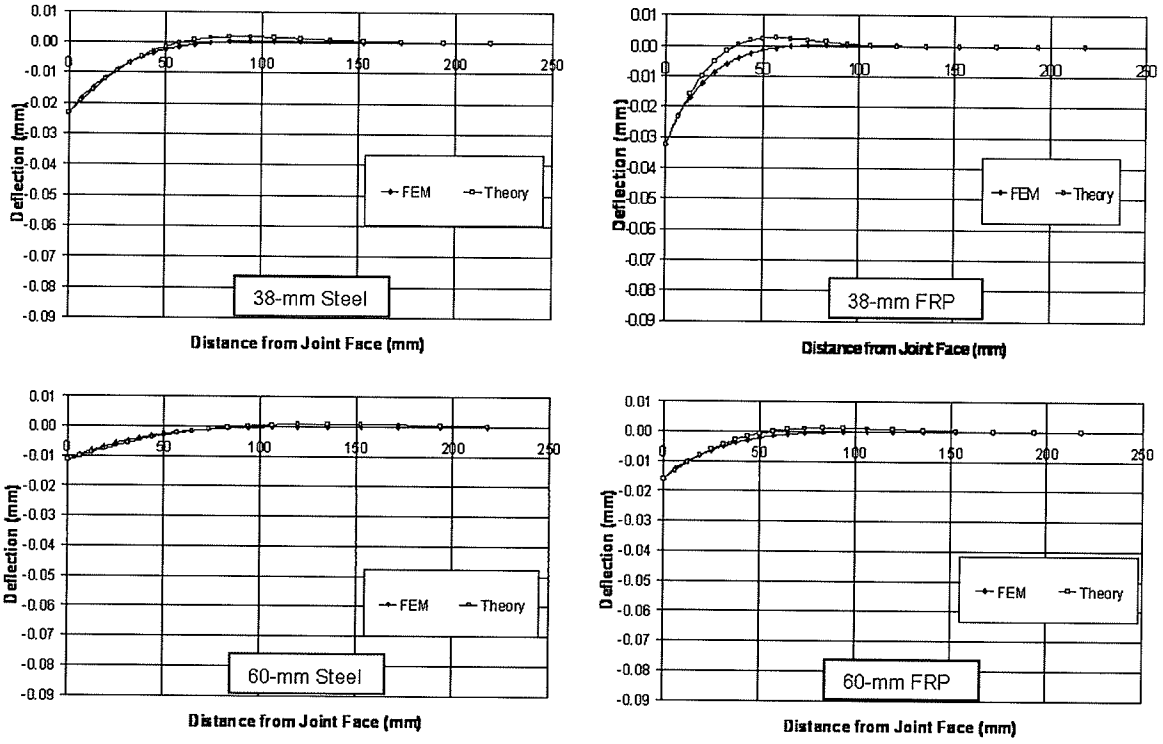

Figure 3.2: Deflection of dowel bars – FEM versus Theory

The FE model deflection curves correlate well with the theoretical curves for all dowel types with the exception of the middle portion of the 38-mm GFRP bar. The theory appears to over-predict the rotation of the bar due to the bending moment induced by the point load.

One noticeable difference between the results of the two methods is that the theory tends to predict larger positive (upward) deflections over the middle portion of the dowel than the model. The dowel bars in the model experienced only mild upward deflections and this was consistent for all dowel types.

Correlation between the two methods was sensitive to the value of the modulus of dowel support. It was found that the range of K-values required to match the deflections at the joint face and produce the theoretical curves shown in Figure 3.2 was 635 to 928 GN/m^3 depending on the type of dowel bar. This is significantly higher than the range suggested in the past [Friberg 1938], however, the values are in the same range as those back-calculated from the experiments by Mannava et al.(1999). Experiments by Teller and Cashell [Teller and Cashell 1958] also back-calculated higher K-values that were in the range of 820 GN/m^3 or twice the maximum value suggested by Friberg. This indicated that the back-calculated K-values in the this study were not overly high. The back-calculated K-values used for each type of dowel bar in this study are given in Table 3.1.

Table 3.1: Results and back-calculated K-values

Dowel Material	Diameter (mm)	Young's Modulus (MPa)	K-value (GN/m^3)	Max. Displacement (mm)	Max Bearing Stress (FEM) (MPa)	Max. Bearing Stress (Theory) (MPa)
Steel	38	200,000	760	-0.023	-33.6	-17.7
	60	200,000	643	-0.011	-15.0	-7.3
FRP	38	40,000	928	-0.032	-55.1	-30.0
	60	40,000	740	-0.016	-24.9	-11.9

The FE models incorporated a 200 mm thick base material beneath the slab which experienced deflections as well. The theoretical expressions for deflection are independent

of the support of the slab. Large changes in the stiffness of the base material in the FE model had negligible impact on the results. This verified the theoretical approach.

3.3.2 Bearing Stress

Correlation between the model and theory was not as good for the computed bearing stresses as it was for deflections (Figure 3.3).

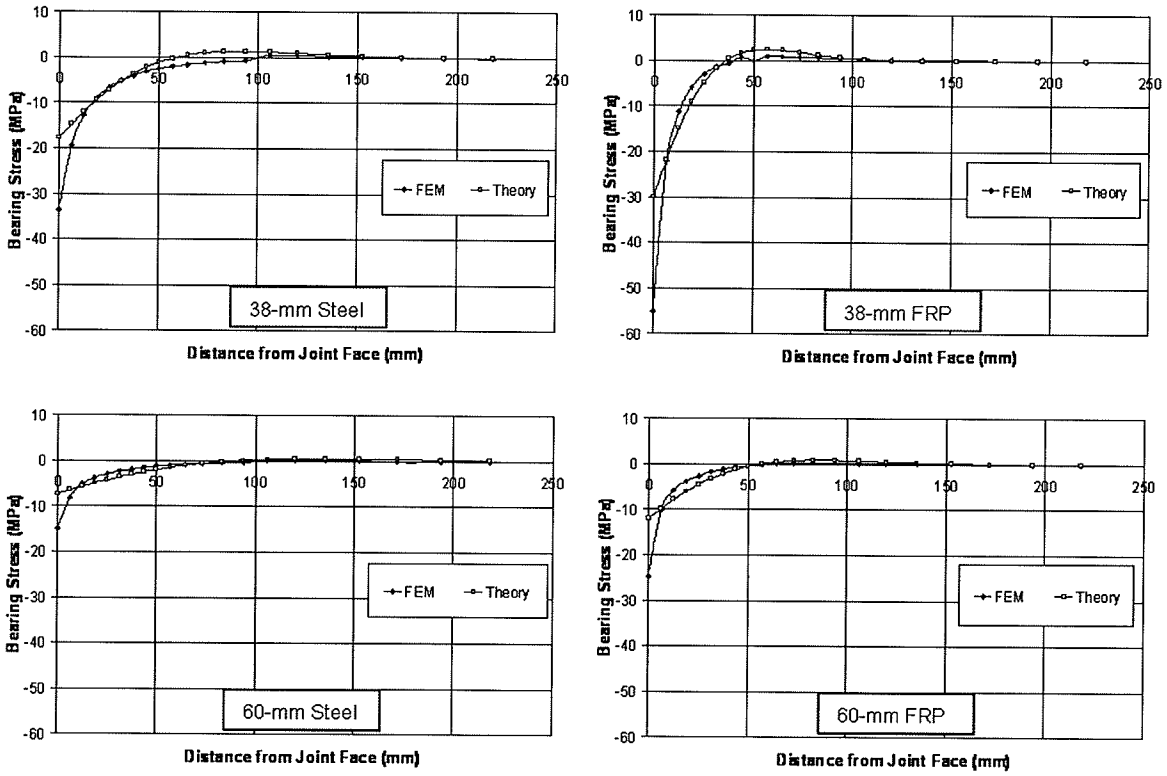

Figure 3.3: Bearing stresses in concrete beneath the dowel bar – FEM versus Theory

In theory, the bearing stress is obtained by multiplying the deflection by the K-value, which means that bearing stress is highly dependant on the selection of that parameter. The finite element model calculates stress from strain and the modulus of elasticity of the concrete and therefore eliminates the use of a K-value. It can be clearly seen in the graphs in Figure 3.3

that the bearing stresses computed at the joint face by the FE model are much higher than those calculated by theory. The stresses dissipate far more rapidly with distance from the joint face for the FE model and are lower in magnitude for the remaining length of the dowel bar compared to theory.

The critical bearing stresses obtained for the 38-mm dowel bars in the model exceed the compressive strength of the concrete which would suggest that crushing or spalling might occur over the first 5 to 10 mm from the joint face. This type of distress is commonly observed in the field and would suggest that the high stresses computed at the joint face by the FE model are not unreasonable. A snapshot of the plotted bearing stresses around the bottom surface of a 38-mm GFRP dowel bar at the joint face is given in Figure 3.4.

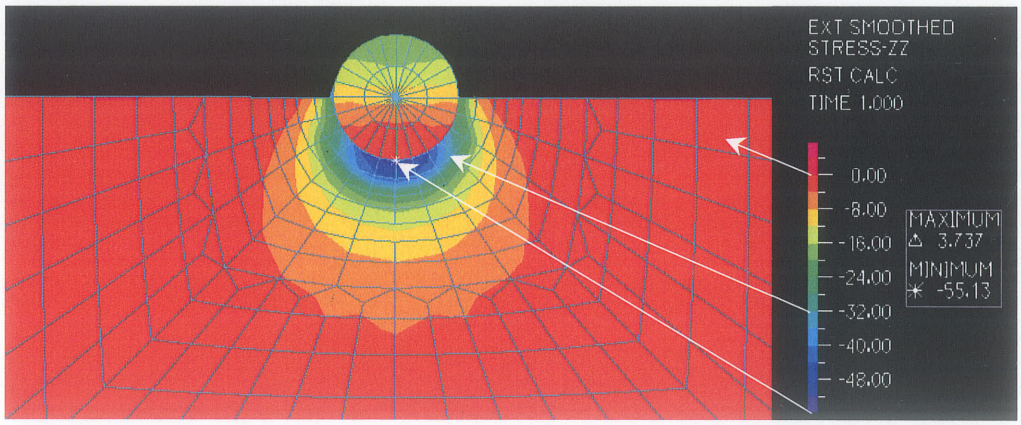

Figure 3.4: Snapshot of bearing stresses below a dowel bar at the joint face plotted by ADINA

The predicted bearing stresses calculated from theory are much lower at the joint face than those computed for the FEM. This may be due to the fact that the analytical solution only accounts for vertical stress on the slab imposed by the deflection of the dowel bar. The finite element solution takes into account the combined state of stress near the joint face which

may produce different results. Also, the result may show that the analytical solution does not accurately predict the true bearing stress near the joint face.

3.4 Comparison Of Dowel Bar Performance

There are significant differences observed between the four types of dowels investigated in this study. Both the finite element model and analytical expressions provided similar results. Figure 3.5 shows the deflection and bearing stress plots for the four dowel types combined.

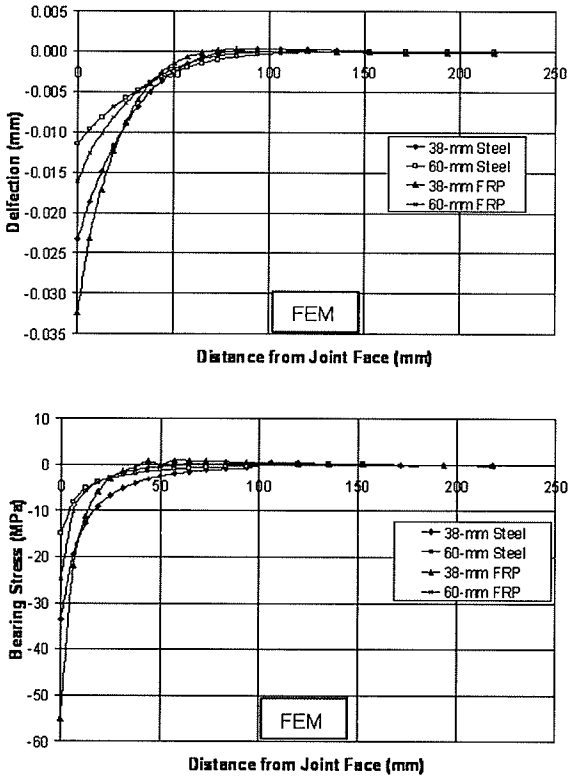

Figure 3.5: Combined dowel bar deflections and bearing stresses

The clear trend is that deflections near the joint face increase with a reduction in stiffness of the dowel bar. The deflections of the lower strength bars were observed to dissipate more rapidly with distance from the joint face than for the steel bars. Because the bar has a lower stiffness, it cannot transfer or 'spread out' the load along the length of the dowel, causing a

higher concentration of force near the joint face. This causes larger deflections and higher bearing stresses near the joint face. The magnitude of the deflections decreases substantially for the 60-mm diameter bars. Obviously the greater size spreads out the load and relieves the stress. The deflections at the joint face produced by the 38-mm bars were more than double the magnitude of the 60-mm bars.

The same trend was evident for the bearing stresses as they are directly related to the deflection of the dowel bar. In Figure 3.5 it can be seen that the GFRP bars produce higher bearing stresses than the steel at the joint face, however, the magnitude of stress dissipates more rapidly with distance away from the joint face. At the joint face the 38-mm GFRP bar produced 64% higher stress than the 38-mm steel bar. The 60-mm GFRP bar produced 26% less stress at the joint face than the 38-mm steel bar and as much as 50% less at 6.5 mm inward. The 60-mm steel bar produced less stress than the 60-mm GFRP, but the magnitudes were almost identical at 6.5 mm inward from the joint face of the slab.

It was found that correlation between the FEM and theory was sensitive to the input value of the modulus of dowel support, K. Past studies have shown that the K-value can vary greatly depending on several factors including load level [Mannava 1999], concrete strength, and depth of concrete below the dowel [Friberg 1938]. The selected K-values used in this investigation to match the maximum deflections of the dowel bar appear to show a trend. As shown in Table 3.1, the K-value increased with a decrease in stiffness of the dowel bar and increased with a decrease in diameter of the bar.

3.5 Summary

Dowel bar deflections and concrete bearing stresses computed using analytical expressions appeared to correlate well with solutions obtained from the finite element model. However, this correlation is highly dependent on the selection of the K-value which varied considerably between the four dowel bar types. The range of back-calculated K-values is found to be substantially higher than that currently used in design of concrete pavements. According to the theory by Timoshenko, higher K-values give lower dowel displacements. This suggests that the magnitude of the displacements in the FE model could be quite low compared to actual. This study reassured the fact that the determination of a proper K-value for design is extremely difficult. One of the greatest benefits of using the finite element method is that it does not require the input of a K-value to obtain a solution. Only known parameters such as elastic moduli, poisson's ratios, and concrete compressive strength, f'_c, need to be input.

Both the finite element model and theory predicted similar behavioural differences between the four dowel types. It was clear that the GFRP bars with a lower stiffness exhibited higher deflections and bearing stresses at the joint face of the slab than did the steel bars of identical sizes. Bearing stresses were as much as 64% higher for the 38-mm GFRP bars, however, the difference dropped substantially a small distance in from the joint face and were 11% less at 12.5 mm inward. The larger diameter of 60 mm clearly reduced deflections and bearing stresses considerably.

Chapter 4

Experimental Program

4.1 General

The experimental program was conducted to study the performance of various dowel types under simulated vehicle axle loads. The dowels, cast into full-scale depth concrete slabs, were loaded in shear by a steel loading device. The mechanism simulated the effect of an adjacent slab being loaded and transferring that load across the joint via the dowel bars. Elastic solutions by Friberg [Friberg 1938], the finite element analysis in this study, and other past experimental work have all shown that lower dowel deflections produce less strain in the concrete and therefore less bearing stress in the concrete. Reduction of bearing stresses will result in less damage to the concrete. By measuring the dowel deflections, it is possible to determine the optimum dowel design for use in concrete pavement joints.

The experimental program comprised two phases. Phase I involved static and cyclic loading of four slabs, each cast with a different type of dowel. The slabs were loaded up to a service level of 12 kN and then unloaded. Static tests were repeated after sets of 250,000 cycles up to a total of 1,000,000 cycles. The second phase comprised four similar slabs that were loaded monotonically until failure of the dowels. The steel dowels, which have a significantly greater stiffness, were loaded until the strain in the bar reached yield. For all tests, the dowels and slabs were instrumented to measure load-deflection and load-strain responses as well as plot the deflected shape of each dowel under load.

4.2 Materials

This section describes the different types of dowels used in the study and details on the fabrication of the concrete-filled GFRP tubes including properties of the concrete mix design. Data are provided for the concrete mixes used for casting the slabs as well.

4.2.1 Dowels

There were four types of dowels tested in this study. These are a 38-mm (1.5") diameter epoxy-coated steel dowel, a 38-mm pultruded GFRP dowel, and two sizes of concrete-filled GFRP tube dowels with outside diameters of 50.8 mm and 63.5 mm (2" and 2.5"). The GFRP tube thickness for both dowel sizes was 6.2 mm (1/4"). All dowels were 456 mm (18") in length. Figure 4.1 shows a photo of the four dowel types. The 38-mm steel and GFRP dowel bars tested are typical of those most commonly used in the field today. Testing of these dowels allows for a direct comparison of the effect of bar stiffness on dowel performance as the size of each bar is identical. The concrete-filled GFRP dowel bars were selected because of their larger size and economical construction along with the non-corrosive properties of GFRP and concrete. Comparisons between the concrete-filled dowels and the 38-mm diameter dowels provided information on the effect of bar size on dowel performance.

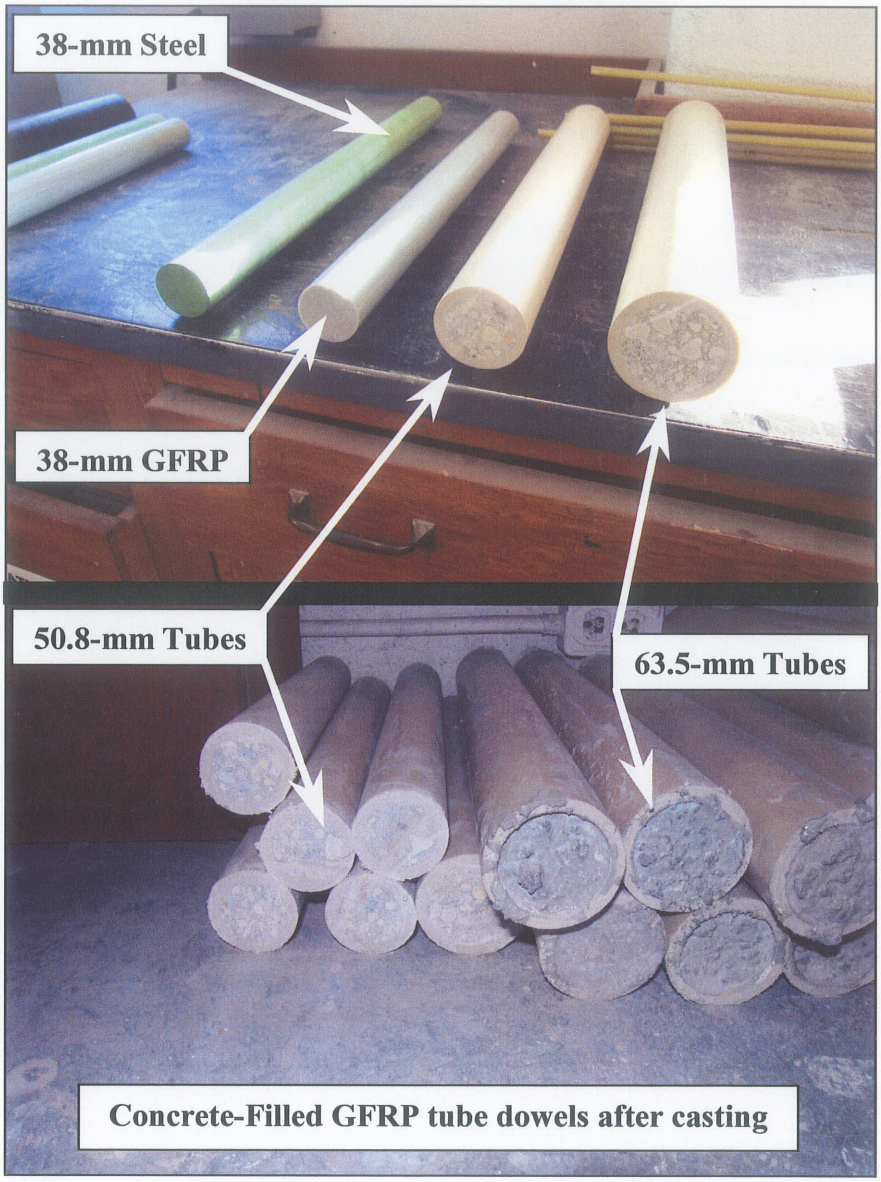

Figure 4.1: Dowel Bars Tested

The 38-mm diameter epoxy-coated steel dowels tested in this study comprised mild steel with a yield strength of approximately 300 MPa and were provided by Cowen Steel in Winnipeg, Manitoba. The elastic modulus was 200,000 MPa with a poisson's ratio of approximately 0.3.

The 38-mm GFRP dowels were manufactured by RJD Industries in Laguna Hills, California. They comprise 70% pultruded glass fibres / 30% resin by volume as provided by the manufacturer. The dowels had an elastic modulus of approximately 40,000 MPa. Tensile and shear strength data for these dowels provided by the manufacturer are given in Table 4.1.

Table 4.1: Shear and Tension Test Data for FiberDowel GFRP Dowels (As per Manufacturer)

FiberDowel	Tensile Tests -			Single Shear Tests -	
Diameter mm (inches)	Fail Load kN	Elongation	Failure Mode	Fail Load kN	Failure Mode
12.5 (.500")	90	0.08%	Tensile	30	Shear
19.0 (.750")	174	0.09%	Tensile	91	Shear
22.2 (.875")	234	0.09%	Tensile	114	Shear
25.4 (1.00")	287	0.08%	Tensile	128	Shear
31.8 (1.25")	458	0.24%	Tensile	131	Shear
38.1 (1.50")*	630	0.39%	Tensile	146	Shear
44.4 (1.75")	856	0.39%	Tensile	193	Shear

* The dowel size used in the experimental program

The GFRP tubes used for the concrete-filled dowels were provided by Strongwell, Inc. in Bristol, Virginia. The tubes are part of the Extren Series 625 pultruded GFRP products fabricated by Strongwell. They comprise layers of continuous strand mat that provide multi-directional strength and pultruded layers that provided strength in the longitudinal direction. The GFRP tubes have a vinyl-ester resin that is corrosion resistant and fire retardant. The composition of the tubes is 70% glass fibres by volume and 30% resin. The Extren Series 625 tubes have a synthetic veil on the outer layer that provides additional protection against corrosion. The concrete cores were cast by filling 508 mm long (20") sections standing upright and using tamping rods and a vibrator to consolidate the concrete. Figure 4.1 shows

the dowels after they were cast. Once the cores hardened, the ends of the tubes were cut off with a diamond blade to provide smooth ends and leave a 457 mm (18") long dowel. Properties of the Extren Series 625 GFRP tubes and the concrete mix for the core are provided in Tables 4.2 and 4.3 respectively. The concrete core of the dowel is expected to crack under service load based on earlier tests on concrete-filled dowels at the University of Manitoba [Murison 2000]. These tests showed that the ultimate shear and flexural strength of the dowel is provided mainly by the GFRP tube. The concrete core provides internal support to reduce ovalizing and prevent crushing of the surrounding GFRP tube.

Table 4.2: Extren Series 625 Tube Minimum Ultimate Coupon Mechanical Properties (As per Manufacturer)

Mechanical Property	Value	Units	ASTM Test
Tensile Stress, LW	207	MPa	D638
Tensile Modulus, LW	17.9	10^3 MPa	D638
Compressive Stress, LW	207	MPa	D695
Compressive Modulus, LW	17.9	10^3 MPa	D695
Modulus of Elasticity, E	19.3	10^3 MPa	-
Short Beam Shear, LW	31.0	MPa	D2344
Poisson's Ratio	0.330	mm/mm	D3039

LW – Lengthwise Direction of Dowel

Table 4.3: Properties of Concrete Mix For GFRP Dowel Cores

Mix Properties		Mix Design Components	
Cement	Type I	**Water/Cement**	0.35
Slump	200 mm	**Water Content**	150 l/m^3
Aggregate Size	10-mm max.	**Cement Content**	429 kg/m^3
28-Day Compressive Strength	f'c = 48 MPa	**Course Aggregate**	1150 kg/m^3
	Std. Dev. = 0.9	**Fine Aggregate**	734 kg/m^3
		Air Content	1.5-3 %
	C.V. = 0.018	**Total Volume**	1 m^3
		Total Weight	2463 kg/m^3

4.2.2 Concrete

The concrete used for the pavement slabs was supplied by a local mixing plant and had a specified 28-day compressive strength of at least 35 MPa. Results of the cylinder tests as provided in Table 4.4 showed the strengths to be significantly higher (in the range of 46 MPa or greater). There were two batches of concrete cast into the slabs. The first batch was used to cast six of the eight slabs while the second batch was used to cast the remaining two slabs as shown in Table 4.5.

Table 4.4: Pavement Slab Concrete Compressive and Tensile Strength Cylinder Tests

Aug. 30, 2002	Batch 1	(MPa)	Batch 2	(MPa)
(28-day)	1	48.8	1	53.3
	2	45.1	2	50.4
	3	44.4	3	51.2
	Average:	**46.1**	**Average**	**51.6**
Oct. 2, 2002	Batch 1	(MPa)	Batch 2	(MPa)
(8 weeks)	1	53.65	1	-
(Phase I)	2	53.28	2	-
	3	51.21	3	-
	Average:	**52.7**	**Average:**	**-**
Nov. 10, 2002	Batch 1	(MPa)	Batch 2	(MPa)
(14 weeks)	1	59.4	1	63.7
(Phase II)	2	58.3	2	63.4
	3	59.0	3	65.7
	Average:	**58.9**	**Average:**	**64.3**
Tensile Stength	Batch 1	(MPa)		
28-Day	1	4.2		
	2	5.1		
	3	4.6		
	Average:	**4.6**		

Table 4.5: Test Specimen Identification

Specimen	Concrete Batch Number	
	Phase I	Phase II
38-mm Epoxy-coated Steel	1	2
38-mm FiberDowel Pultruded FRP	1	1
50.8-mm Concrete-Filled FRP Tube	1	2
63.5-mm Concrete-Filled FRP Tube	1	1

4.3 Test Specimens

A total of eight concrete pavement slabs were constructed. There were two sets of four slabs containing a pair of each of the four types of dowels. The two dowels in each slab were placed at mid-depth and were spaced 305 mm (12") apart centre to centre as shown in Figure 4.2.

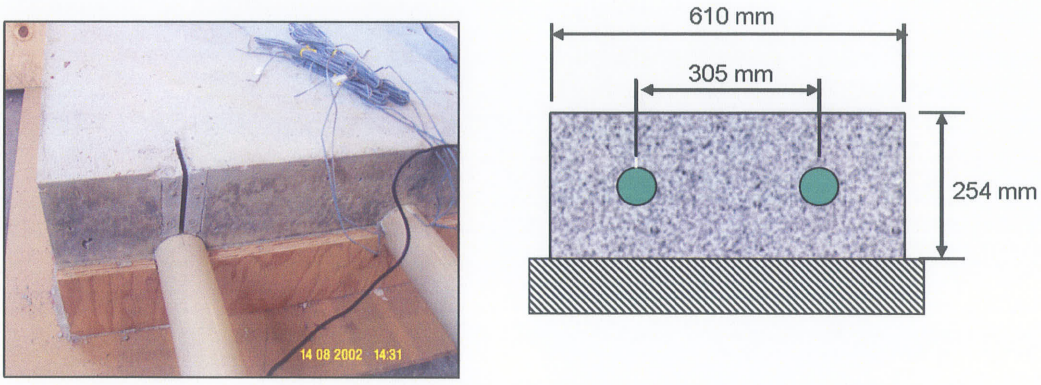

Figure 4.2: Pavement Slab Test Specimen

The dimensions of the slabs were 610 mm x 610 mm x 254 mm thick (24" x 24" x 10") and the thickness is typical of a freeway or expressway pavement. The dowels were embedded 229 mm or half their length into the slab. A small shaft was cast in the slab above one of the dowels in each slab. This shaft that lead down from the top of the slab to the top of the embedded dowel bar was used to measure the dowel deflections directly. During the tests,

the protruded ends of the dowels were loaded directly eliminating the need to cast an adjacent slab. The main objective of not having an adjacent slab was to eliminate any deflections of the bar within the loaded slab and to have the joint face open for visual monitoring of damage. A steel cross-head that applied load directly to the dowels was placed at a specified distance from the concrete joint face (12.5 mm) simulating the loading conditions on a typical pavement joint opening.

4.3.1 Instrumentation

Instrumentation was used to measure several parameters including strain in the dowel bars due to bending, strain in the concrete in the critical region directly below the dowel bar, and dowel bar deflections. The displacement of the loading device was measured by linear variable differential transducers (LVDTs) located at each dowel and were attached to the steel cross-head. These displacements along with the load and stroke and all other strains and displacements were recorded using a computerized data acquisition system.

4.3.1.1 Dowel Bar Deflection

The main objective of this study was to capture the deflected shape of each dowel bar type under load. In order to accomplish this task, several steps needed to be taken. The first step was to cast a short narrow slot in the concrete slab that would lead from the top surface of the dowel bar up though the concrete slab. This slot allowed for the use of small LVDTs to measure the dowel displacements at specified distances along its top surface. The slot measured approximately 6 mm wide and 60 mm long parallel to the direction of the dowel bar. It was expected that the dowel bar would exhibit upward force at a distance greater than

60 mm so the slot did not extend further. This was done so that the behaviour of the dowel would not be affected by the removal of concrete above it.

A compact support fixture was manufactured to house the LVDTs in a way that would allow for several displacement measurements to be taken within close proximity to each other. The LVDTs were held in place by the device and measured the displacement of the dowel through stainless steel extension rods resting against the top surface of the dowel bar. Small cavities were pre-tapped into the top surface of the dowel bar prior to casting of the slabs at the specified locations where the measurements were required. A total of five LVDTs were required to measure displacements over a 50 mm long section of the dowel bar. The critical section is the region where displacements are highest and extends from the location of the joint face up to 50 mm inward where displacements are approximately zero. This was estimated from the finite element model developed in this study as well as the experimental work conducted by Mannava [Mannava et. al. 1999]. The locations of the five points were zero (at the joint face), 10, 20, 35, and 50 mm inward from the joint face as shown in Figure 4.3. The first three LVDTs closest to the joint face were spaced more closely together because there was an exponential decrease in displacement with distance from the joint face as seen with Equation [5] in Chapter 2. In order to read displacement measurements that were closely spaced, the LVDTs needed to be stacked on top of each other in a way that extension rods from the top LVDTs would pass down in-between the bottom ones as shown in Figure 4.3. The LVDTs were otherwise too large to place side by side. The LVDTs had a total travel of 6.35 mm and an accuracy of 0.001 mm. This high level of accuracy was required as the expected displacements at service loads ranged between zero and 0.1 mm.

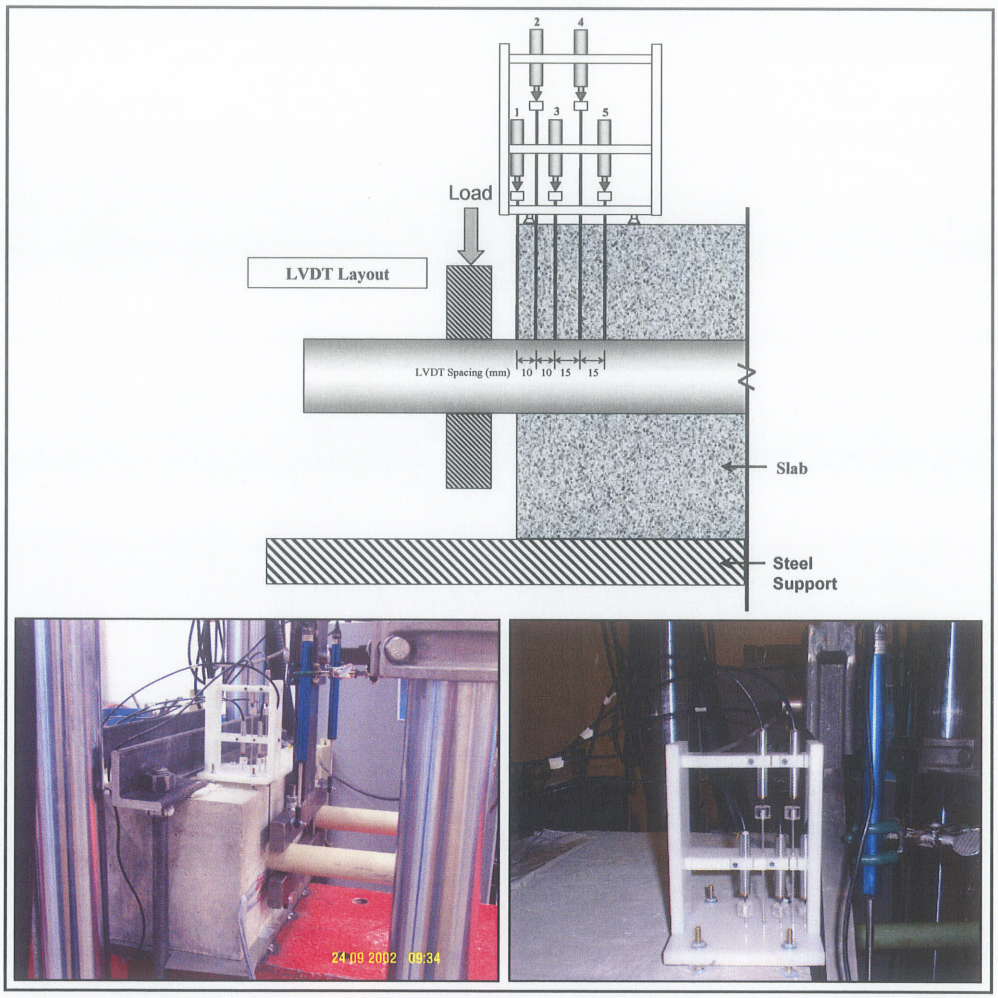

Figure 4.3: LVDT dowel-deflection measuring system

4.3.1.2 Dowel Bar Flexural Strain

One of each pair of dowels in every slab was instrumented with electrical resistance strain gauges to measure longitudinal strains due to bending. The strain gauges used were Type FLA-3-11-5L with a 3-mm gauge length manufactured by Tokyo Sokki kenkyujo Co., Ltd. The gauges were attached using M-Bond 200 adhesive and coated for protection against moisture. The gauges were then covered with a thin, smooth layer of fast-curing epoxy to prevent damage that may be caused by the casting of the concrete. A total of six gauges were

placed on each bar, three on the top and three on the bottom, as shown on the diagram in Figure 4.4. In theory, the maximum bending moment that would occur in the bar under load would exist within the region instrumented with strain gauges. Therefore, the gauges were placed at 3 mm, 19 mm and 38 mm (1/8", 3/4", and 1.5") inside of the face of the concrete. This arrangement would allow for a better approximation of the maximum strain due to bending of the dowel bar and would provide information on the curvature of the deflected bar.

4.3.1.3 Concrete Strain

Strain gauges were selected to monitor the behaviour of the concrete loaded by the dowel bar above. In theory, when load is applied to the dowel, a series of bearing stress bulbs form beneath it decreasing in magnitude with distance away from the dowel. In this study, a series of five small 2-mm strain gauges were used in an attempt to capture this strain gradient. The electrical resistance strain gauges were Type QFXV-1-11-002LE, 120 Ohm, manufactured by Tokyo Sokki Kenkyujo Co., Ltd. Each strain gradient gauge contained five 2-mm length strain gauges for a total gauge-length of 12 mm. Figure 4.5 shows a photograph of one of these gauges and a diagram showing the placement of the gauge on the concrete slab.

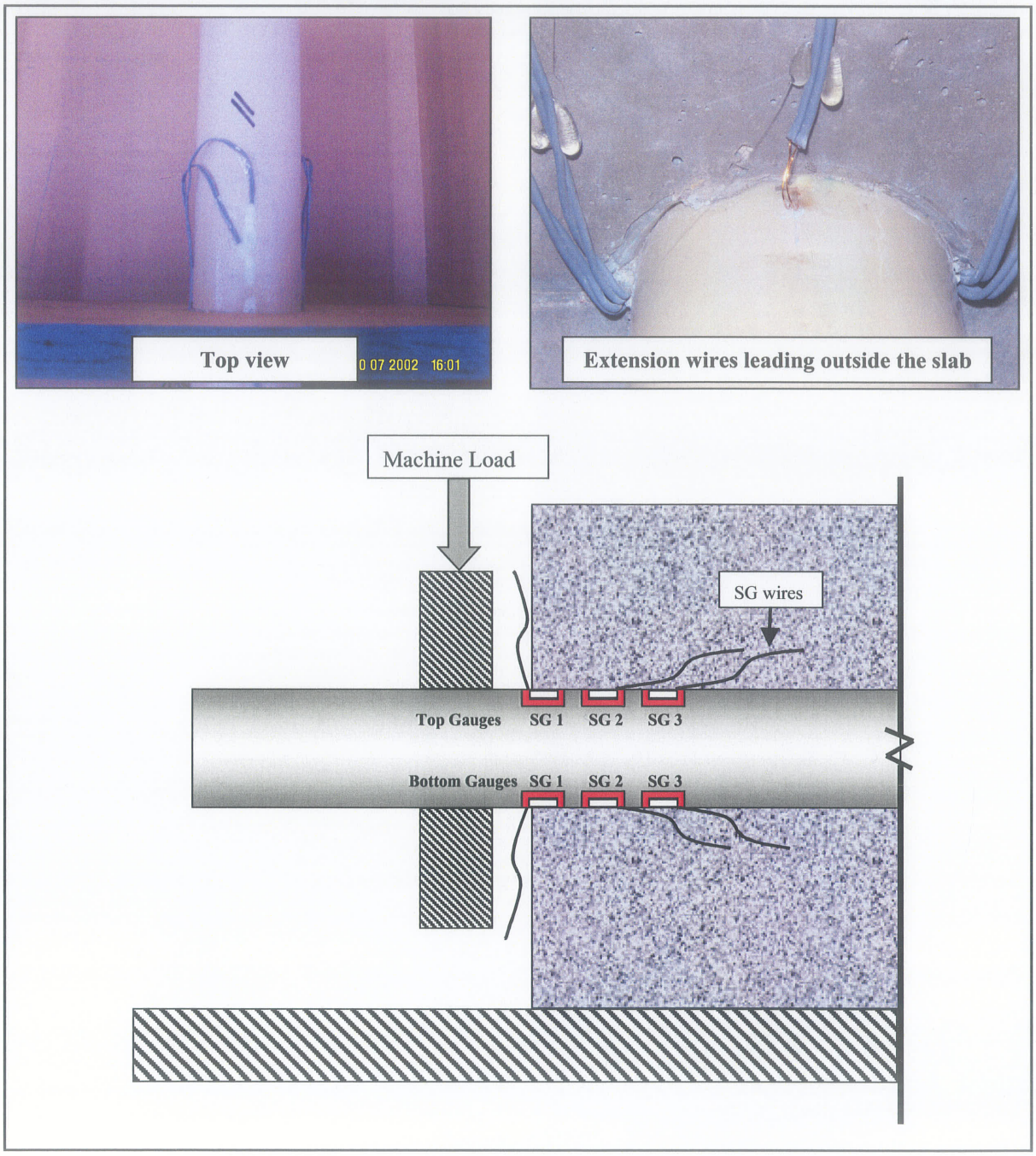

Figure 4.4: Strain gauge layout for measuring bending strains

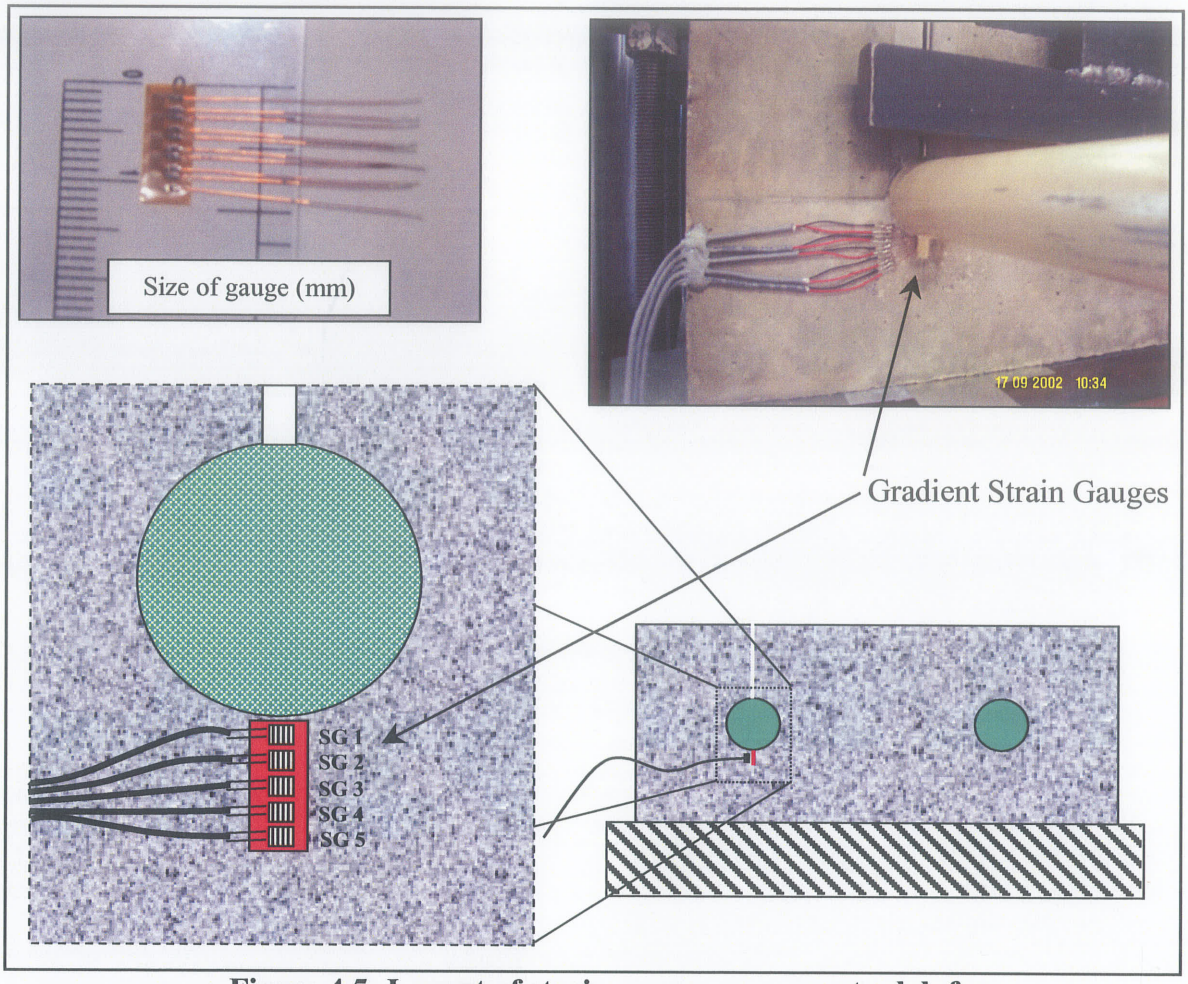

Figure 4.5: Layout of strain gauges on concrete slab face

4.3.2 Fabrication of the Test Specimens

A total of eight slabs were fabricated for the experimental program. There were two dowels cast in each slab that were embedded half their length. For each slab, one of the dowel bars was instrumented with electrical resistance strain gauges to measure flexural strains. The extension wires for these gauges had to be placed in such a way that they would not affect the bearing area above and below the dowel. The two strain gauges nearest the joint face were placed so that the attached wires were directed outwards from the slab and therefore were not embedded in the concrete. The extension wires for the remaining four gauges were routed

back outside of the slab by placing them along each side of the dowel where the bearing stress would be virtually zero.

The second dowel cast into the slab was prepared for measuring vertical displacements using the LVDT set-up described earlier. This dowel had small cavities pre-tapped on its upper surface before being placed in the formwork. The small shaft above this bar was cast using thin galvanized sheet metal as shown in Figure 4.6 along with other photos of the formwork. The bottom edge of the sheet metal that rested above the dowel surface was sealed using glue from a hot glue-gun. The glue prevented cement paste from seeping in and filling the pre-tapped cavities in the dowel. A small metal shim was placed inside the metal slot to prevent the shaft from caving in during casting of the concrete. Two bolt anchors were cast into the sides of each slab to facilitate transport and placement of the slabs in the test set-up.

The formwork was removed after curing for 12 days. Each slab had to be instrumented with the strain gradient gauges. These gauges were placed on the concrete surface directly below the dowel bar that had the shaft cast above it. The concrete was prepared by placing a thin coat of epoxy on the surface to fill any voids and to leave a smooth surface for bonding the strain gauges. The gauges were bonded to the sanded epoxy surface using M-Bond 200 adhesive. Extension wires were soldiered on the ends of the lead wires that were attached to the strain gauges as shown in Figure 4.5.

Figure 4.6: Fabrication of the Test Specimens

4.4 Test Set-up

For all tests, the concrete pavements slabs were anchored down to a large rigid support beam. The slabs were anchored down by bolting together steel angles placed above the slab and below the rigid spreader support beam as shown in the diagram in Figure 4.7. The requirement for a rigid support for the slab led to the use of the large spreader beam. The beam was raised off the ground by placing it across two steel 10" square hollow steel sections and then anchored to the floor using tie-down bars. In theory, the deflection of the dowel bar within the concrete slab is unaffected by the amount of base support. Therefore a rigid base could be used instead of a compacted granular material. Using the rigid beam reduced the overall stroke of the test machine allowing for a higher frequency to be used during cyclic testing. It also eliminated the complexities of setting up a simulated subbase material to support the pavement slab. The slabs were loaded using an MTS 1000 kN capacity closed-loop servo-hydraulic testing machine.

For Phase I, the MTS machine was set up so that its total voltage would range over a maximum limit of 100 kN. This was done because the dowels were not loaded above the 100 kN level, and spreading the voltage change over a smaller load range increased the accuracy of the load measurements. For example, a total voltage of 10 Volts could be divided up over a range of 100 kN instead of 1000 kN. For Phase II, the full 1000 kN load range was used because the dowels were loaded to failure.

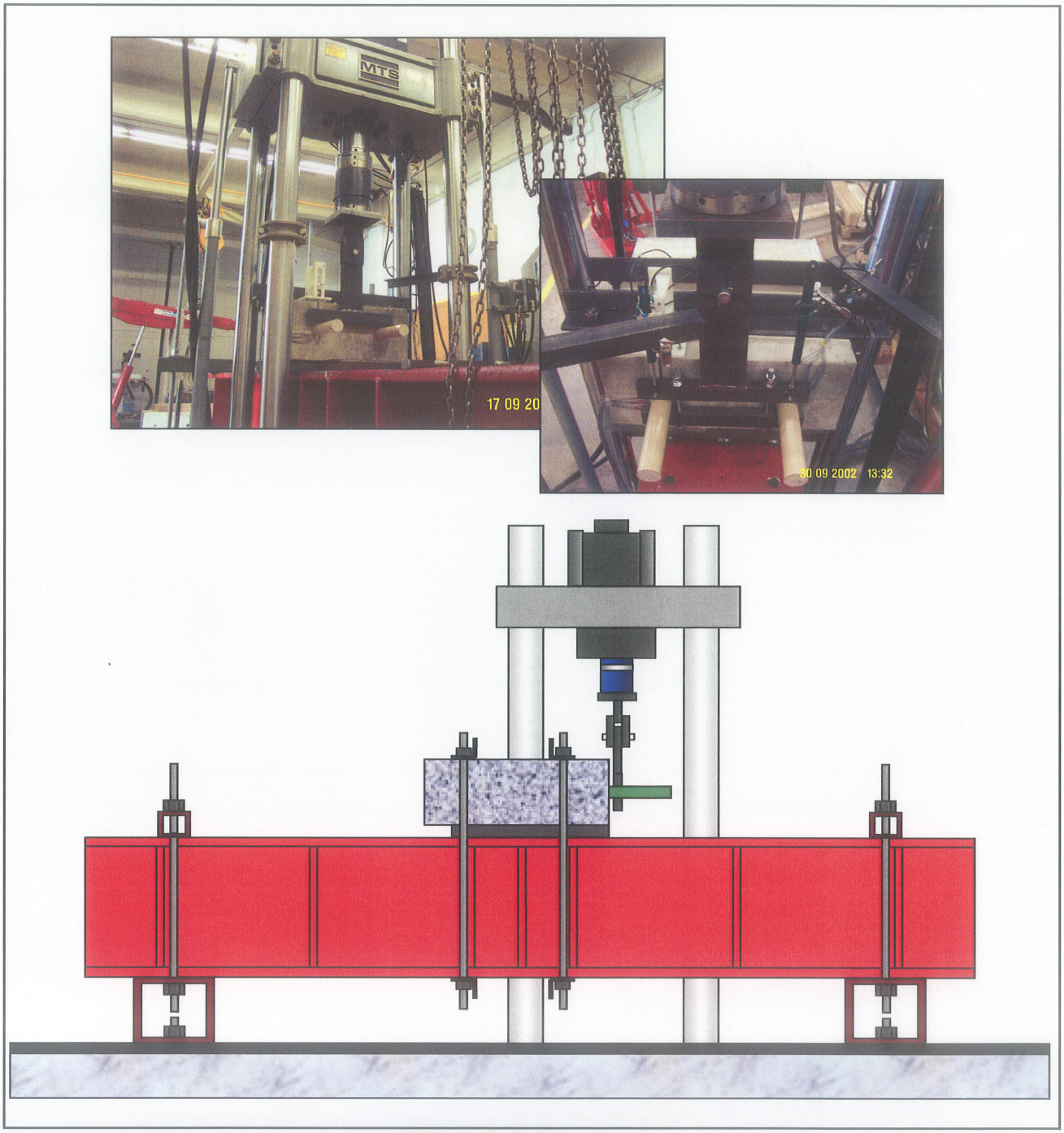

Figure 4.7: Test Set-up

Load was applied to the dowels using a steel device shown in Figure 4.8. The device comprised a loading cross-head welded to a vertical shaft. The shaft was hinged with a

single shear-pin to allow the cross-head to contact and apply load evenly to each dowel. The hinge was made to be a tight fit to prevent any movement between the dowels and the loading machine during cyclic loading. Any movement would create a difference between the machine stroke and the displacement of the cross-head. The dowel bars were clamped together by bolting the top cross-head to a bottom cross-head. The initial purpose of this was to make the loading device capable of reverse-loading during cyclic testing, but the actual testing involved only downward loading in order to reduce the total stroke of the MTS machine.

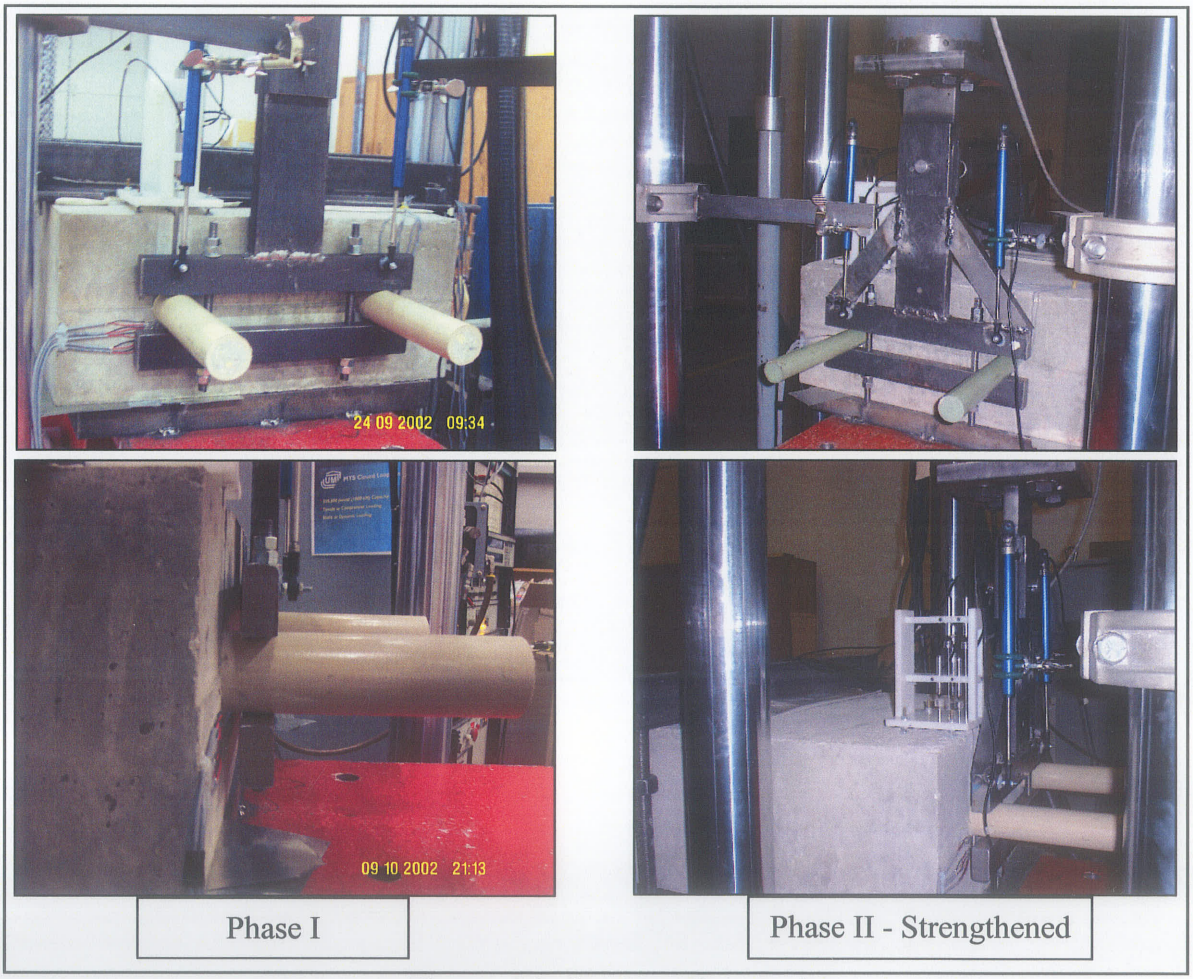

Figure 4.8: Steel loading device

4.5 Phase I – Static and Cyclic Testing at Service Load

The first phase of tests involved static and cyclic loading of the dowels at a service load level. The applied load was estimated from the pavement design theory [Friberg, 1938] as provided in Chapter 2. The load applied per dowel was 12 kN making the machine load reach a total force of 24 kN. Static tests were conducted initially and again after every 250,000 cycles up to a total of 1 million cycles. The cyclic loading was done at a rate of 5 Hz which was the maximum rate possible for the amount of machine stroke experienced.

4.6 Phase II – Loading Dowels to Failure

The second phase of testing involved four similar pavement slabs containing each of the four dowel types. In this phase the slabs were loaded up to failure of the dowels. In the case of the steel dowels, which had a much greater strength than the GFRP dowels, the loading was ceased when the dowel bar began to yield. The test set-up was identical to the one in Phase I, however, the steel loading device was strengthened as shown in Figure 4.8 to provide the required capacity to fail the dowels.

Chapter 5

Results of The Experimental Program

5.1 General

This chapter presents the test results for the experimental program. The results are organized under four major topics which compare dowel displacements, load-deflection behaviour, dowel bar flexural strain, and concrete compressive strain below the dowel bar. Data on these topic areas is provided for both phases of testing. Phase I of the experimental program involved repeated static tests on the pavement slabs conducted after successive cyclic loading sets of 250,000 cycles. Each slab was loaded up to at least 1 million cycles. One of the four slabs which contained the 63.5-mm (2.5") concrete- filled GFRP dowel was loaded for an additional 1 million cycles. The additional cycles were applied for the purpose of investigating the performance of the concrete core of the dowel in addition to the performance of the concrete slab. Phase II involved static tests of a second set of similar pavement slabs where they were loaded up to failure of the dowels. A discussion of the test results is provided in Chapter 6.

5.2 Phase I – Static and Cyclic Testing At Service Loads

A total of four slabs were tested in this phase. Each slab contained a pair of each different type of dowel bar, a 38-mm epoxy-coated steel, 38-mm pultruded GFRP, and a 50.8-mm and 63.5-mm concrete-filled GFRP tube dowel. Each dowel differed mainly in size and flexural stiffness. The embedded lengths of each bar in the slab were identical, a depth of 22.9 cm

(9"). The slabs were loaded to a service level of 12 kN per dowel for a total machine load of 24 kN applied to the steel cross-head. Monotonically loaded static tests were conducted every 250,000 cycles for a total of five static tests. It should be noted that there was an error in the final static test for the steel dowels and therefore only four static test results are provided. The following sections present the results of experimental Phase I. A summary of the test results for each slab is provided in Table 5.1.

Table 5.1: Summary of the Test Results

Test Phase	Dowel Type	Peak Top-Surface Displacement of Dowel at Service Load (mm)	Peak Tensile Strain in Dowel at Service Load (millistrain)	Peak Compressive Strain in Dowel at Service Load (millistrain)	Peak Compressive Strain in Concrete at Service Load (millistrain)
Phase I	38-mm Steel	0.063	0.317	-0.272	-1.96
	38-mm FRP	0.143	1.562	-1.837	-3.94
	50.8-mm C-F FRP	0.071	1.218	-0.829	-1.75
	63.5-mm C-F FRP	0.053	0.771	-0.370	-1.68
Phase II	38-mm Steel	0.042	0.239	-0.203	-1.42
	38-mm FRP	0.100	1.325	-1.621	-1.51
	50.8-mm C-F FRP	0.065	1.096	-1.055	-2.29
	63.5-mm C-F FRP	0.039	0.600	-0.644	-0.31

Test Phase	Dowel Type	Peak Load at Failure (kN)	Comments
Phase I	38-mm Steel	-	No data for static test after 1 M cycles
	38-mm FRP	-	One dowel strain gauge failed after .25 M cycles
	50.8-mm C-F FRP	-	One dowel strain gauge failed after .25 M cycles
	63.5-mm C-F FRP	-	One dowel strain gauge failed after .25 M cycles
			Modes of Failure
Phase II	38-mm Steel	100	Steel yielding at all six gauges
	38-mm FRP	39	Dowel splitting due to inter-laminar shear stress
	50.8-mm C-F FRP	55	Dowel splitting / crushing under load
	63.5-mm C-F FRP	80	Dowel splitting / crushing under load

5.2.1 Dowel Deflection Behaviour

5.2.1.1 Deflected Shape of the Dowel

Figures 5.1(a) and 5.1(b) show the deflected shapes of each dowel type at service load for the initial static test and for the final static test after 1 million cycles. The curve plotted for the steel dowel in Figure 5.1(b) is for the test after 750,000 cycles because of the error in the final static test. The deflected profiles of the dowels were measured with the five small LVDTs whose measurement locations are indicated by the nodes on each curve. The face of the concrete slab would be located at the vertical axis of the graph and is where the dowel displacements are highest. The displacements decrease rapidly with distance from the joint face. Only the first 50 mm in length of the displaced dowels are plotted in the graphs.

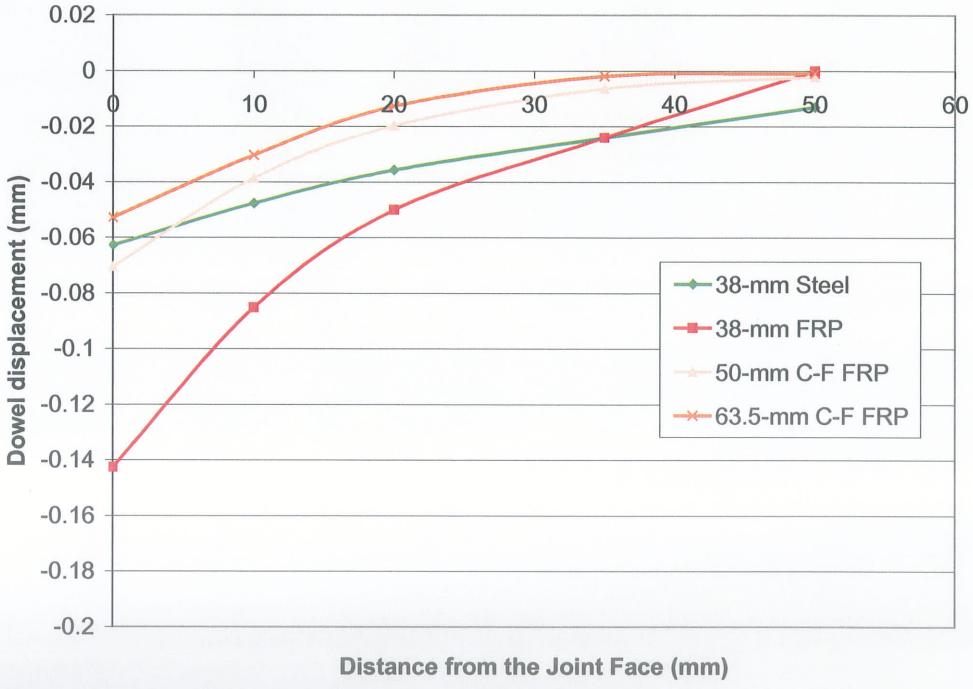

Figure 5.1(a): Deflected Shape of Each Dowel Bar at Service Load – Phase I Initial Test

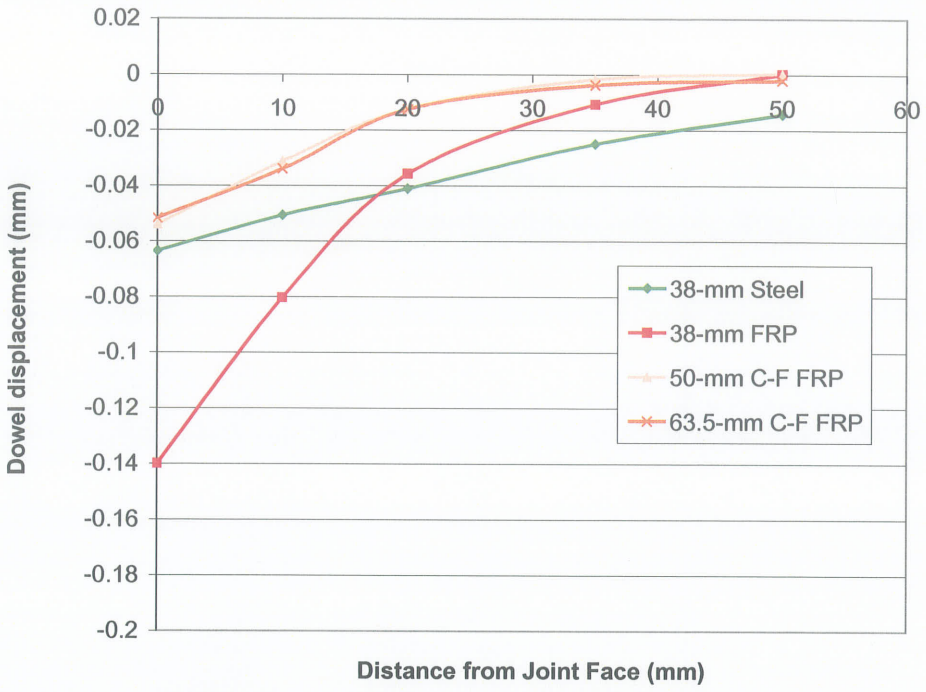

Figure 5.1(b): Deflected Shape of Each Dowel Bar at Service Load – Phase I Test After 1 Million cycles

It should be noted that the LVDTs measured the deflection of the top surface of each dowel bar. The GFRP dowels have a lower strength and stiffness in the transverse direction compared to steel, thus the GFRP bars experience some transverse deformations or ovalizing of the bars. For this reason, the magnitude of deflection of all the GFRP dowels in the concrete slab will actually be lower than shown on the graphs. Therefore, the top deflections were used as a reference to compare deflections after each set of load cycles in Phase I and to compare results of Phase I and II. Further discussion on this issue is provided in the next chapter.

5.2.1.2 Load-Deflection Behaviour

Figure 5.2 shows the load-deflection plots for each dowel type. The dowel displacements shown were measured at the joint face of the slab using the first small LVDT (LV1). There are two sets of curves provided which include the results of the initial test and final test after 1 million cycles (750,000 cycles for the steel dowels). It was observed that with each static test conducted after every 250,000 cycles, the magnitude of displacement for each dowel varied slightly, but not greatly enough to indicate any damage to the concrete slab. There was, however, a noticeable difference observed with the 50.8-mm concrete-filled GFRP dowel. This dowel exhibited higher displacements in the initial static test, but lower after the first set of 250,000 cycles. This indicated a possible change in the physical properties of the dowel that will be discussed in the following chapter.

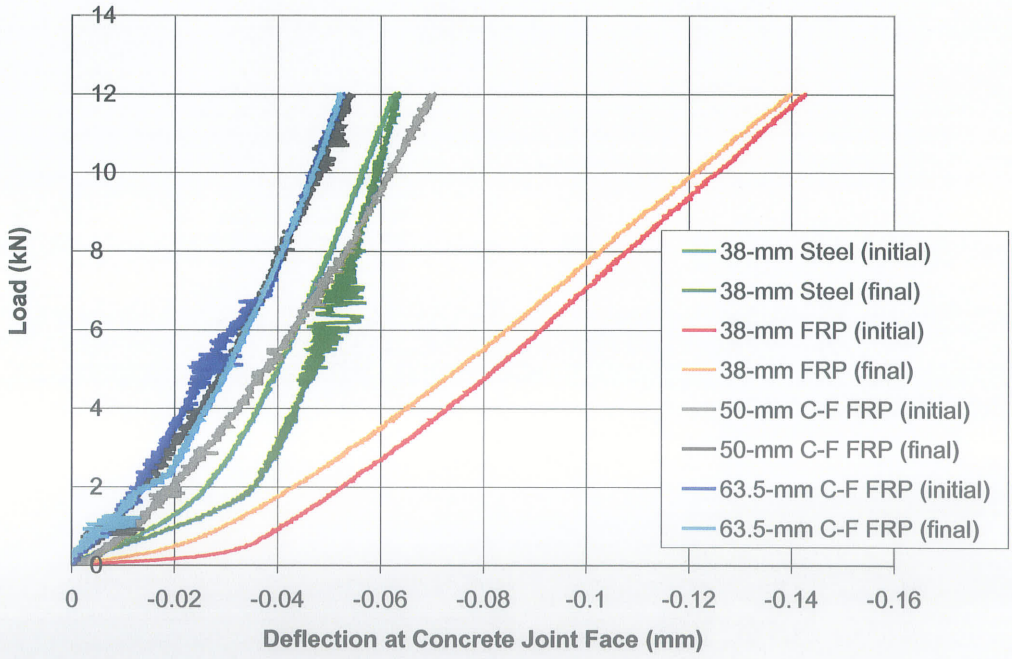

Figure 5.2: Load-Deflection Behaviour Before and After 1 Million Load Cycles - Phase I (Measured by LV1 at the joint face of the slab)

5.2.1.3 Dowel Displacements During Cyclic Loading

Figure 5.3 shows the dowel displacements at the joint face of the slab measured during cyclic loading. The maximum and minimum deflections for each dowel are captured during a 1 second interval. There were 160 data points plotted per second of loading. The epoxy-coated steel dowels and both of the concrete-filled GFRP dowels were loaded at a rate of 5 Hz and therefore a total of five load pulses can be seen on the graph. The cyclic loading rate is dependant on the total travel or stroke of the hydraulic MTS testing machine. The 38-mm GFRP dowel exhibited substantially higher displacements than the other three dowel types and it was found that the MTS machine could not maintain a loading rate of 5 Hz for this dowel type. The loading rate was adjusted to 4.5 Hz for the 38-mm GFRP dowel as shown by the load pulses plotted in Figure 5.3. The peak magnitudes of displacement are similar to those measured in the static tests.

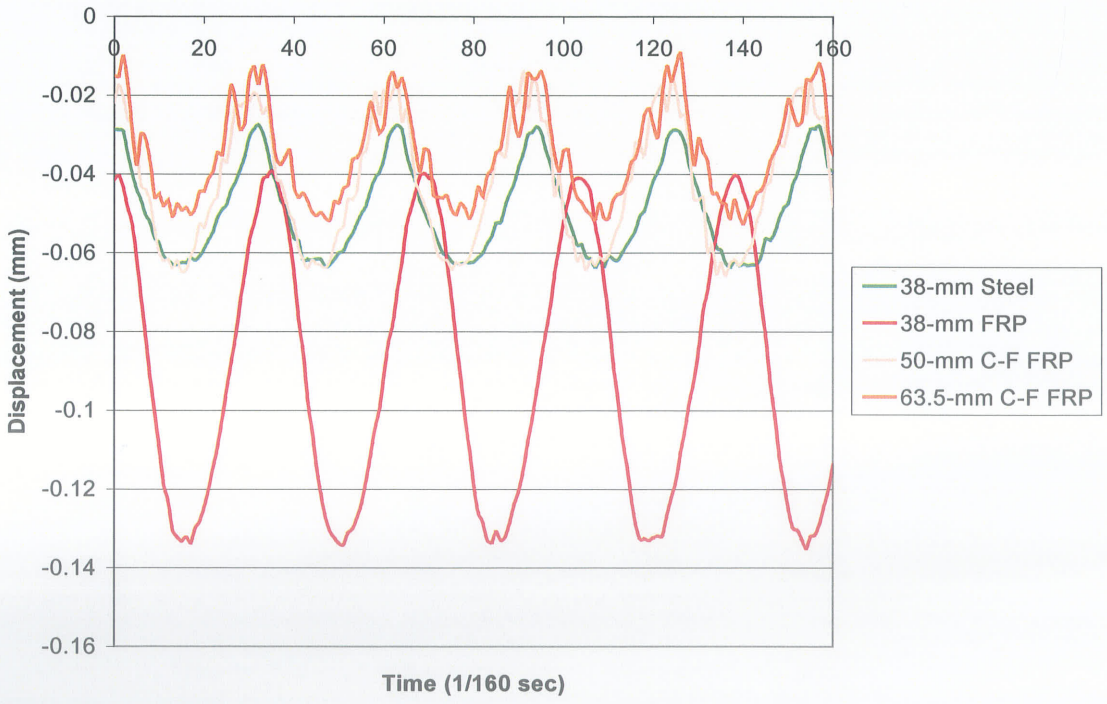

Figure 5.3: Deflection of dowels under cyclic loading – At Service Load (12 kN)

The dowels were loaded in a haversine function in the compression range only. This was done to reduce the total stroke of the MTS machine in order to achieve the fastest loading rate possible. Another step taken to reduce total actuator travel and ensure the stability of the system was to maintain a minimum load on the dowels of approximately 10% of peak load. Therefore, the displacement of each dowel ranged from a minimum value under the seating load of approximately 1.3 kN per dowel and a maximum value under service load.

Figure 5.4 shows the load pulses for the epoxy-coated steel dowels captured at each set of 250,000 cycles. The curves of the load pulses varied slightly but, they are fairly consistent and do not provide any indication of damage occurring with increased number of cycles. There were similar findings for the other three dowel types that are not shown. One of the curves appears to have more noise than the others (Test at 750,000 cycles).

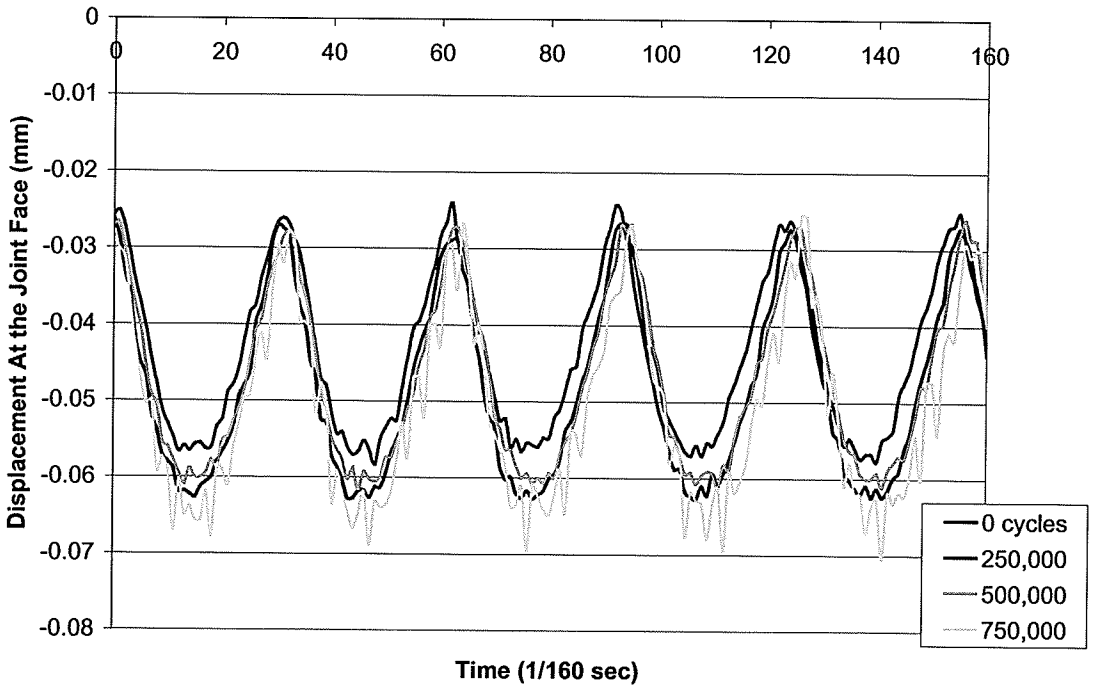

Figure 5.4: Deflection of epoxy-coated steel dowel under cyclic load – After each set of 250,000 cycles

5.2.3 Dowel Bar Strain Measurements

5.2.3.1 Dowel Bar Strain at Service Load

Figure 5.5 displays the longitudinal bending strain measurements in each of the four dowel types captured at service load. There were a total of six gauges, 3 pairs on the top and bottom, placed at three different distances inward from the joint face, 3.2, 19.0, and 38.1 mm. These strain readings were used to monitor the curvature of the dowel for comparison with measured displacements and to approximate where the maximum moment or curvature occurs along the length of the dowel. The figure shows a clear difference between the steel and GFRP dowels. For instance, the magnitude of the bending strains were far greater for the GFRP dowels than for the steel. The values were higher but they were not very large compared to the GFRP rupture strain.

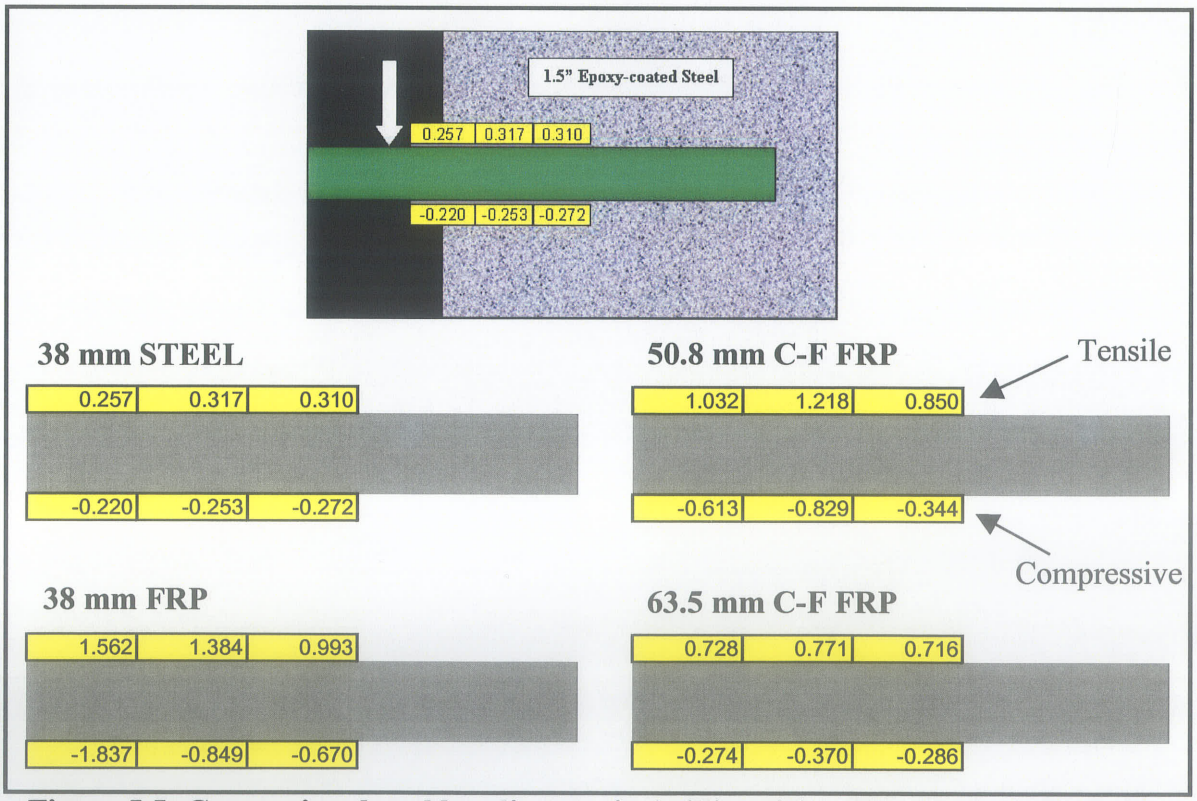

Figure 5.5: Comparing dowel bending strain (millistrain) – Phase I at service load

The steel dowel appeared to behave in a linear-elastic fashion. The distribution of tensile and compressive strain was more evenly distributed. The 38-mm GFRP dowel exhibited high compressive strain near the joint face as indicated by the high value measured by that particular gauge. The flexural strain distributions on this dowel and both of the concrete-filled GFRP dowels indicate a different type of bending behaviour. The dowels appear to be bending more like a hinge and bending about the edge of the concrete slab face below.

Figure 5.6 shows the dowel bar strains at service load measured after each set of 250,000 cycles. The graph shows only the values plotted by the two strain gauges closest to the joint face (the front top and bottom gauges). Some data on the steel dowels is missing from this graph due to errors in the data.

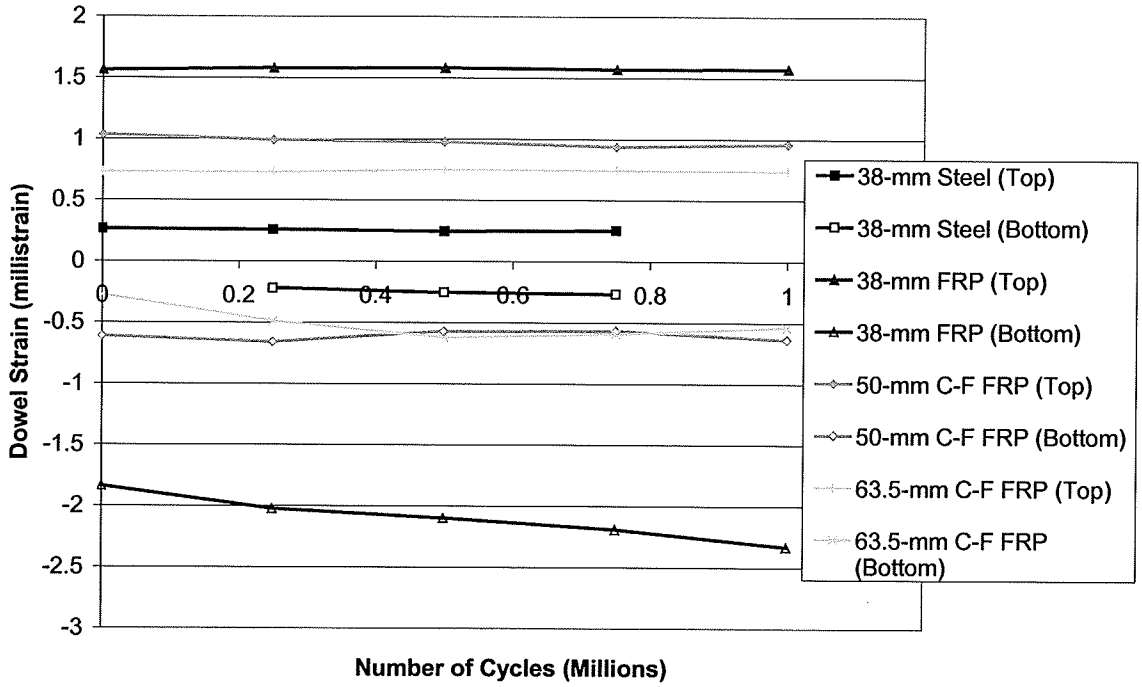

Figure 5.6: Bending strain in each dowel at service load – Phase I
Measured at joint face after each set of 250,000 cycles
(3 data points missing for steel dowel due to loss of data)

The graph shows that there is no significant change in measured longitudinal strain for any of the dowel types, however, the 38-mm GFRP dowel does show some consistent increases in strain. If any damage had occurred to the dowel or the concrete slab, it was not visible.

5.2.3.2 Load-Strain Behaviour

Figures 5.7(a) to 5.7(d) provide the load-strain plots for each of the four dowel types. Figure 5.7(d) shows that the concrete core of the 63.5-mm concrete-filled GFRP dowel cracks at approximately half the service load-level. Figure 5.7(e) shows the load-strain curve for the repeated static test on the same dowel that shows no sign of cracking. This shows that the flexural strength of the concrete-filled dowels relies primarily on the GFRP tube surrounding the concrete core. The positive strains indicate tension on the top of the dowel and the negative values are compressive strains on the bottom. The GFRP dowel bars exhibit differences in behaviour between tension and compression regions. The tensile strains on the top of the bar are more spread-out over the three top strain gauges. On the compression side, the strain increases substantially near the joint face, but the strain in the other two gauges embedded further along the length of the bars have much smaller magnitudes. This is an indication of the poor compressive strength of GFRP. It is also an indication that the dowel bar experiences a 'hinge' type of bending about the joint face of the concrete slab. The strains measured in the GFRP dowels are much higher than those measured in the steel showing that the GFRP bars have a much lower flexural modulus and stiffness. The rupture strain of GFRP is approximately 0.016 therefore, the strains experienced under service load are only approximately 10-15% of failure. These strains are very low, therefore no damage to the dowel bars would be expected after 1 million cycles or more.

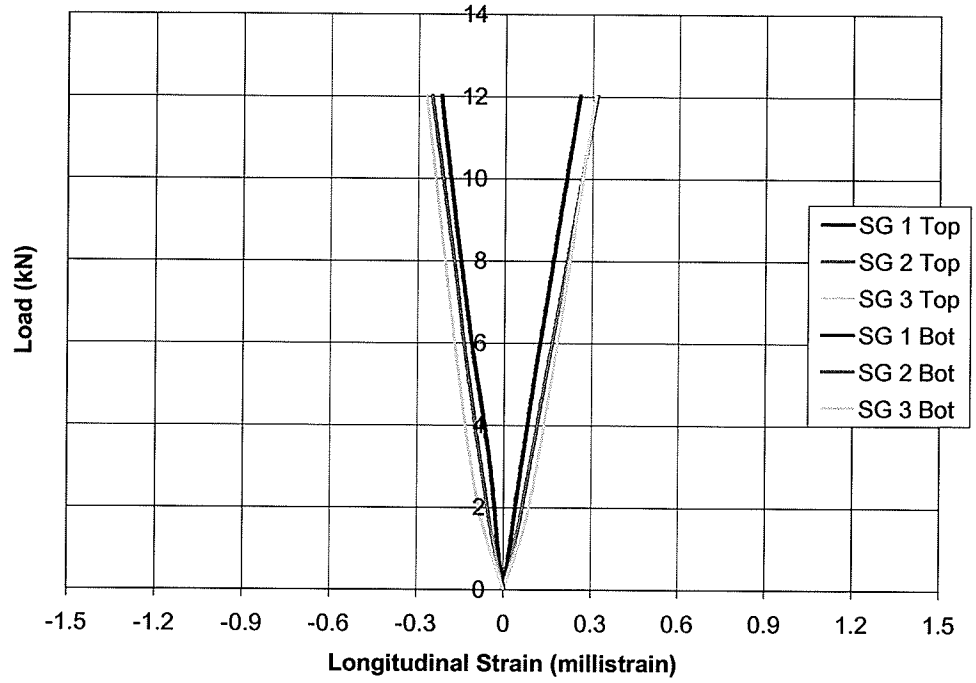

Figure 5.7 (a): Load-Strain graph for 38-mm Steel Dowel - Phase I

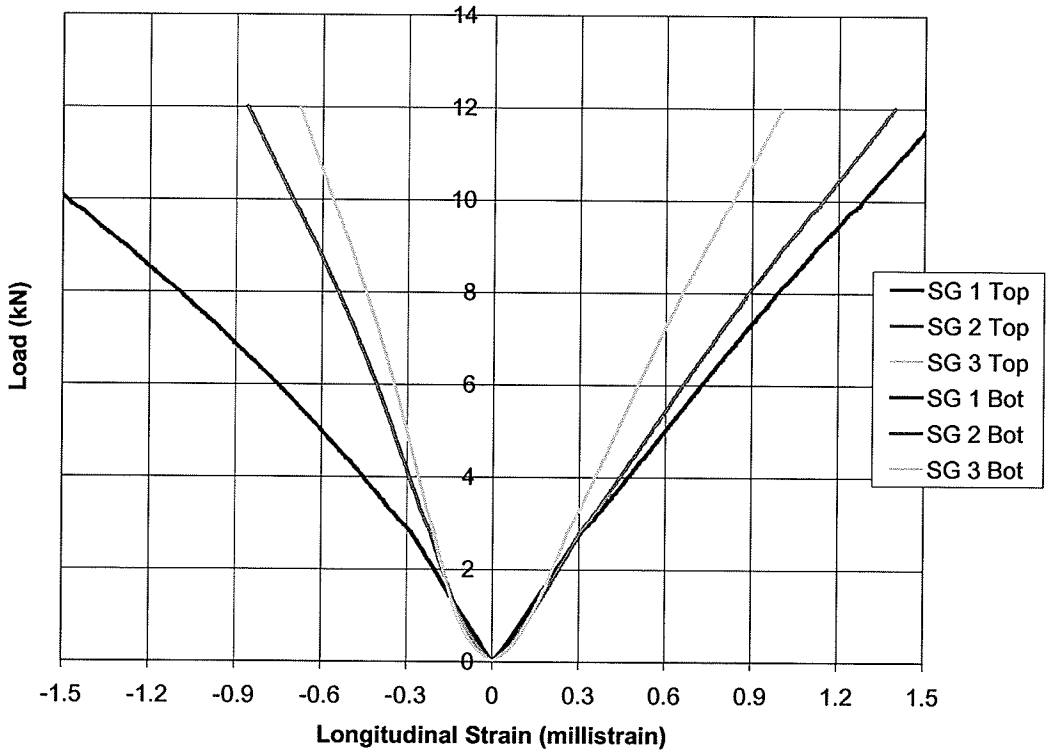

Figure 5.7 (b): Load-Strain graph for 38-mm Pultruded GFRP Dowel - Phase I

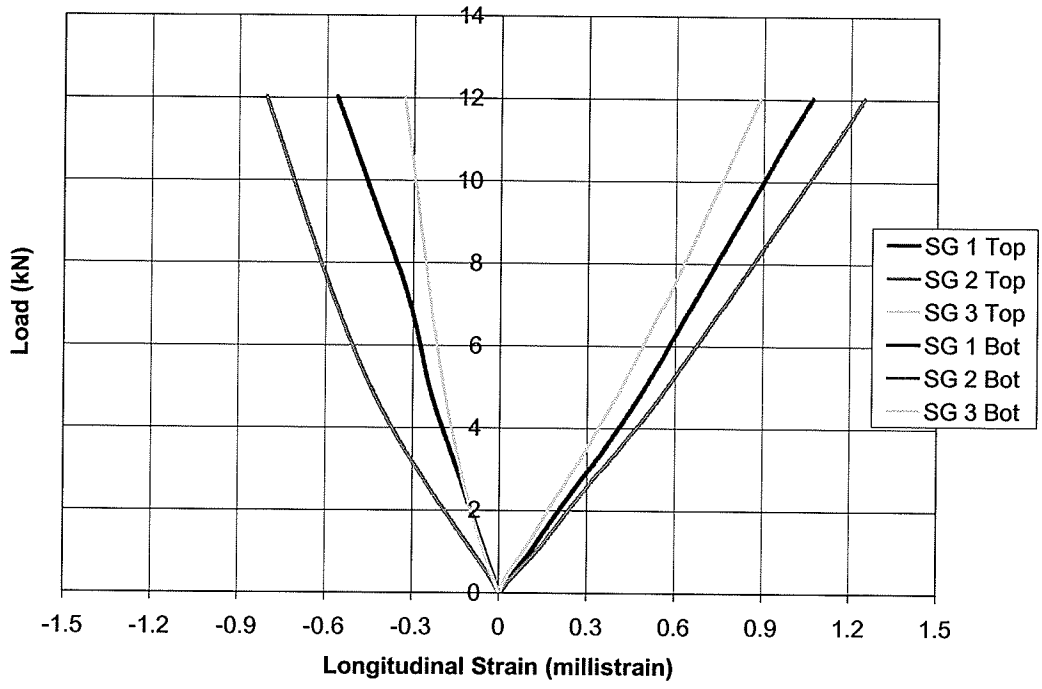

Figure 5.7 (c): Load-Strain graph for 50.8-mm concrete-filled GFRP Dowel - Phase I

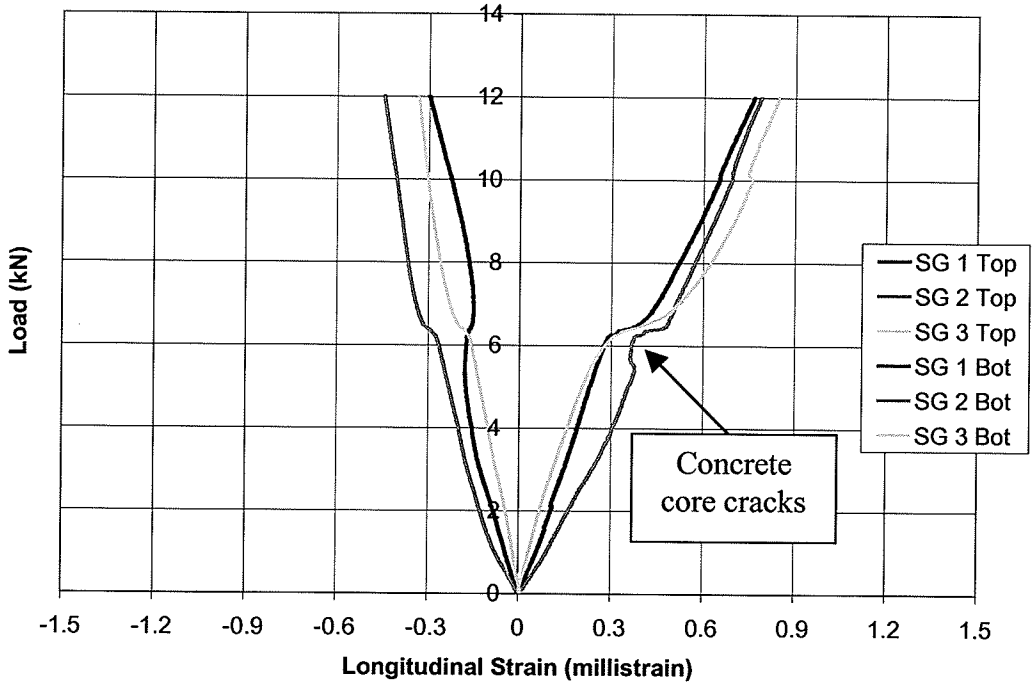

Figure 5.7 (d): Load-Strain graph for 63.5-mm concrete-filled GFRP Dowel - Phase I

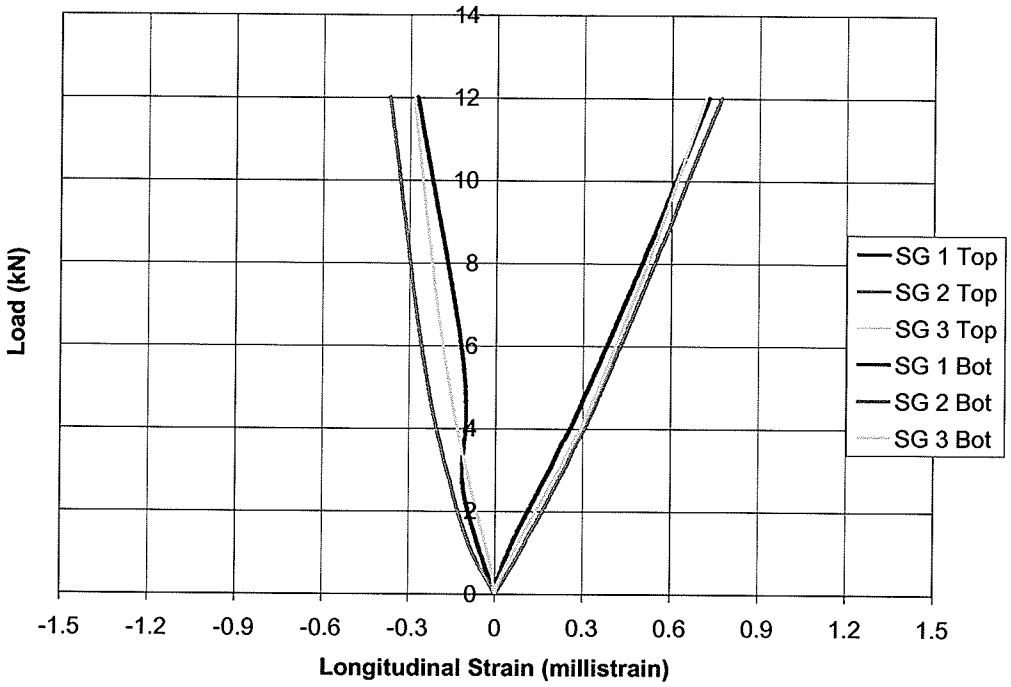

Figure 5.7 (e): Load-Strain graph for 63.5-mm concrete-filled GFRP Dowel – Repeat static test - Phase I

5.2.3 Concrete Compressive Strain Below the Dowels

Figure 5.8 shows the strains for each dowel bar type measured at service load. The strain readings were measured by the five small strain gauges below the dowel spaced 2 mm apart on centre with the first gauge located 2.5 mm below the bottom surface of the dowel bar. It was expected that obtaining accurate measurements of the true vertical compressive strain in the concrete would be difficult because the concrete is not homogeneous and the gauges were extremely small. For a homogeneous, linear-elastic material, the strains should decrease with increasing distance below the dowel bar similar to stress bulbs in the soil under a footing. The plots in Figure 5.8 indicate a similar trend, however, some of the strain readings appear erratic. The strain gauge readings may be affected by the epoxy used to fill in small air

pockets formed on the outer surface of the slab. The top gauge readings are the most important as they should indicate the greatest amount of strain in the concrete below the bar. The top gauges are centred 2.5 mm below the actual surface of the bar. The highest concrete strains would be expected to exist immediately below the bar. The magnitude of strain in the top gauge of the slab containing the 38-mm GFRP dowel is lower than the other three dowel types which is quite unexpected. The results may indicate errors in the data or errors in the methods for obtaining concrete strain measurements. Further discussion on this issue is provided in the next chapter.

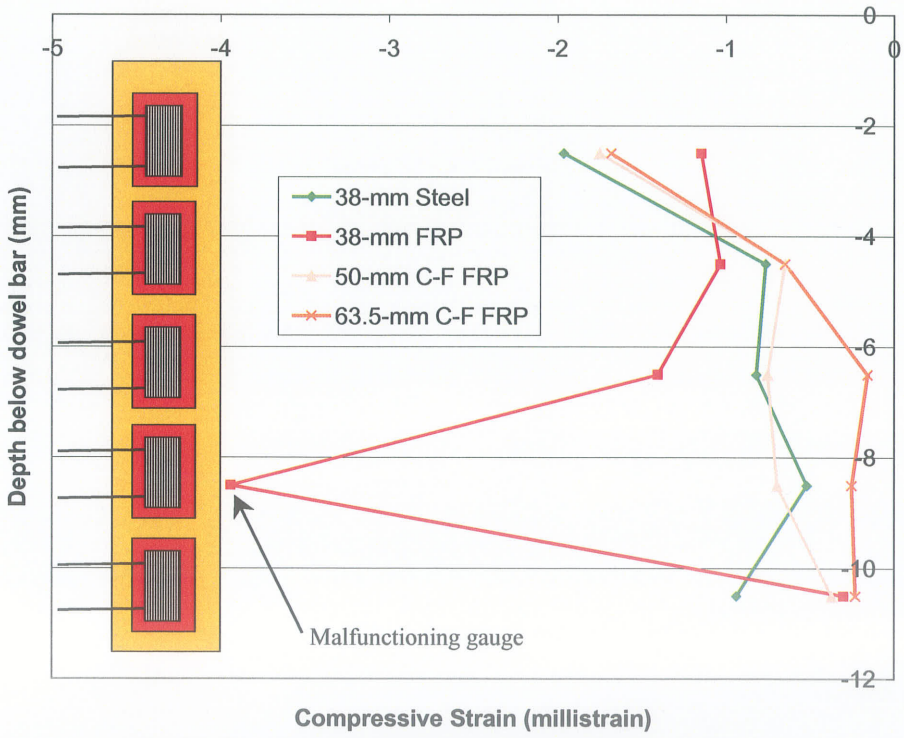

Figure 5.8: Vertical compressive strain in concrete below each dowel bar type – Phase I (Strain versus depth below dowel at service load)

Figures 5.9(a) to 5.9(d) show the concrete strain profiles for each dowel measured after each set of 250,000 cycles. The plots show that the strain values appear to decrease after each set

of cycles. Some gauges show substantial decreases indicating some form of damage. For example, the bottom gauge for the 50.8 mm (2") concrete-filled GFRP dowel drops from approximately 2.3 millistrain to 0.4 millistrain after the first 250,000 cycles. Similar decreases were observed for the other dowel types as well. The decreases are possibly due to micro-cracking of the concrete below the dowel. Figures 5.10(a) to (d) show the load-concrete strain curves up to service load for the four pavement slabs. The curves show no indication of damage to the concrete occurring to any of the dowel types. There are no abrupt changes in strain values or changes in the slope of the curves to indicate accelerated crack propagation.

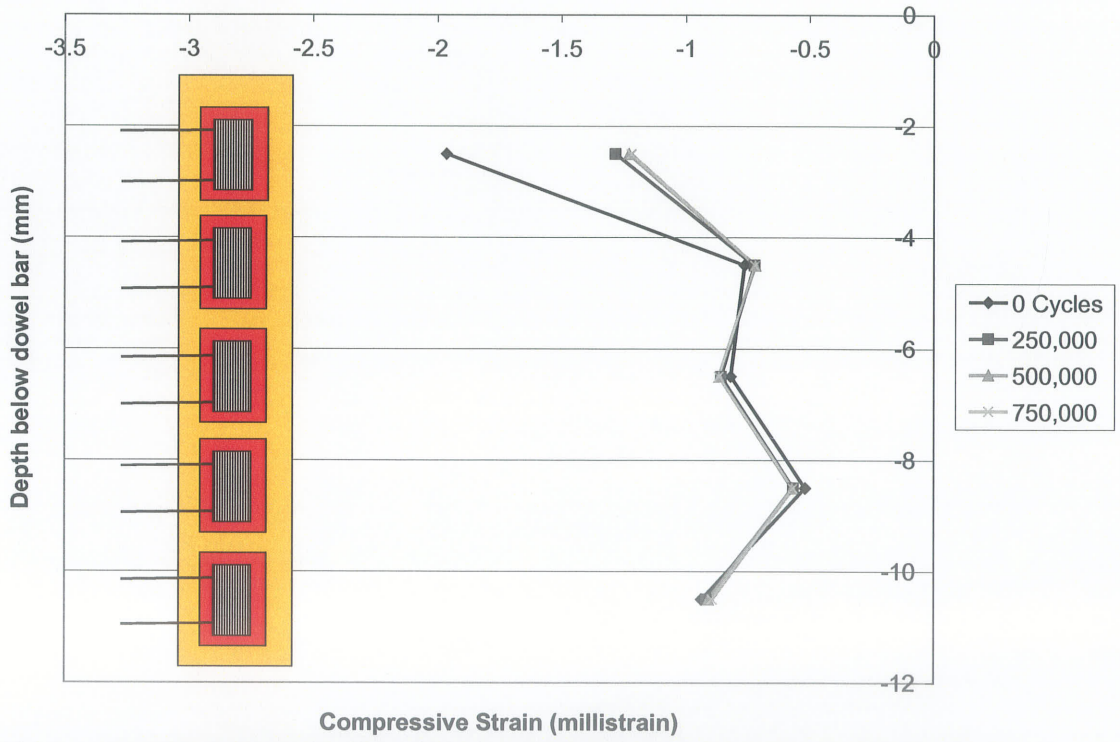

Figure 5.9 (a): Vertical compressive strain profiles for 38-mm Steel Dowel after each set of cycles (Service Load)

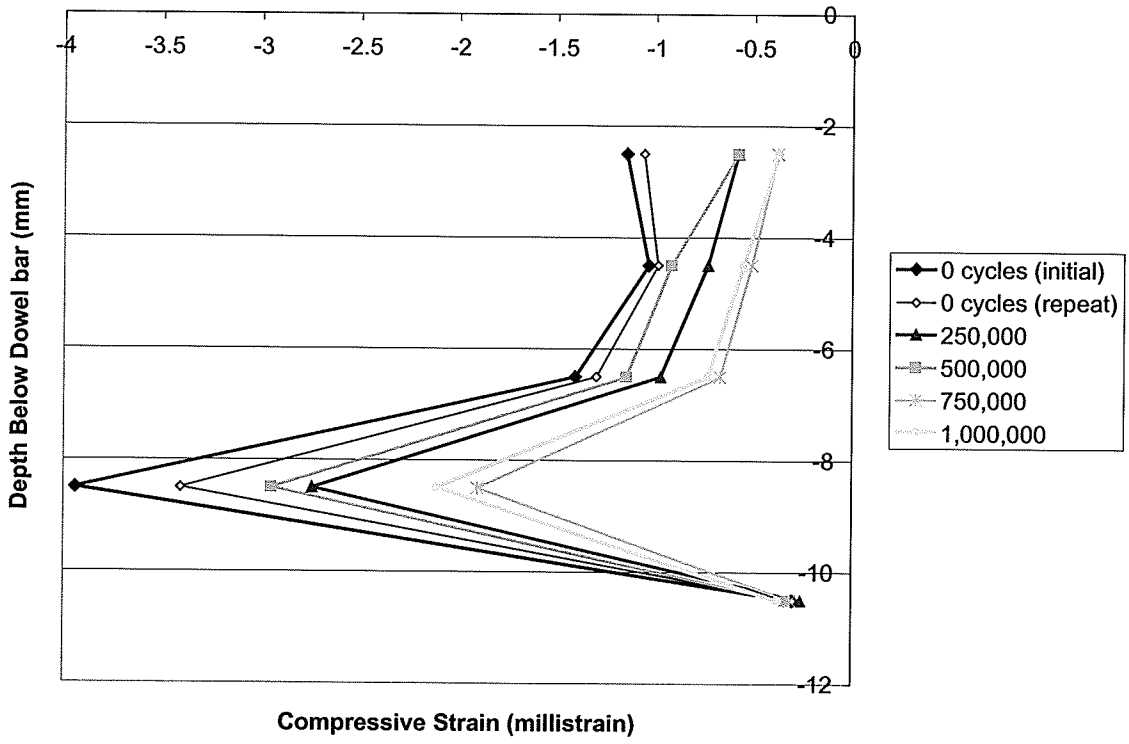

Figure 5.9 (b): Vertical compressive strain profiles for 38-mm GFRP Dowel after each set of cycles (Service Load)

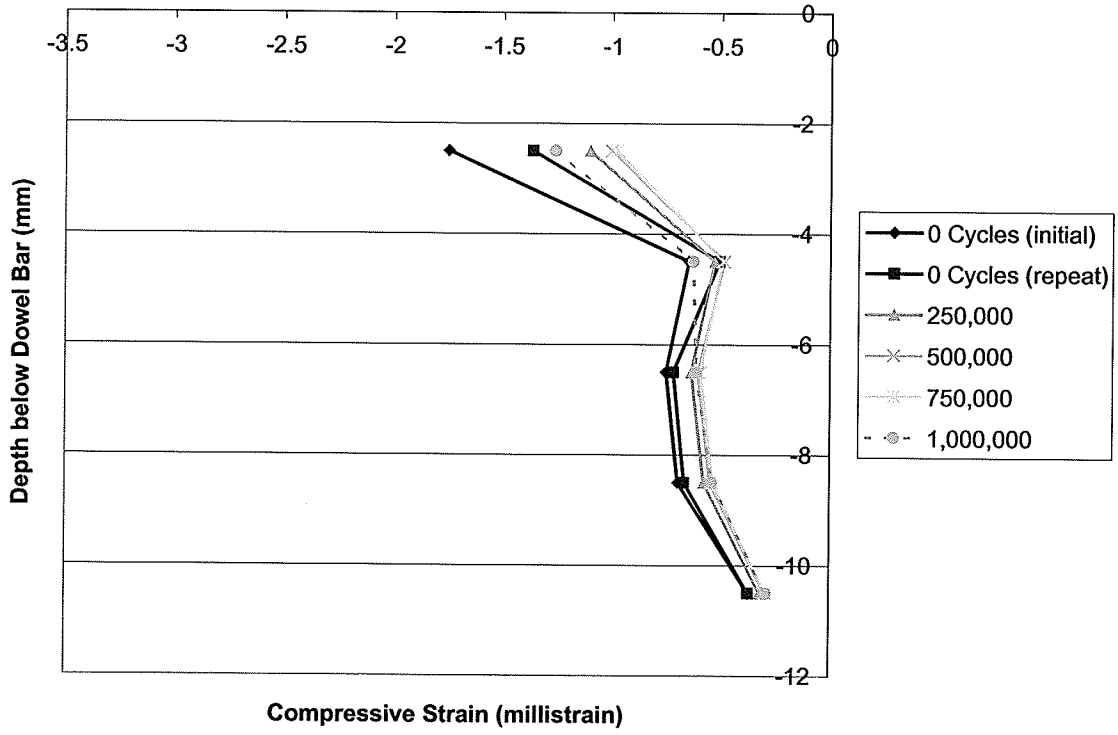

Figure 5.9 (c): Vertical compressive strain profiles for 50.8-mm concrete-filled GFRP Dowel after each set of cycles (Service Load)

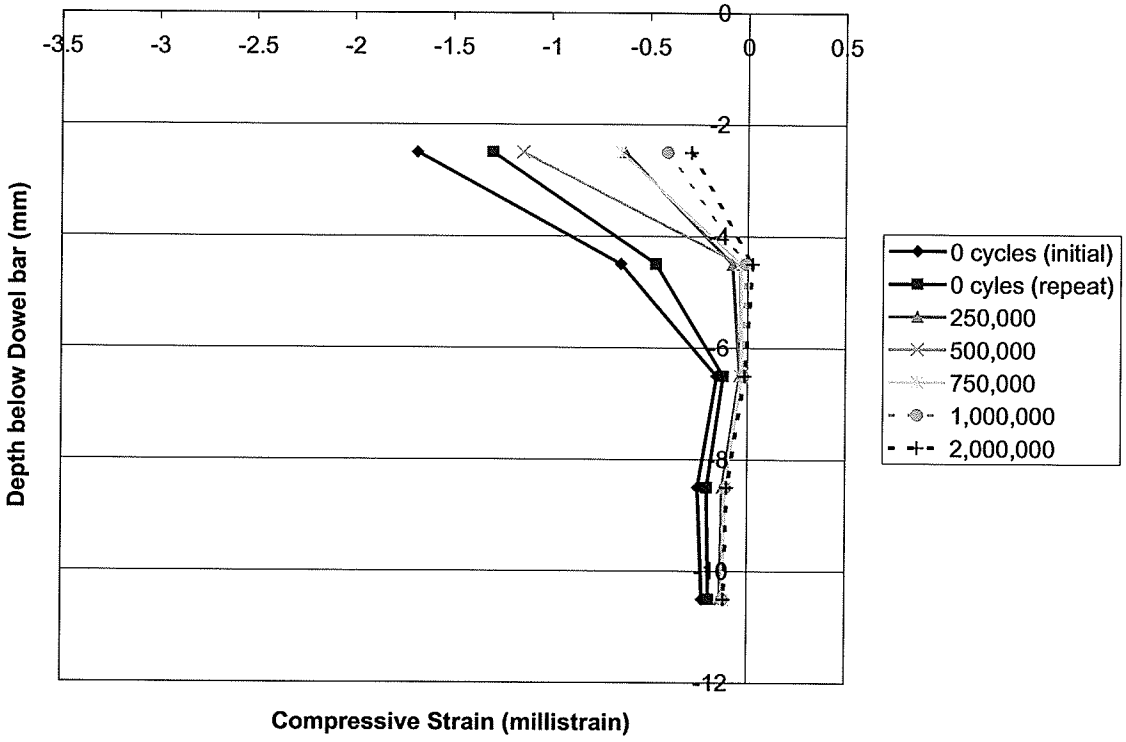

Figure 5.9 (d): Vertical compressive strain profiles for 63.5-mm concrete-filled GFRP Dowel after each set of cycles (Service Load)

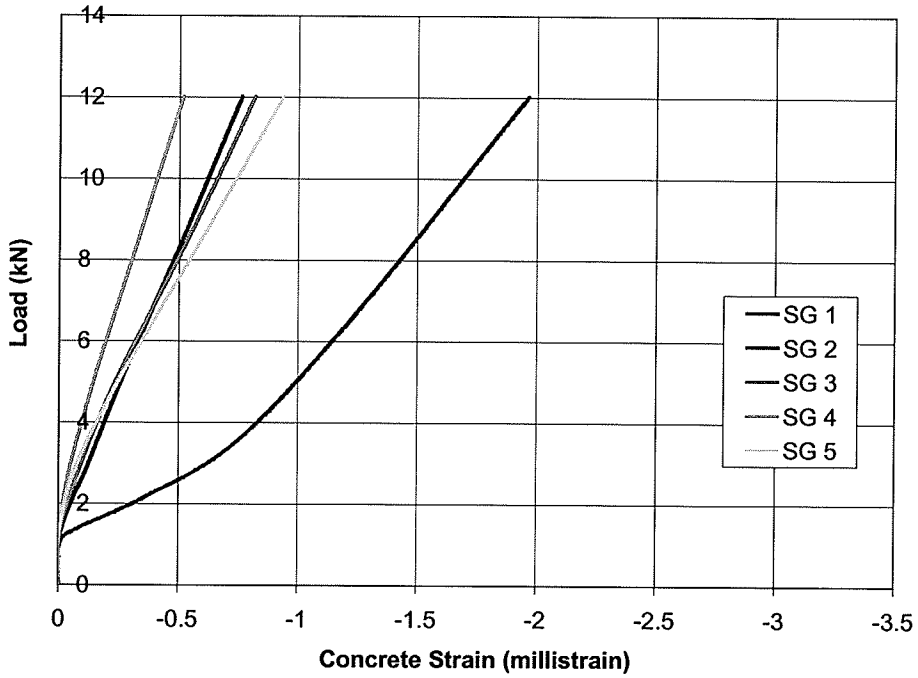

Figure 5.10(a): Load-strain behaviour of concrete below 38-mm Steel dowel – Phase I

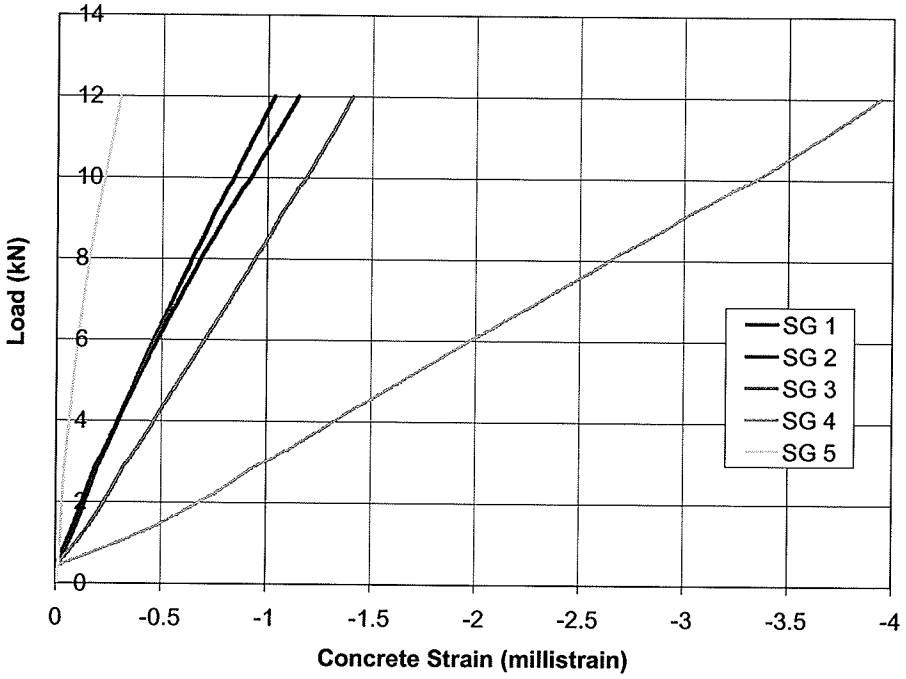

Figure 5.10(b): Load-strain behaviour of concrete below 38-mm GFRP dowel – Phase I

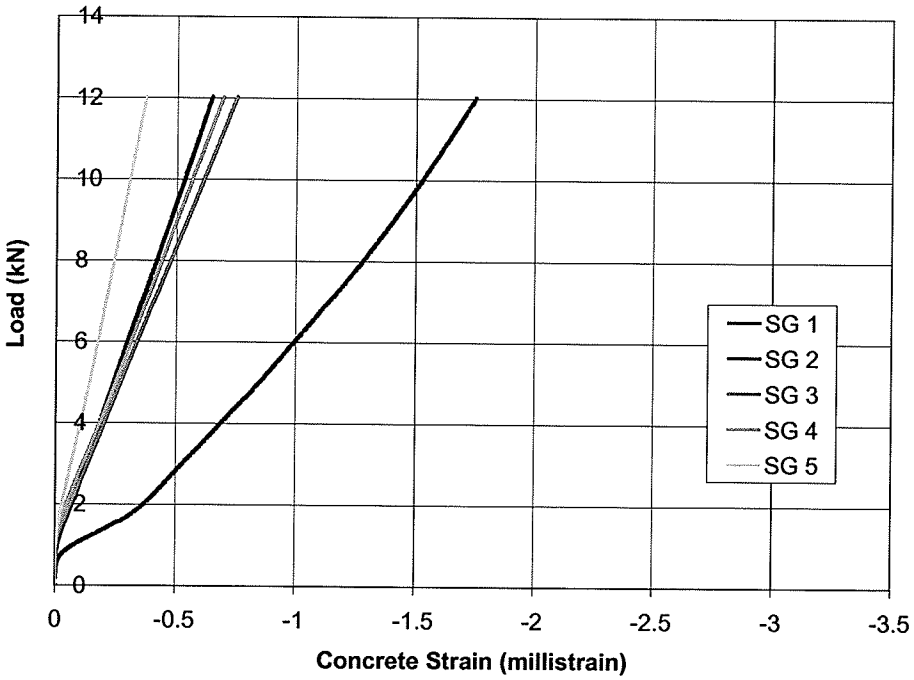

Figure 5.10(c): Load-strain behaviour of concrete below 50.8-mm Concrete-filled GFRP dowel – Phase I

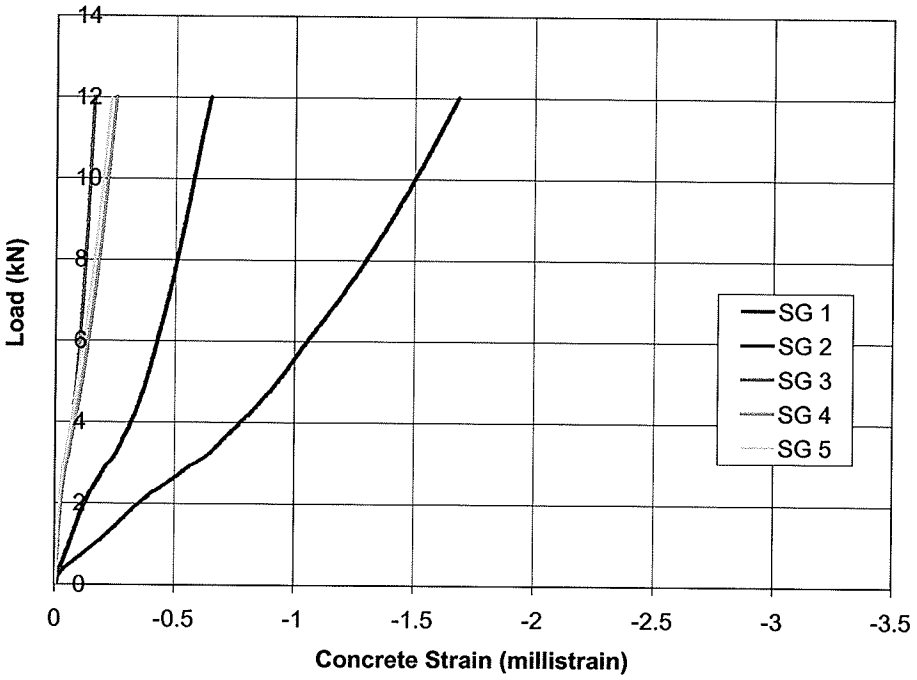

Figure 5.10(d): Load-strain behaviour of concrete below 63.5-mm Concrete-filled GFRP dowel – Phase I

5.3 Phase II – Static Tests up to Failure

The second phase of the experimental program involved static tests up to failure of four pavement slabs similar to those tested in Phase I. The tests were conducted approximately four weeks after the Phase I tests were completed. The compressive strengths of the concrete pavement slabs had increased over this time period. Reductions in dowel displacements and strains were expected in Phase II due to the increase in concrete strength.

Load was applied to the slabs and increased until the dowels failed. The modes of failure were different depending on the type of dowel. Failure initiation of the epoxy-coated steel dowels was considered to occur when yielding of the extreme surfaces was observed. At this point, the test was stopped even though the ultimate capacity had not been reached.

The pultruded 38-mm GFRP dowel and both of the concrete-filled GFRP tube dowels failed quite differently. The GFRP dowels were loaded to ultimate capacity at which point the dowels experienced severe structural damage. The 38-mm solid GFRP dowel experienced splitting of the matrix between the longitudinal glass fibres due to shear and tensile stresses as shown in the photograph in Figure 5.11.

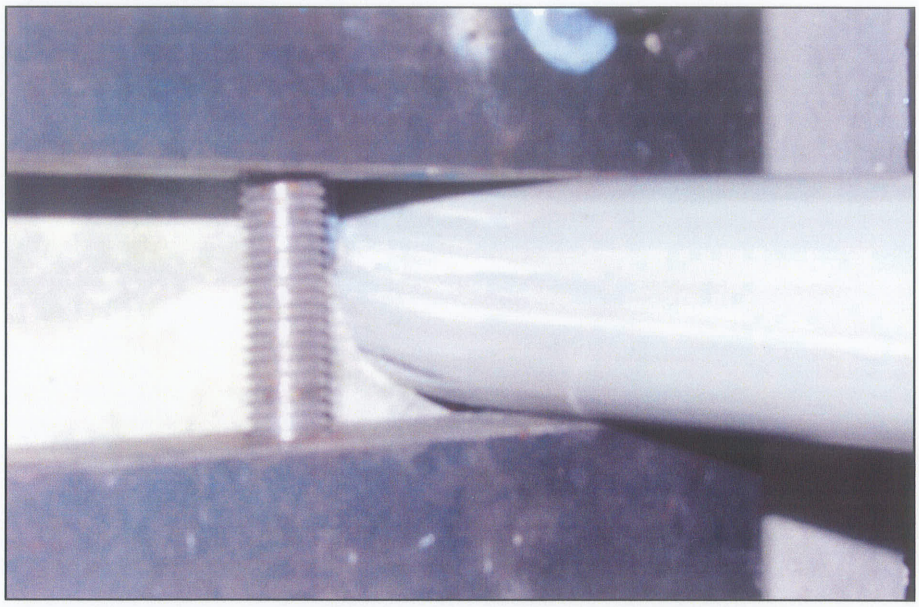

Figure 5.11: Splitting failure of 38-mm GFRP dowel at approximately 39 kN

The concrete-filled GFRP tube dowels both failed in a different fashion. Close to ultimate load, the steel cross-head that applied the load to the dowels began to penetrate, or shear down through, the upper surface of the GFRP tube. The tube was also experiencing a significant amount of ovalizing in shape that deformed the bar in such a way that created high circumferential stresses. These stresses caused longitudinal splitting of the bar that propagated outward from the joint face of the slab. The combination of these failure

characteristics was caused in part by the lack of confinement pressure around the protruded part of the dowel that would be present if the adjacent concrete slab were cast around it.

Later inspection of the concrete-filled GFRP dowels revealed that there were some indentations around the bottom of the tube where the concrete slab edge penetrated the dowel surface. One of the 50.8-mm (2") GFRP tube dowels showed signs of the bottom surface being cut or sheared by the concrete slab edge as the dowel ovalized in shape during loading. This indicated that the dowel was near failure regardless of the steel cross-head shearing through the top surface. Photos of the damage to the concrete-filled GFRP tube dowels are provided in Figure 5.12.

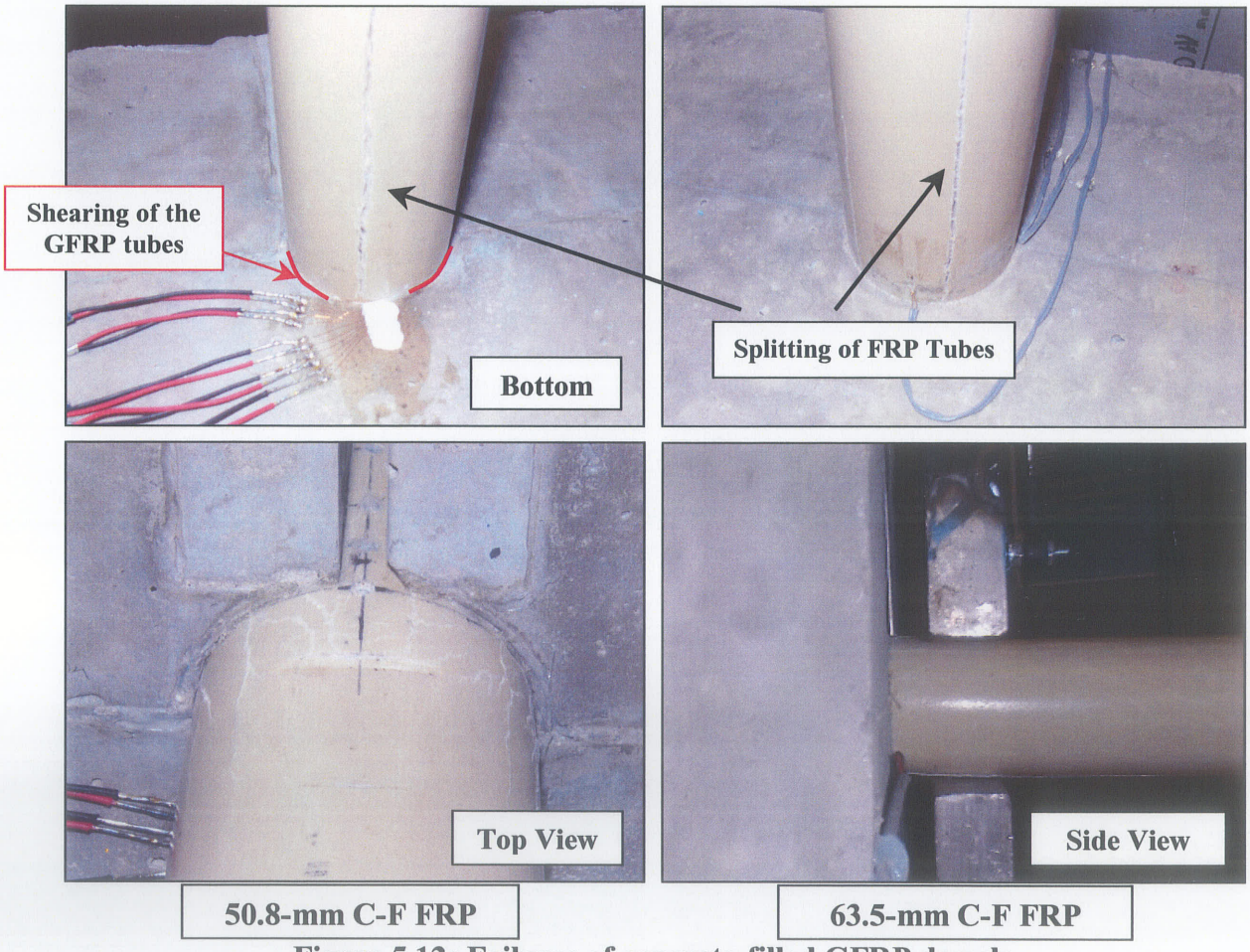

Figure 5.12: Failures of concrete-filled GFRP dowels

5.3.1 Dowel Deflection Behaviour

5.3.1.1 Deflected Shape of the Dowel at Service Load

Figure 5.13 shows the deflected shapes of each dowel bar type measured at service load in the second phase of testing. The magnitudes of the displacements appear to be smaller than those measured in Phase I as expected due to the increase in concrete strength. The steel and 50-mm concrete-filled GFRP dowels were cast in the Batch 2 concrete slabs which had a slightly higher compressive strength than Batch 1. Therefore, an even greater reduction in deflection was expected for these dowel types. Comparing the deflected shapes from both phases of testing, it can be seen that there was a significant reduction in displacement for the steel, however, there was no noticeable change in displacement for the 50-mm concrete-filled dowel.

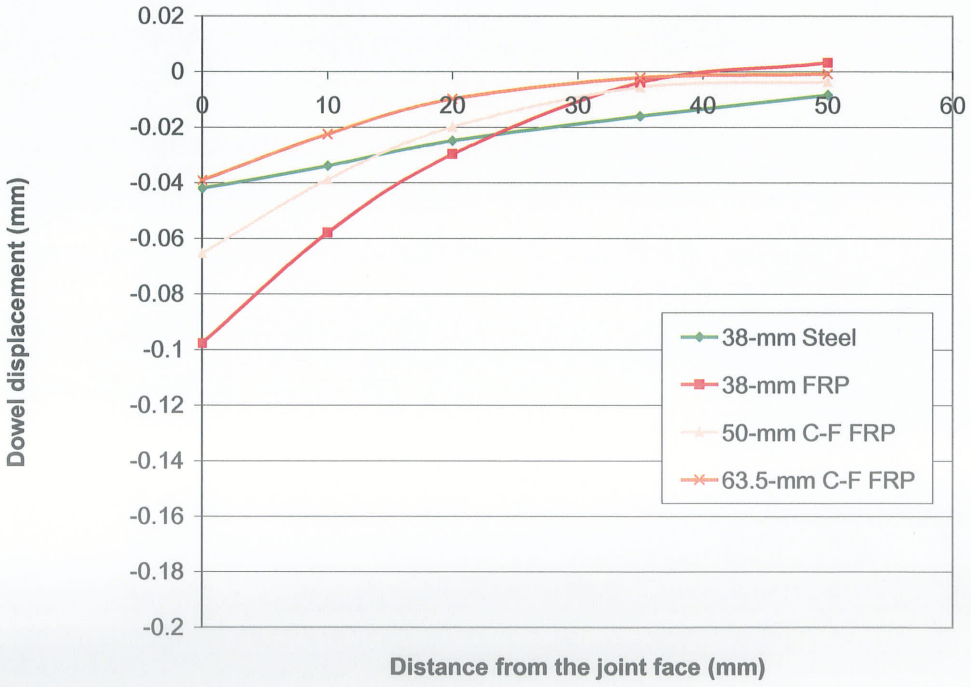

Figure 5.13: Deflected shape of each dowel bar at service load (Phase II) (Top surface of dowel)

The LVDTs were measuring the deflections at the top of the dowel surface and therefore there is not necessarily an indication that the 50-mm dowel performed poorly. It is likely that the dowel bar experienced a different type of deformation and cracking than the dowel tested in Phase I. This is possibly due to differences in the crack formation in the concrete dowel core which would alter the bending behaviour of the dowel. Small differences in the mechanical properties between the dowels used in each phase of testing could also be responsible.

5.3.1.2 Load-Deflection Behaviour up to Failure

Figures 5.14(a) to 5.14(d) provide the load-deflection curves for each dowel bar type. Each figure includes the curves for displacements measured at each of the five points along the length of the dowel bar. Combined load-deflection curves for each dowel type measured at the joint face of the slab are plotted in Figure 5.15(a) (up to failure) and Figure 5.15(b) (up to service). The clear difference in stiffness of each bar is evident from the slopes of the load deflection curves.

The steel dowel had the greatest stiffness and achieved the highest ultimate load. The 63.5-mm concrete-filled GFRP dowel exhibited a higher stiffness than the steel in the early stages of loading (up to service load), however, the slope of the curve began to change soon after as seen in Figure 5.15(a) where the two curves intercept. The 63.5-mm GFRP dowel exhibited a strange behaviour when it reached a load level of 60 kN. It was observed at this point that the steel loading cross-head began to shear down through the top surface of the GFRP tube which caused the upper surface to 'rebound' or displace in the upward direction.

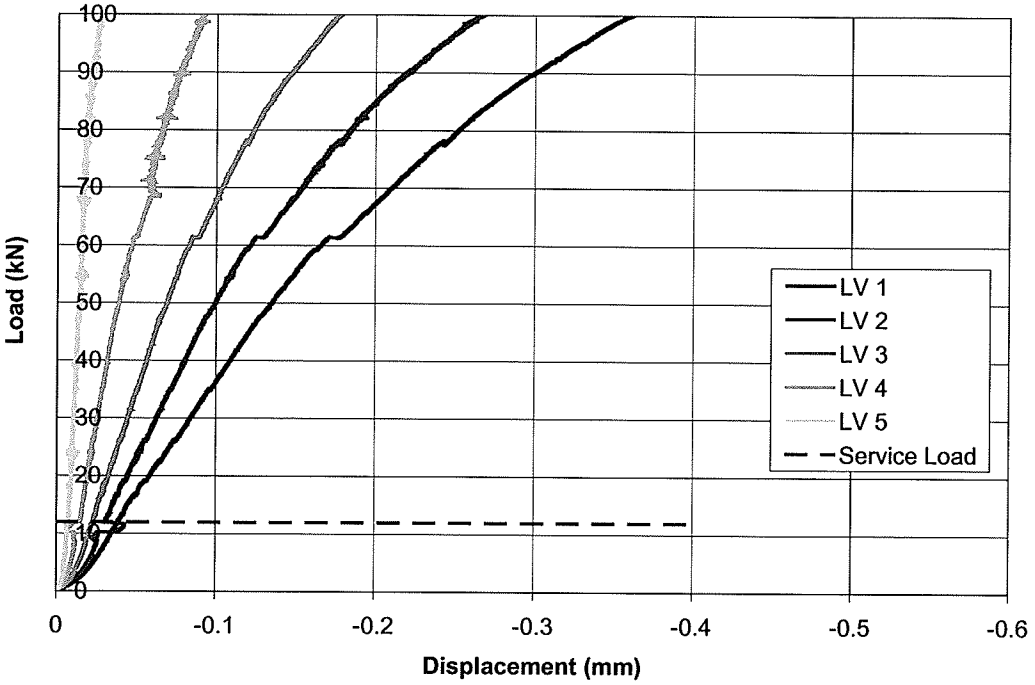

Figure 5.14 (a): Load-deflection plots up to failure for 38-mm Steel dowel For each location measured along the dowel surface (Phase II)

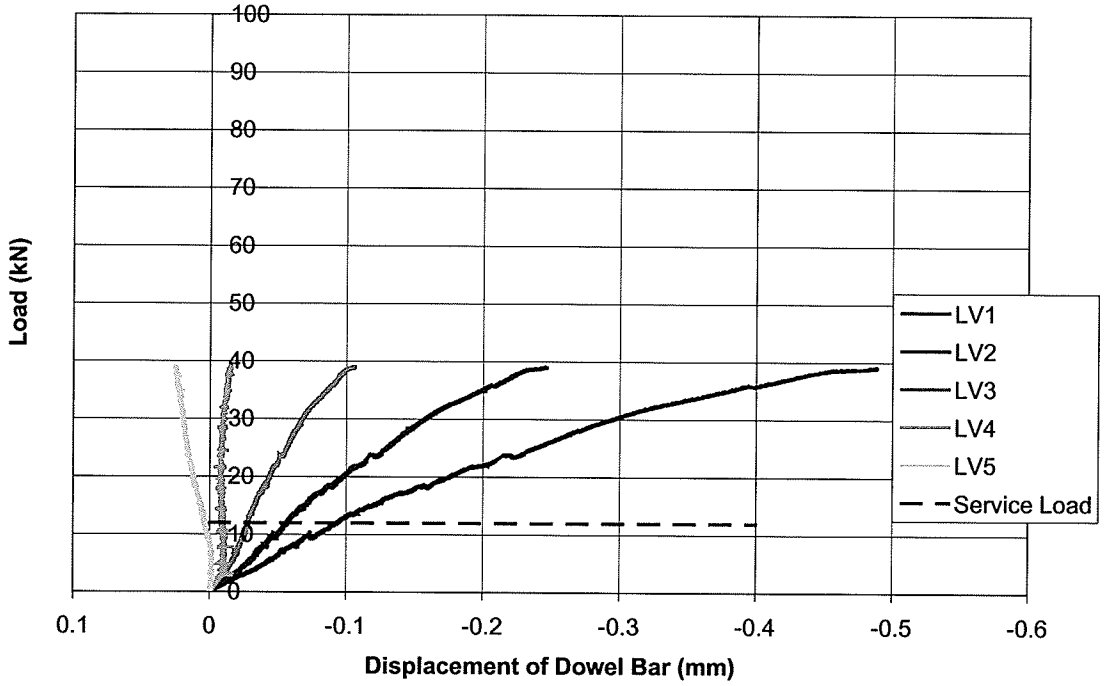

Figure 5.14 (b): Load-deflection plots up to failure for 38-mm GFRP dowel For each location measured along the dowel surface (Phase II)

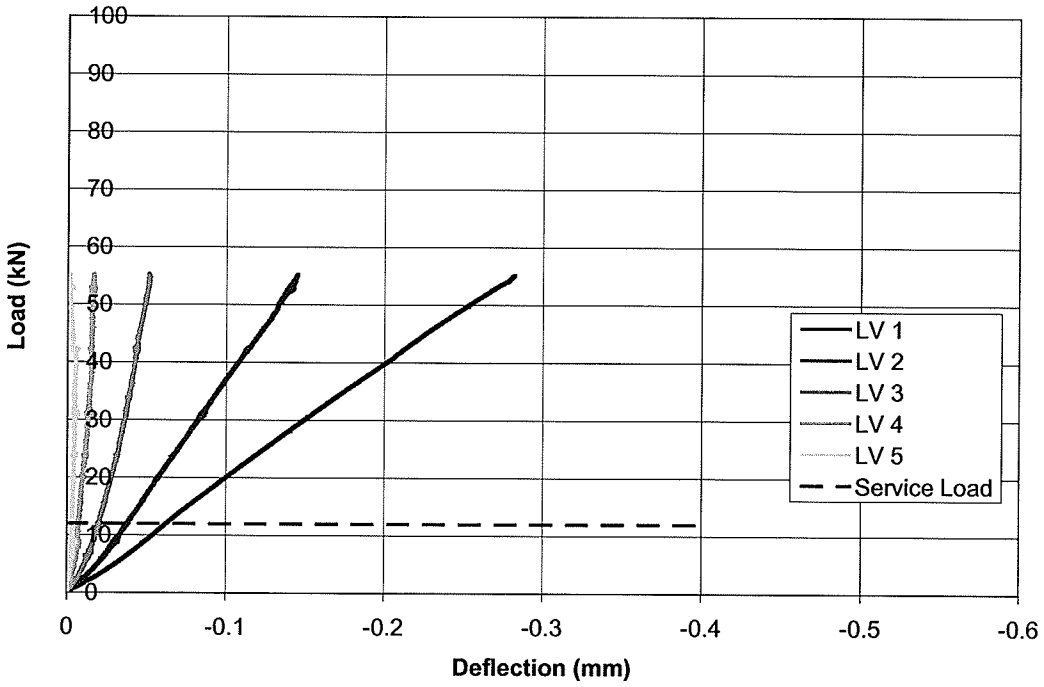

Figure 5.14 (c): Load-deflection plots up to failure for 50.8-mm concrete-filled GFRP dowel - For each location measured along the dowel surface (Phase II)

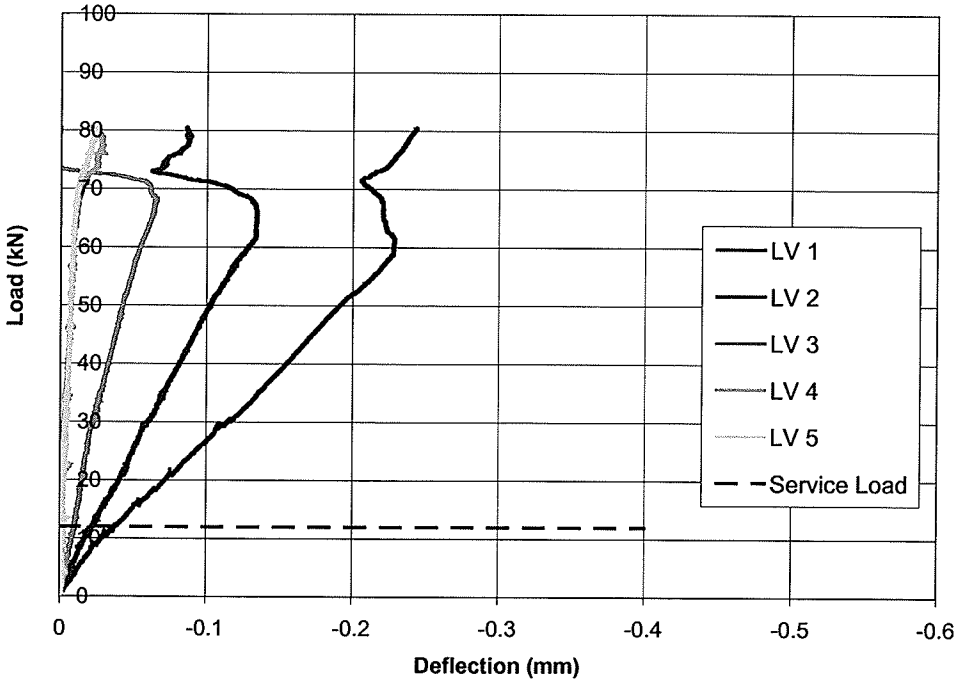

Figure 5.14 (d): Load-deflection plots up to failure for 63.5-mm concrete-filled GFRP dowel - For each location measured along the dowel surface (Phase II)

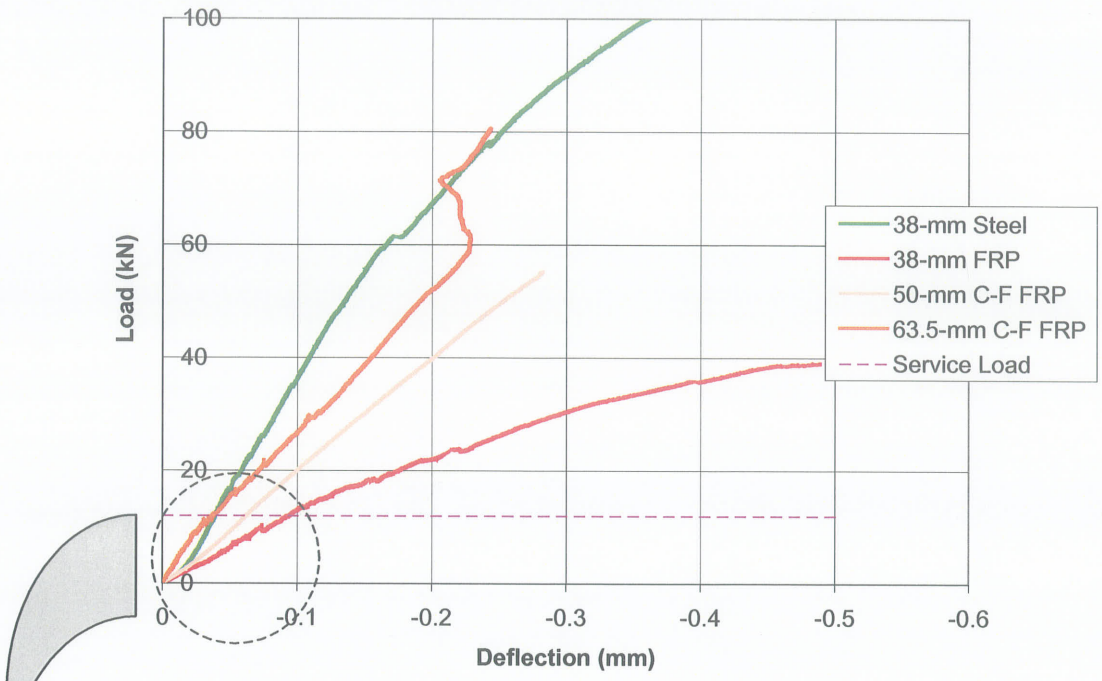

Figure 5.15 (a): Load-deflection behaviour of each dowel type – measured at the joint face location (LV 1)

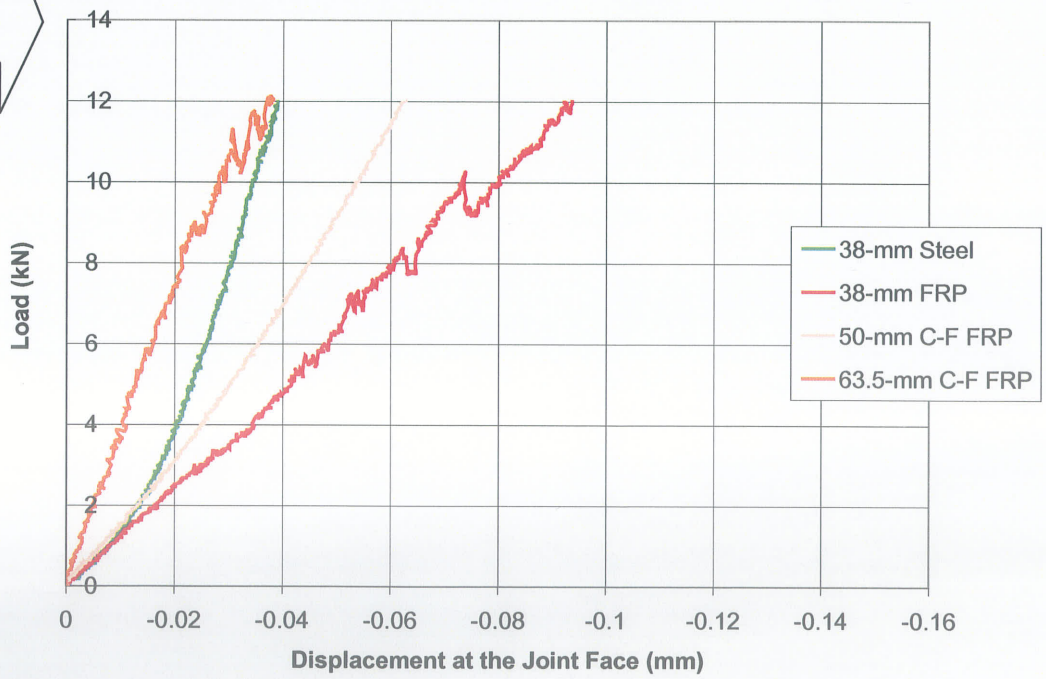

Figure 5.15 (b): Load-deflection behaviour of each dowel type (up to service load) – measured at the joint face location (LV 1)

The stoke of the machine as plotted in the load-stoke curves in Figure 5.16 does not show the same effect because the protruded part of the dowel displaced downward continuously. The stroke is clearly much larger because it is measured from the extended portion of the dowel which cantilevers out from the slab face. The slopes of all curves in the load-stroke graph are affected by the stiffness of each dowel bar in both the longitudinal and transverse directions as well as the stiffness of the concrete supporting it.

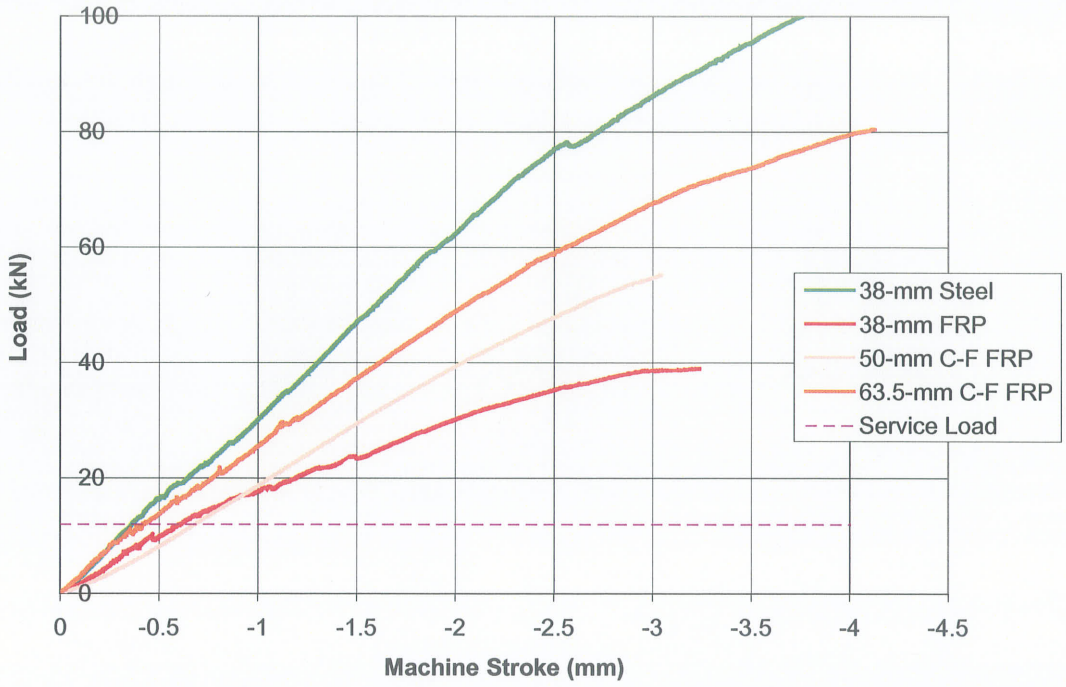

Figure 5.16: Load versus deflection of loading cross-head for each dowel type – Phase II

5.3.2 Dowel Bar Strain

Figure 5.17 shows the longitudinal strains in each dowel bar type at service load for the second phase of testing. In comparison with the results in Phase I, the strains measured in Phase II are smaller. This is consistent with the fact that the concrete strength is higher and

the dowels deflected less reducing the curvature of the bars and therefore reduced the longitudinal strain.

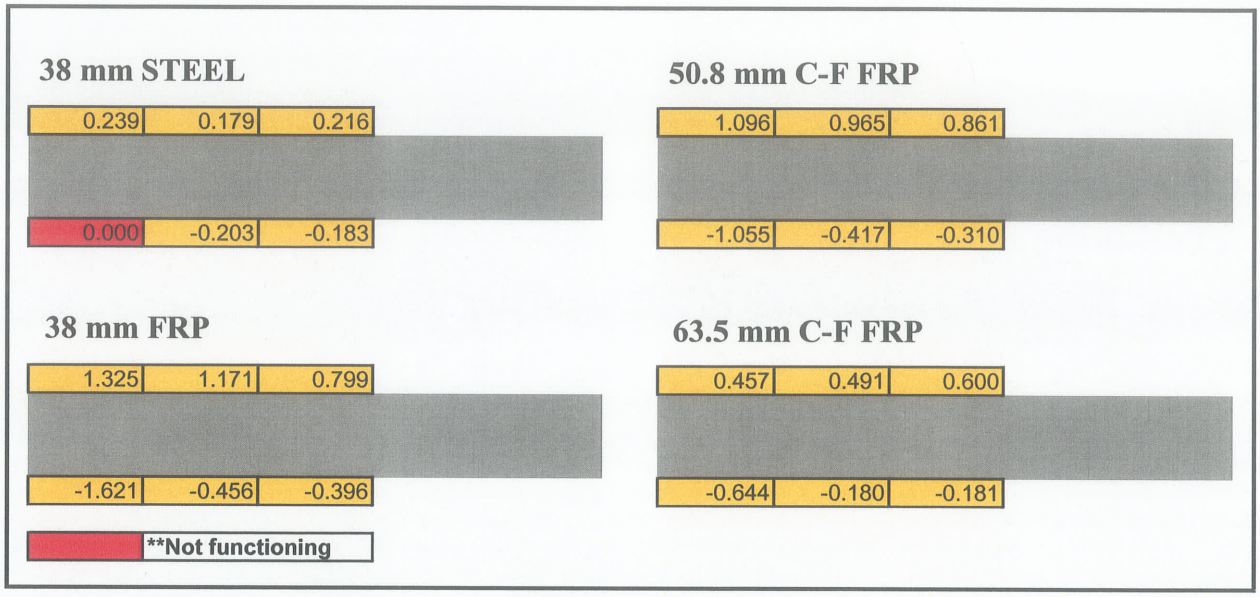

Figure 5.17: Dowel bar bending strains at service load – Phase II (millistrain)

Figures 5.18(a) to 5.18(d) show the load-strain curves for each dowel type. The bottom strain gauge nearest the joint face on the steel dowel bar was damaged so this load-strain curve was eliminated from Figure 5.18(a). The slope of the curve was expected to be very similar to the others just as was observed in the Phase I results.

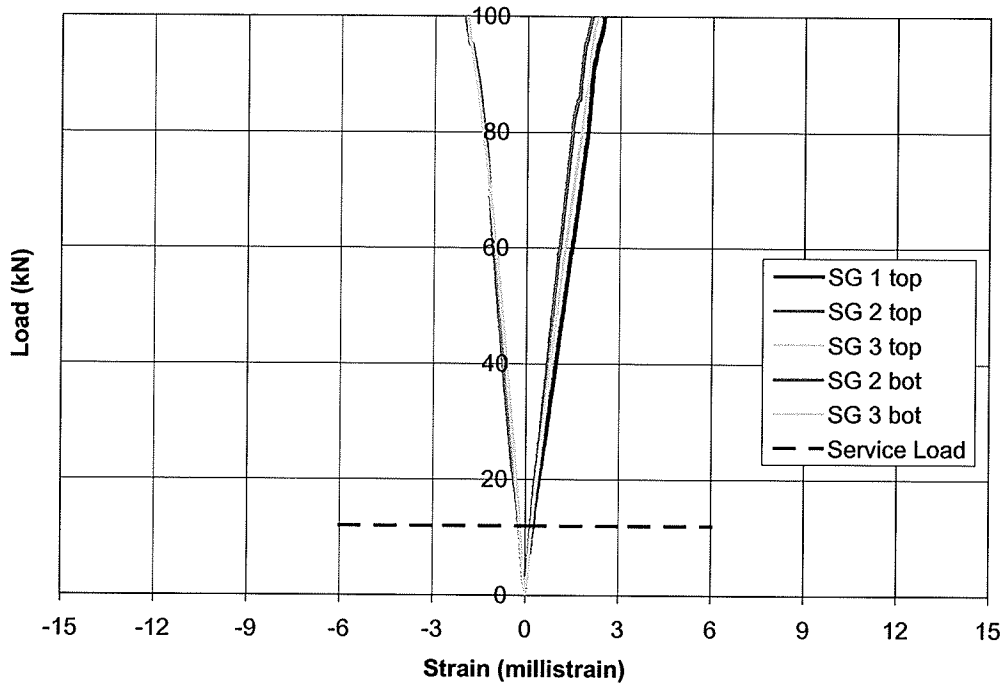

Figure 5.18 (a): Load-Strain behaviour of 38-mm Steel dowel –Phase II

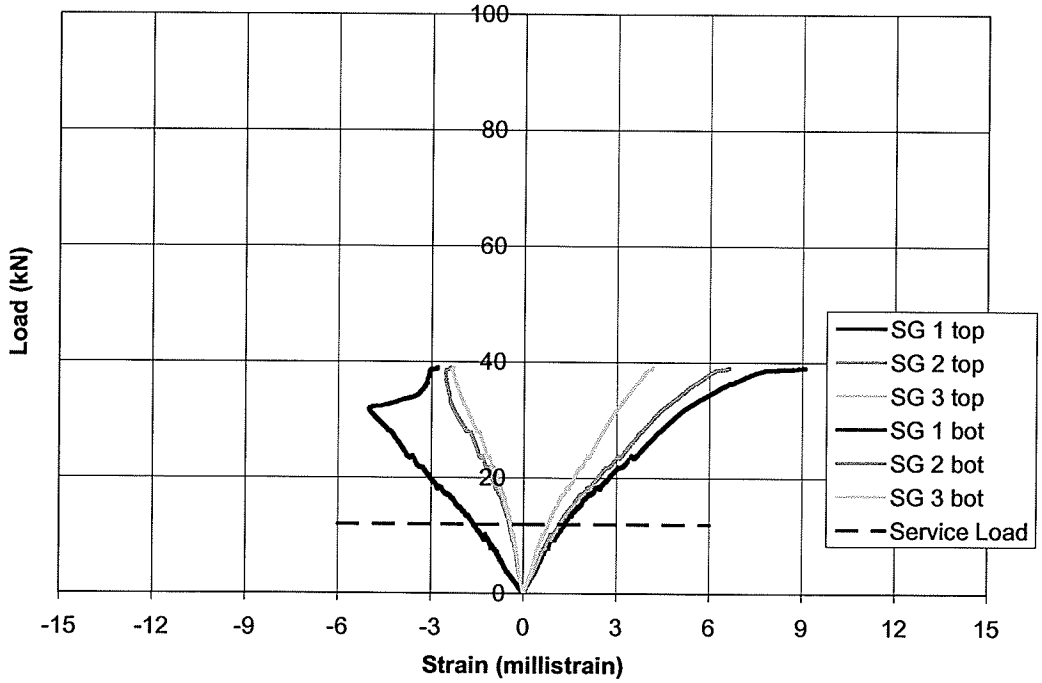

Figure 5.18 (b): Load-Strain behaviour of 38-mm GFRP dowel –Phase II

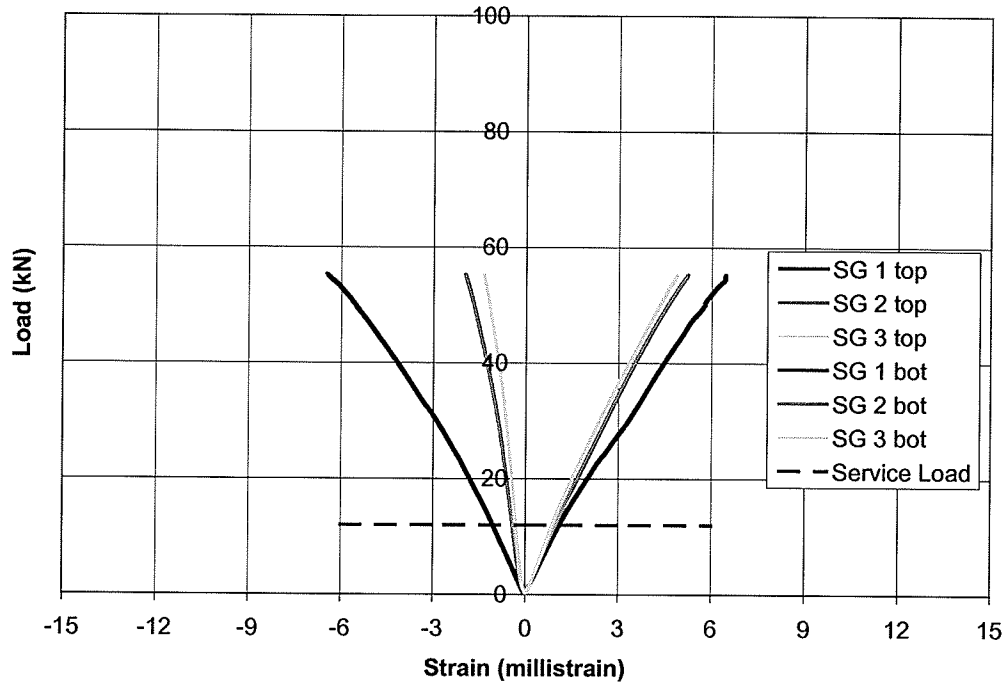

Figure 5.18 (c): Load-Strain behaviour of 50.8-mm concrete-filled GFRP dowel – Phase II

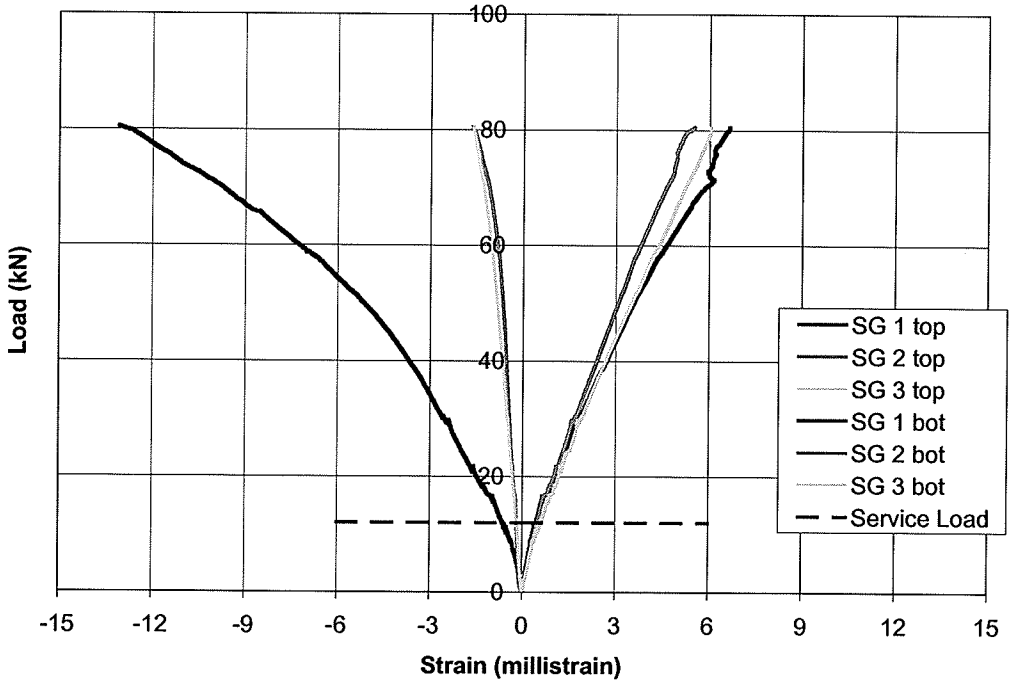

Figure 5.18 (d): Load-Strain behaviour of 63.5-mm concrete-filled GFRP dowel – Phase II

5.3.3 Concrete Strain Below the Dowel Bar

The concrete strain measured below each dowel bar type at service load level is given in Figure 5.19. The top strain gauge for the slab with the steel dowel bars de-bonded from the concrete face almost immediately after loading commenced and therefore the reading on this gauge is eliminated from the plot. The strain profiles appear less erratic than the results of the Phase I tests, however, the results are not as expected. The profiles for the 38-mm bars are similar with the exception of the missing steel gauge, however, it is expected that the 38-mm GFRP should produce significantly larger strains as predicted by the preliminary finite element analysis. The 50.8-mm concrete-filled GFRP dowel appears to produce the highest strain in the concrete compared to the other three types. The 63.5-mm concrete-filled GFRP dowel produces strains lower than the other three dowel types, however, the strain magnitudes are so much lower than in the Phase I result. This massive change does not appear logical.

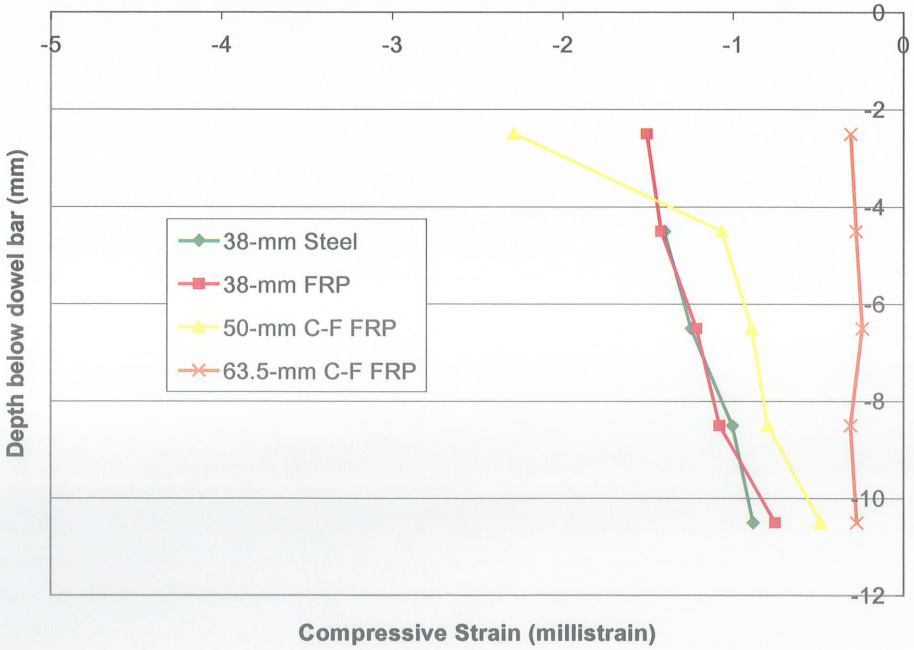

Figure 5.19: Vertical compressive strain versus depth below dowel – Phase II

Figures 5.20(a) to 5.20(d) show the load-strain plots of all the strain gauges up to failure for each of the four dowel types. These plots show when sudden changes occur in the concrete structure below the dowel bar. Each graph shows when the failure of the concrete appears to occur. Inspection of the strain gauges below the 50.8-mm concrete-filled GFRP dowel showed that some of the gauges had debonded from the concrete surface. The concrete surface did not appear to be damaged in any way. Therefore, the sudden change in the strain for four out of five of the gauges appeared to be due to the loss of bond only. Figure 5.20(d), which shows the strains for the 63.5-mm concrete-filled dowel, indicates very low strain in the concrete slab and shows no sign of damage throughout the entire test. Figures 5.21(a) to (d) show the load-strain plots for each slab loaded up to service level.

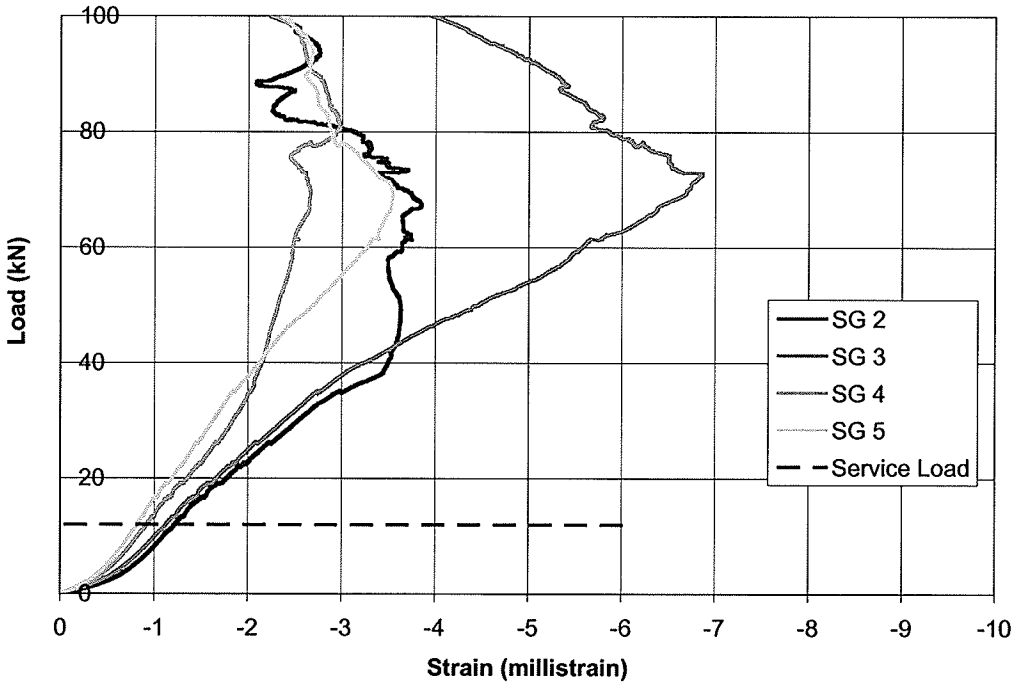

Figure 5.20 (a): Load-strain behaviour of concrete below 38-mm Steel dowel – Phase II

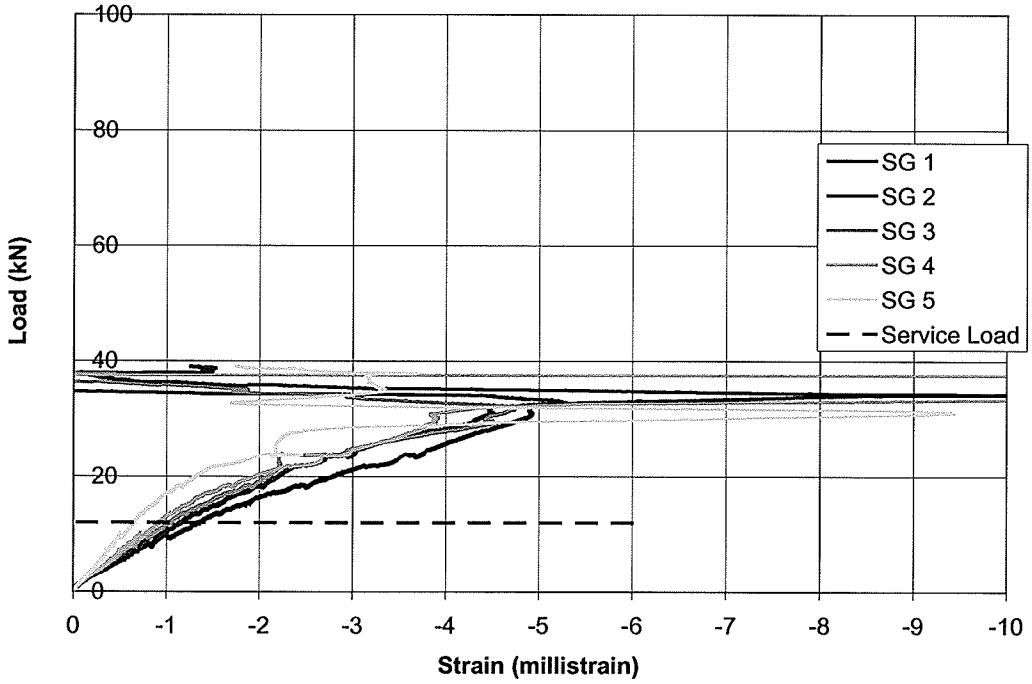

Figure 5.20 (b): Load-strain behaviour of concrete below 38-mm GFRP dowel – Phase II

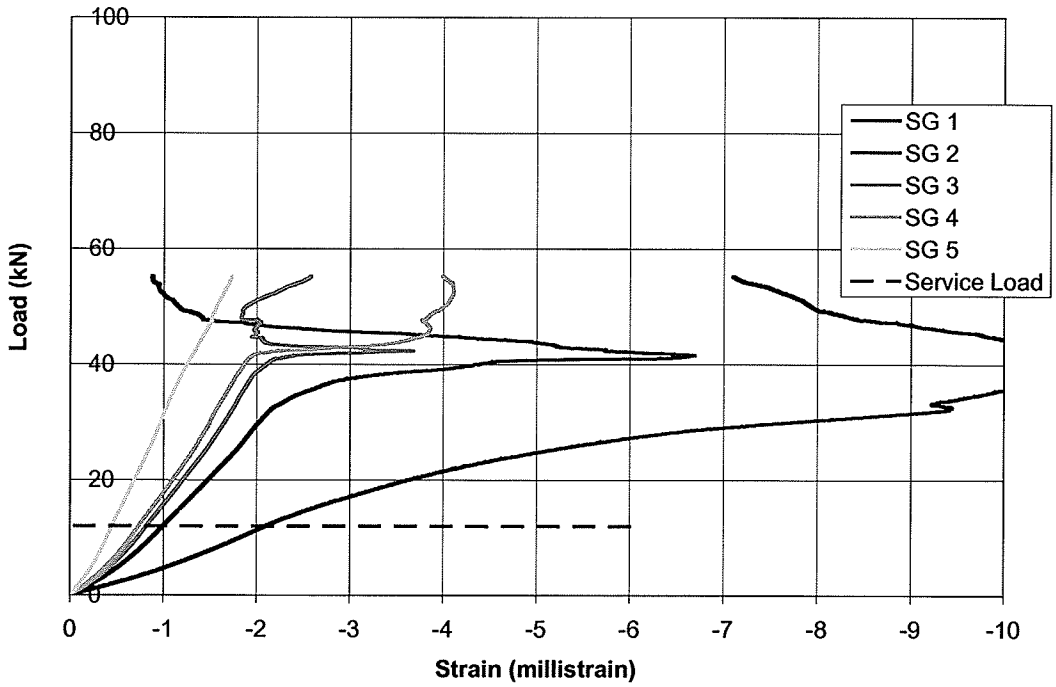

Figure 5.20 (c): Load-strain behaviour of concrete below 50.8-mm concrete-filled GFRP dowel – Phase II

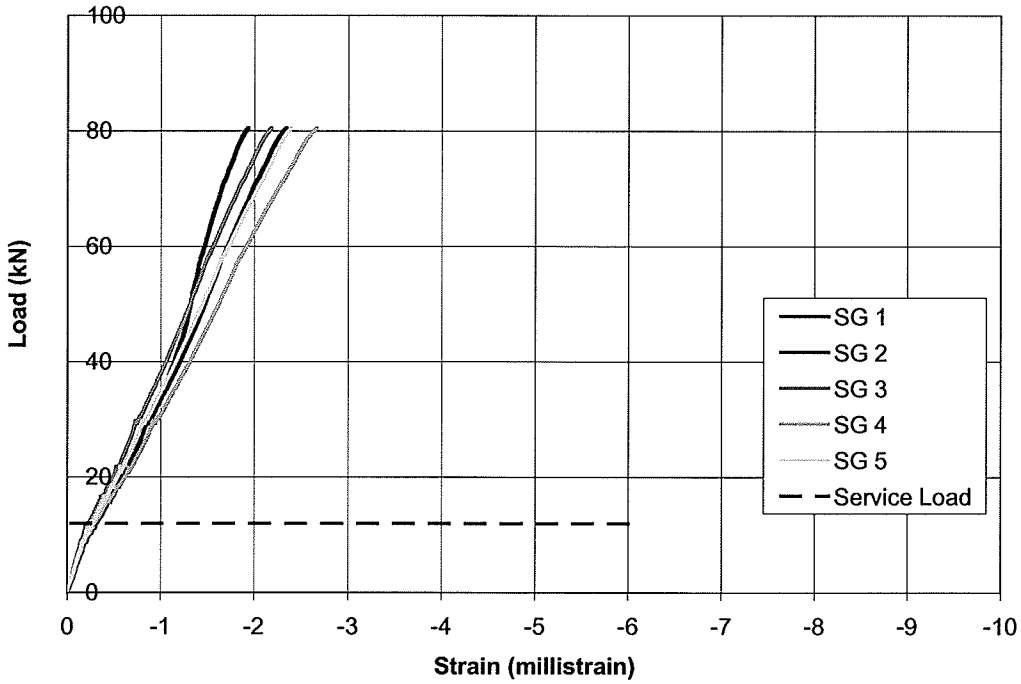

Figure 5.20 (d): Load-strain behaviour of concrete below 63.5-mm concrete-filled GFRP dowel – Phase II

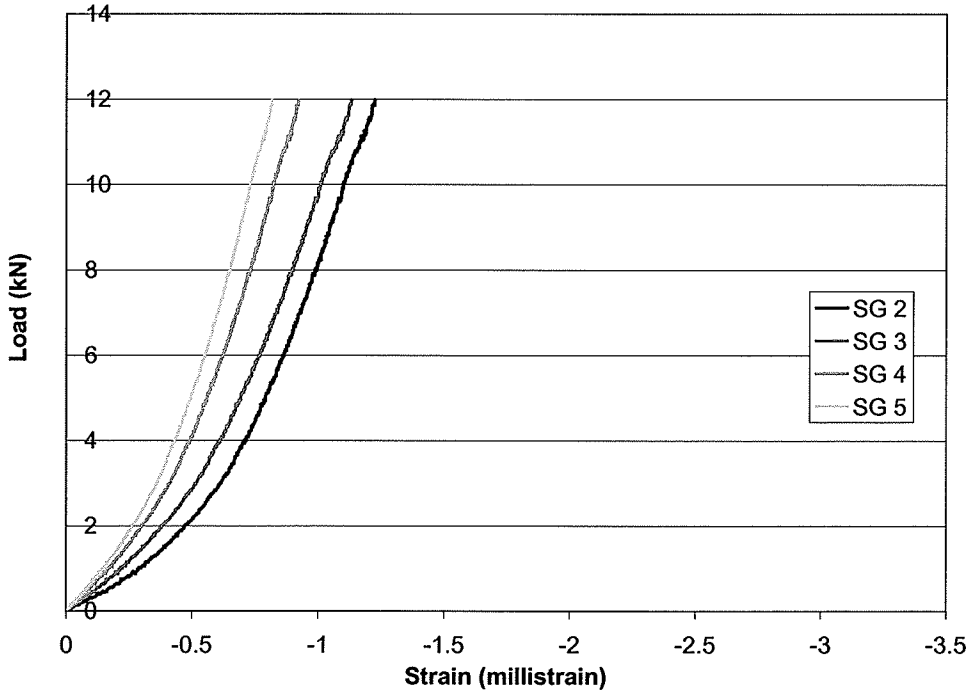

Figure 5.21(a): Load-strain behaviour of concrete up to service load for 38-mm Steel dowel – Phase II

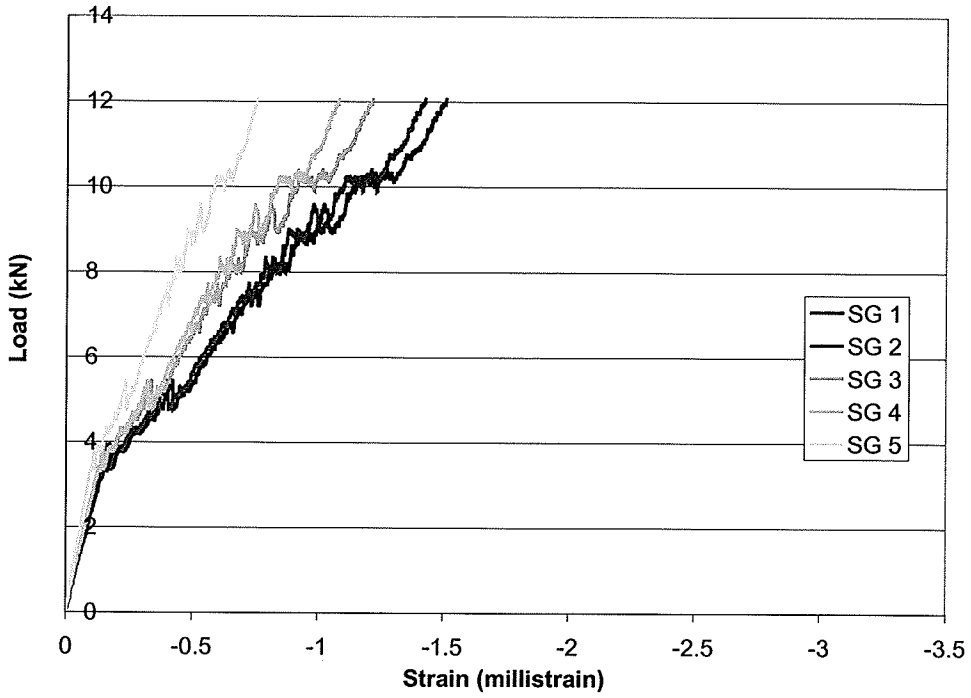

Figure 5.21(b): Load-strain behaviour of concrete up to service load for 38-mm GFRP dowel – Phase II

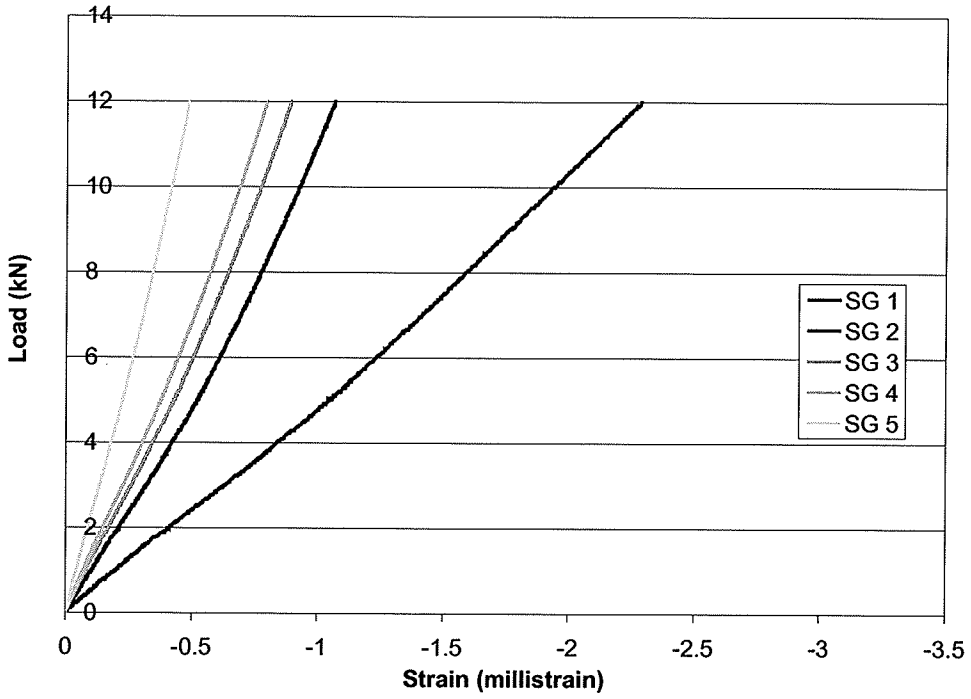

Figure 5.21(c): Load-strain behaviour of concrete up to service load for 50.8-mm concrete-filled GFRP dowel – Phase II

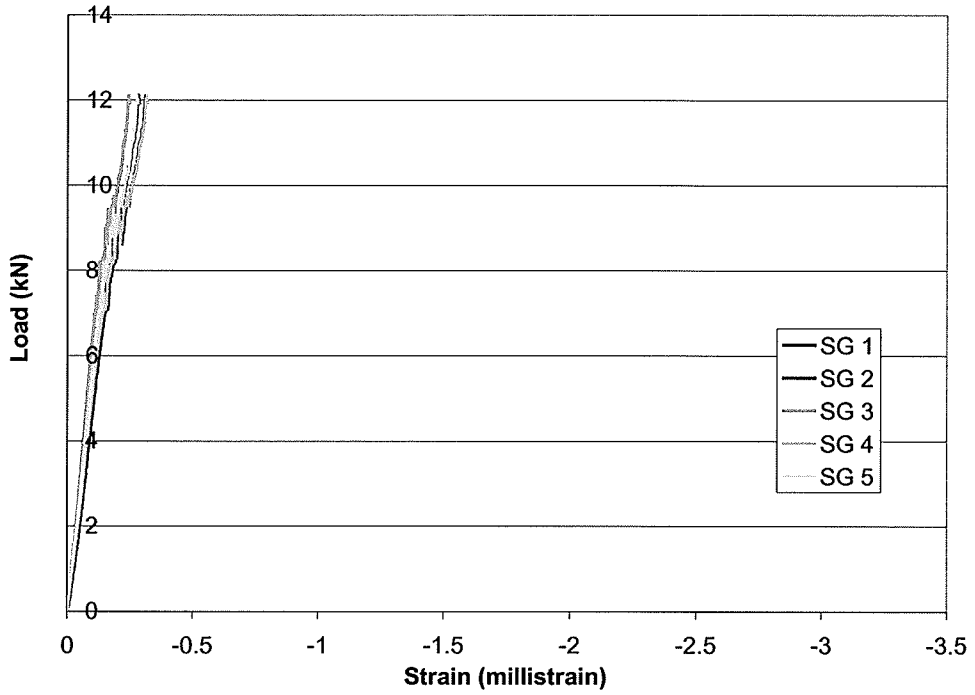

Figure 5.21(d): Load-strain behaviour of concrete up to service load for 63.5-mm concrete-filled GFRP dowel – Phase II

The damage to the concrete in these tests was mainly on a microscopic level. Visual inspections of the slabs after the tests showed little or no damage to the surface of the concrete below the dowel. The 38-mm (1.5") GFRP dowel caused a large flake of concrete to bust out from the face as shown in the photo in Figure 5.22. The steel dowel produced some slight flaking of the concrete surface in close proximity to the dowel (Figure 5.23), but did not produce any other significant visual damage. The concrete-filled GFRP tube dowels did not produce any visual concrete damage as shown in Figure 5.24(a) (50.8-mm GFRP) and Figure 5.24(b) (63.5-mm GFRP).

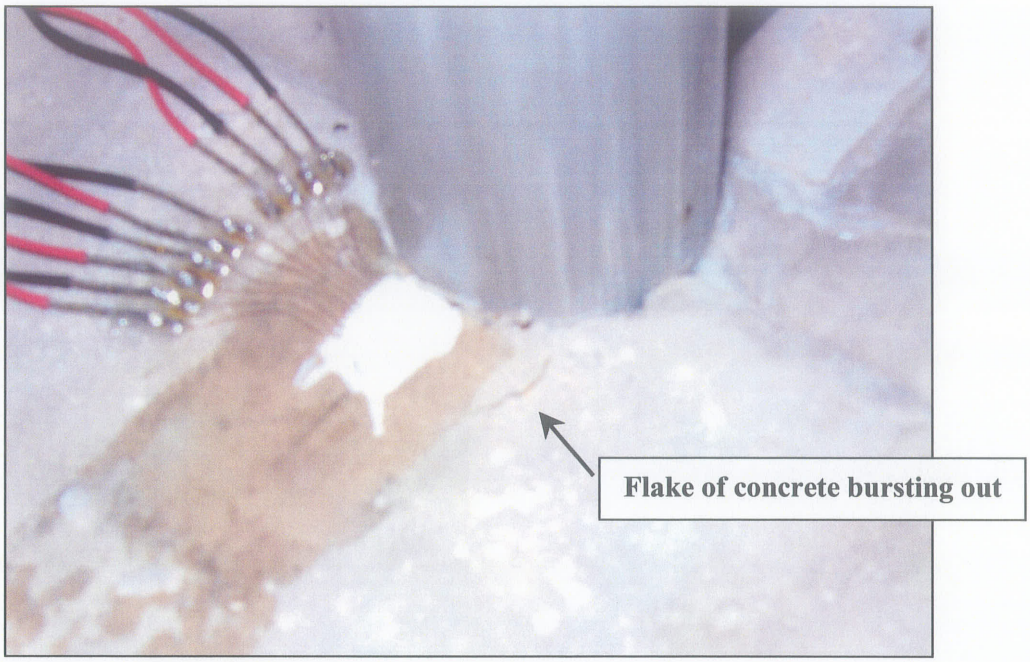

Figure 5.22: Damage to concrete below 38-mm GFRP dowel at approximately 24 kN – Phase II

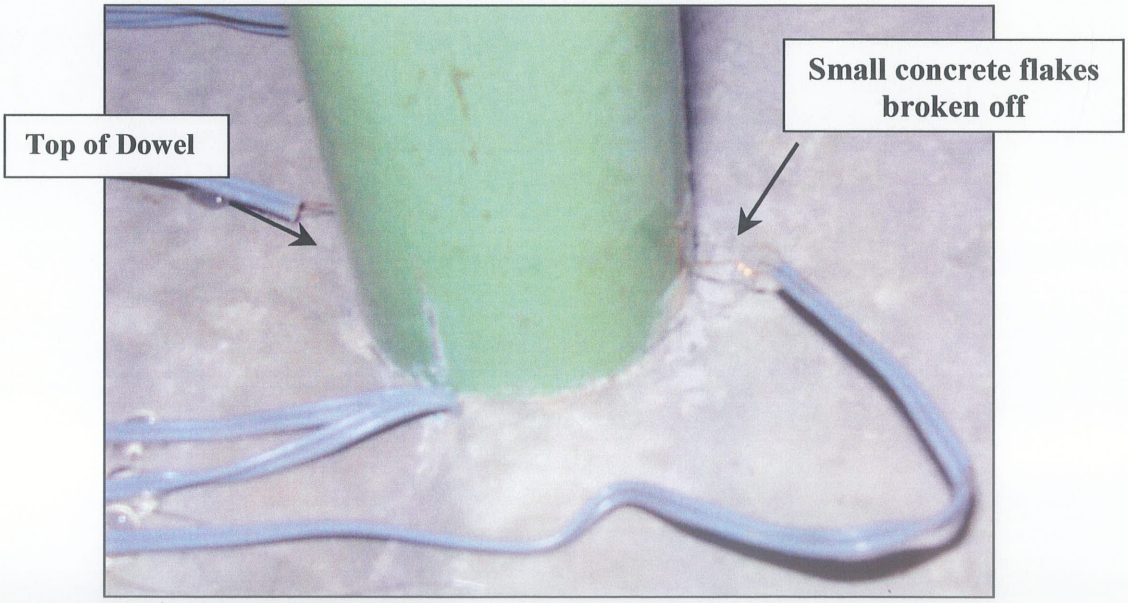

Figure 5.23: Damage to concrete below 38-mm steel dowel at failure (100 kN) – Phase II

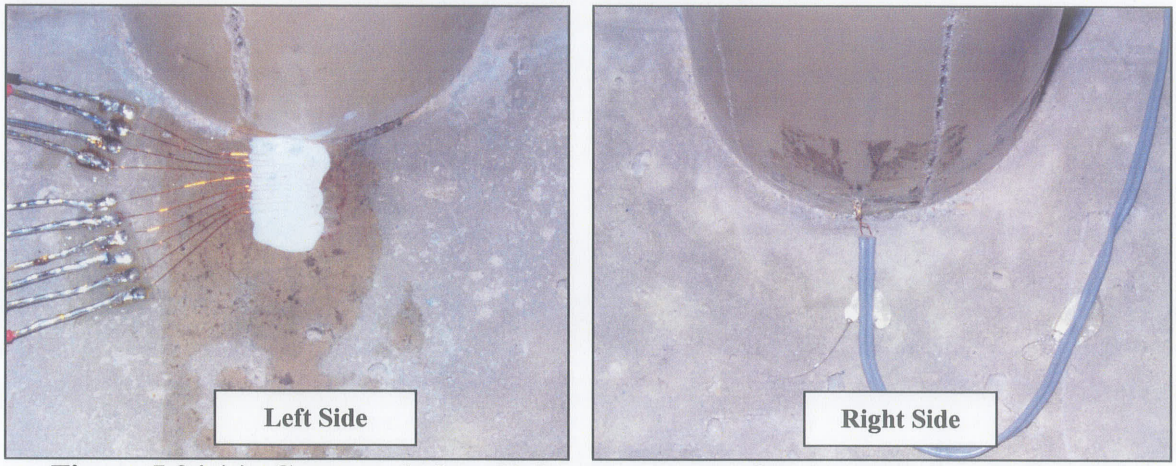

Figure 5.24 (a): Concrete below 50.8-mm concrete-filled GFRP dowel after failure (55 kN) – Phase II – No visible damage to concrete

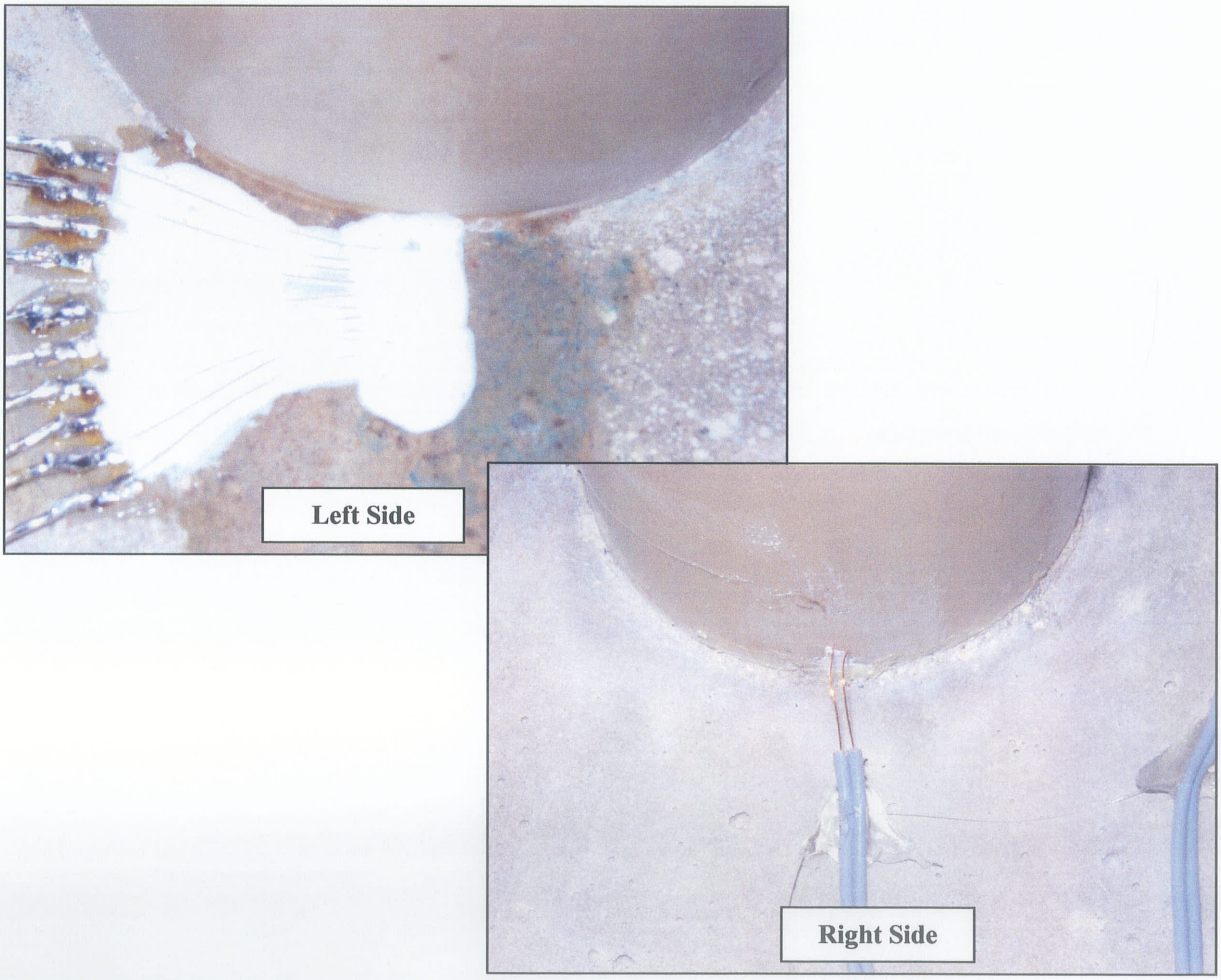

Figure 5.24 (b): Concrete below 63.5-mm concrete-filled GFRP dowel after failure (80 kN) – Phase II -- No visible damage to concrete

Chapter 6

Analysis and Discussion

6.1 General

In this study, the behaviour of a dowel bar encased in a concrete pavement slab subjected to simulated vehicle loads has been examined through the use of preliminary finite element modeling and experimental work. This chapter will discuss the results of the experimental work outlined in Chapter 5 and provide comparisons with results from a finite element analysis that was run using similar properties obtained in the laboratory tests. Results for this revised finite element analysis are provided below. They include an increased concrete slab compressive strength and two sizes of concrete-filled GFRP tube dowels which replace the 60-mm solid dowels used in the preliminary analysis provided in Chapter 3. Discussion will be provided on areas including dowel bar displacements and load-deflection behaviour, dowel bar strains due to bending, load-strain behaviour of the dowels, and concrete strains and bearing stresses in the pavement slab. The validity of the analytical solutions proposed by Friberg (1938) and their use in designing with GFRP dowels is also discussed.

6.2 Finite Element Analysis

6.2.1 Introduction

There were three reasons for conducting a revised finite element analysis comprising similar material properties as those measured in the experimental program. The first reason was to

provide a computer model containing ideal properties that could be used to compare with the experimental results. In addition, the finite element model can provide valuable information about the internal stresses in the dowel and pavement slab that cannot be determined easily through laboratory tests. The third reason for conducting the finite element analysis was to estimate the amount of transverse dowel deformation that occurs when the dowel is loaded. As was first mentioned in the experimental results of Chapter 5 for the dowel deflection measurements, the dowel deflections were measured from the top of the dowel surface and do not account for the transverse deformation or ovalizing of the bar. Therefore, the magnitude of deflection of the bar into the concrete below, which is directly related to the bearing stress, is lower than the deflections measured at the top surface of the bar.

It was determined to be impossible to directly measure the deformation of the bottom surface of the dowel with the test slabs used in the experimental program without affecting the integrity of the concrete surrounding the dowel. Methods for measuring the transverse deformation of GFRP bars through different laboratory tests were examined and it was determined that there was not a test that would provide accurate results. For this reason, the finite element method was employed.

6.2.2 Description of the Model

The dimensions and mesh properties of the revised FE model were identical to those used in Chapter 3. The changes made to the model included an increase in concrete compressive strength to 53 MPa, and the use of a two sizes of concrete-filled GFRP tube dowels. The elastic modulus of the GFRP tube was lowered to more closely match the properties of the

Extren Series 625 tubes used in the laboratory tests. Table 6.1 provides the properties of the dowels and other geometries in the model. A 38-mm steel dowel and a 38-mm solid GFRP dowel were analyzed along with 50.8-mm (2") and 63.5-mm (2.5") diameter concrete-filled GFRP tube dowels.

Similar to the model in Chapter 3, a 12 kN load was applied to the dowel and was centered 12.5 mm from the joint face of the pavement slab. The slab rested on a solid base material. The material properties of the base did not affect the interaction between the dowel and concrete. The model was run using both a soft base material as well as a steel base. The magnitude of the slab deflections were affected, but the dowel deflections into the surrounding concrete and the stresses in that concrete were unaffected.

6.2.3 Results and Discussion of the Finite Element Analysis

6.2.3.1 Deflected Shape of the Dowel Bar

Figure 6.1 shows the deflected shapes of the four dowel types modeled. The deflected shapes represent the bottom surface of each dowel. The 38-mm GFRP dowel has the highest displacement among the four dowel types. The 63.5-mm concrete-filled dowel has the lowest. The 38-mm GFRP dowel has higher displacement than the 38-mm steel due to the lower flexural stiffness. The 38-mm steel dowel and the 50.8-mm concrete-filled GFRP tube dowel exhibit approximately the same peak deflections. The elastic modulus for the GFRP tube is less than one-third that for the 38-mm solid GFRP dowel, which shows that the larger diameter of the concrete-filled tube has a significant effect in reducing deflections and

therefore bearing stresses. The larger, 63.5-mm concrete-filled GFRP dowel reduces deflections even more as was determined from the experimental results.

As was found in the preliminary finite element analysis, the magnitudes of the dowel deflections are quite low. This can clearly be seen when the FEM results are compared with the experimental results shown in Chapter 5, however, the experimental results represent the top-surface deflections for the dowels. The figure below shows the deflections at the bottom surface of each dowel. It is the bottom surface deflections that correlate with the bearing stress in the concrete.

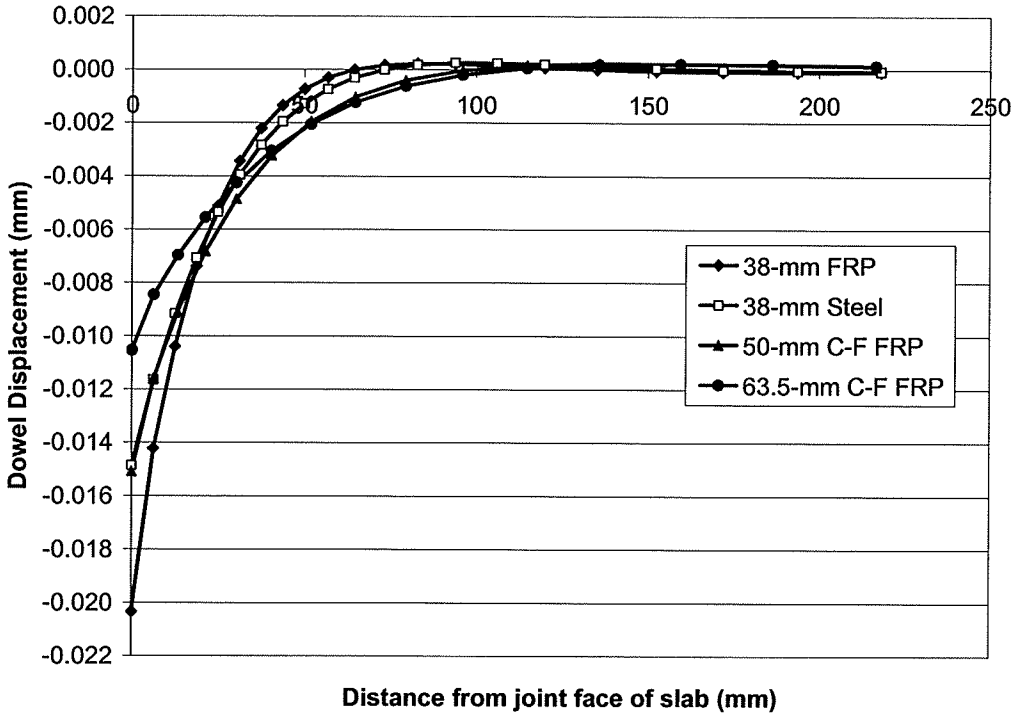

Figure 6.1: Deflected Shape of Each Dowel Bar

6.2.3.2 Stress and Strain in the Concrete Slab Under the Dowel

As seen in Figure 6.2 and 6.3, the 38-mm GFRP dowel produced the highest vertical compressive stress and strain in the concrete which corresponds with this dowel exhibiting the highest deflection. The large 63.5-mm diameter concrete-filled GFRP dowel produced the lowest strain. Clearly, the dowels that exhibit higher displacements produce higher stain and bearing stress. The stress in the concrete below the 38-mm GFRP dowel is close to the ultimate compressive resistance of 53 MPa which is very high. Figure 6.4(a) and 6.4(b) show snapshots of the vertical compressive stress under each of the four dowel types.

The vertical compressive strain in the concrete is plotted with depth below each dowel bar in Figures 6.5(a) and 6.5(b). Figure 6.5(b) shows a zoomed-in view of the strains in the region directly below the dowel bar. The magnitude of the strain and therefore, bearing stress, dissipate rapidly with depth below the dowel bar. The strain values for the nodes located second from the top are higher than actual because the extreme values for each element were plotted instead of the smoothed or averaged values, but the differences between the dowels are clear.

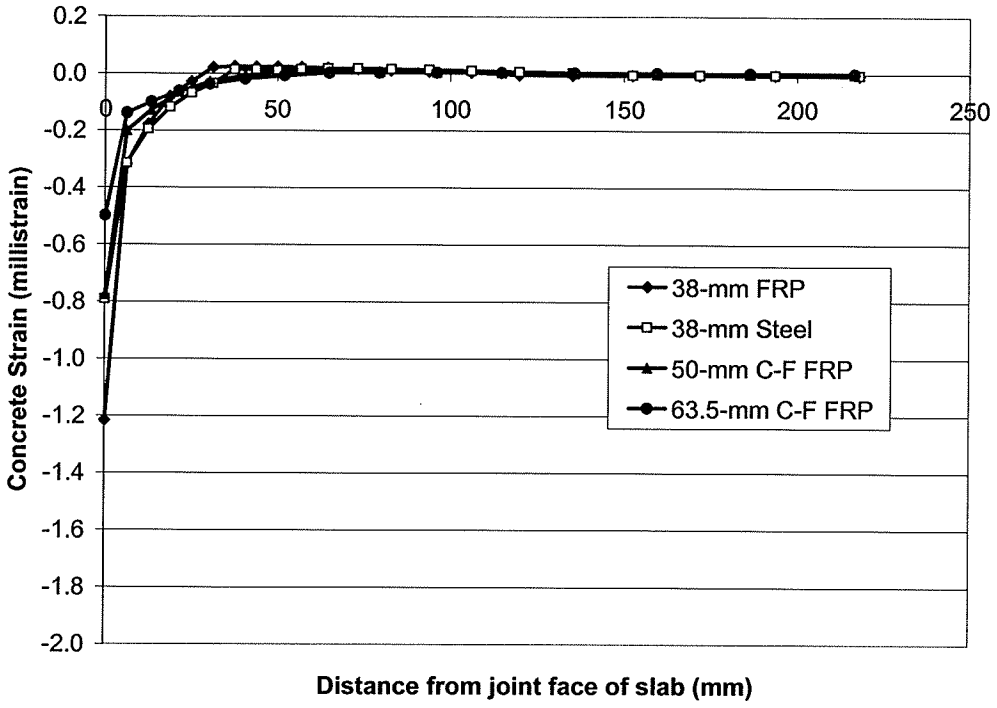

Figure 6.2: Vertical Compressive Strain in Concrete Below Dowel Bar vs Dowel Length

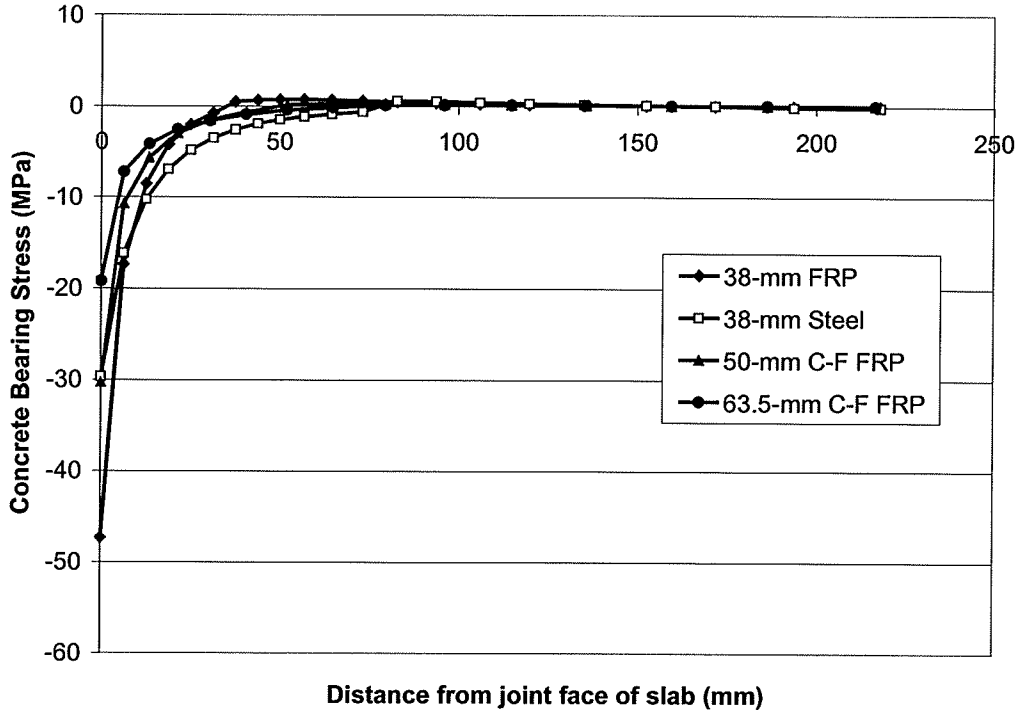

Figure 6.3: Vertical Compressive Stress in Concrete Below Dowel Bar vs Dowel Length

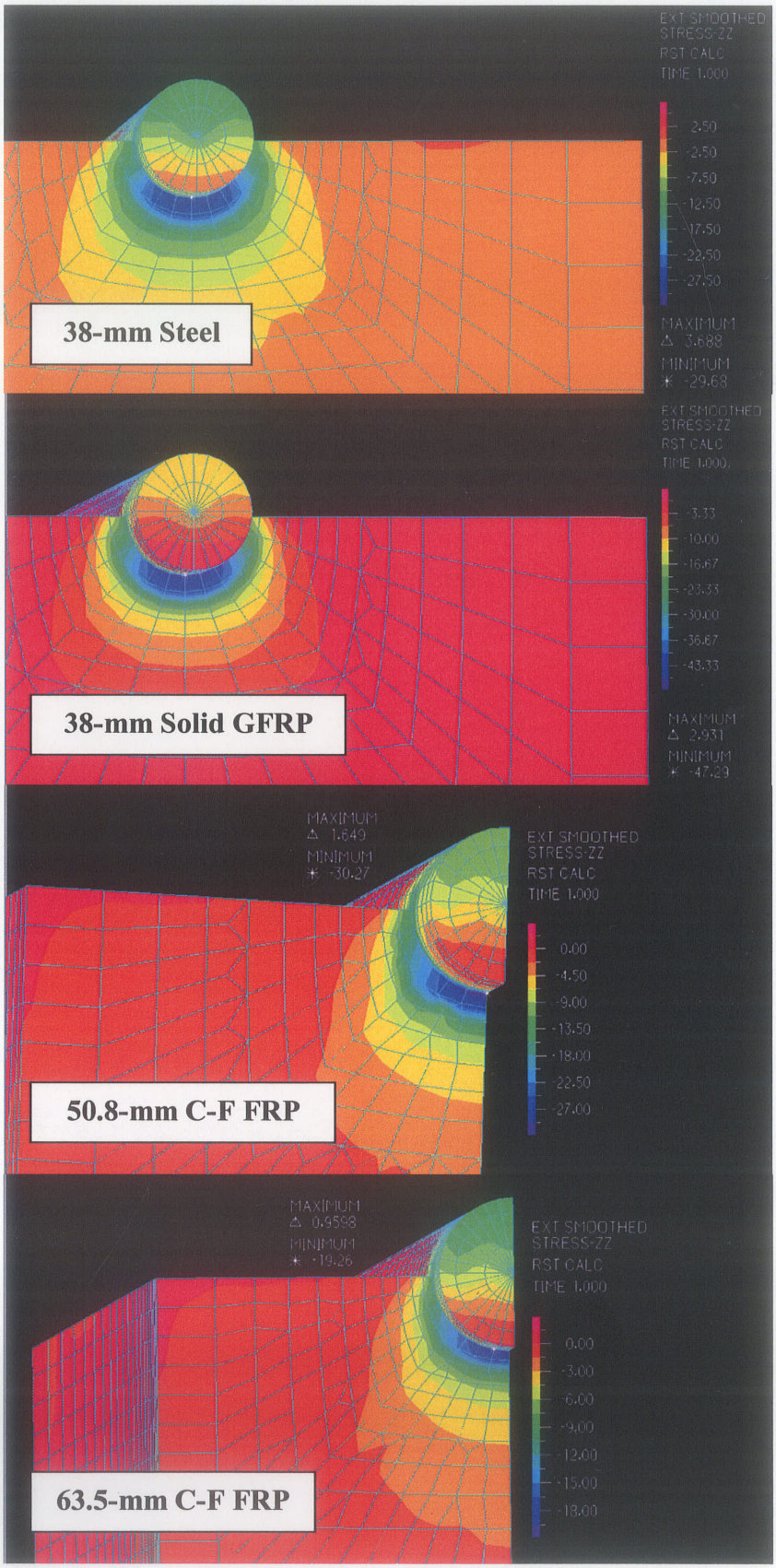

Figure 6.4(a): Snapshots of Vertical Stress Distributions Around Dowel at the Joint

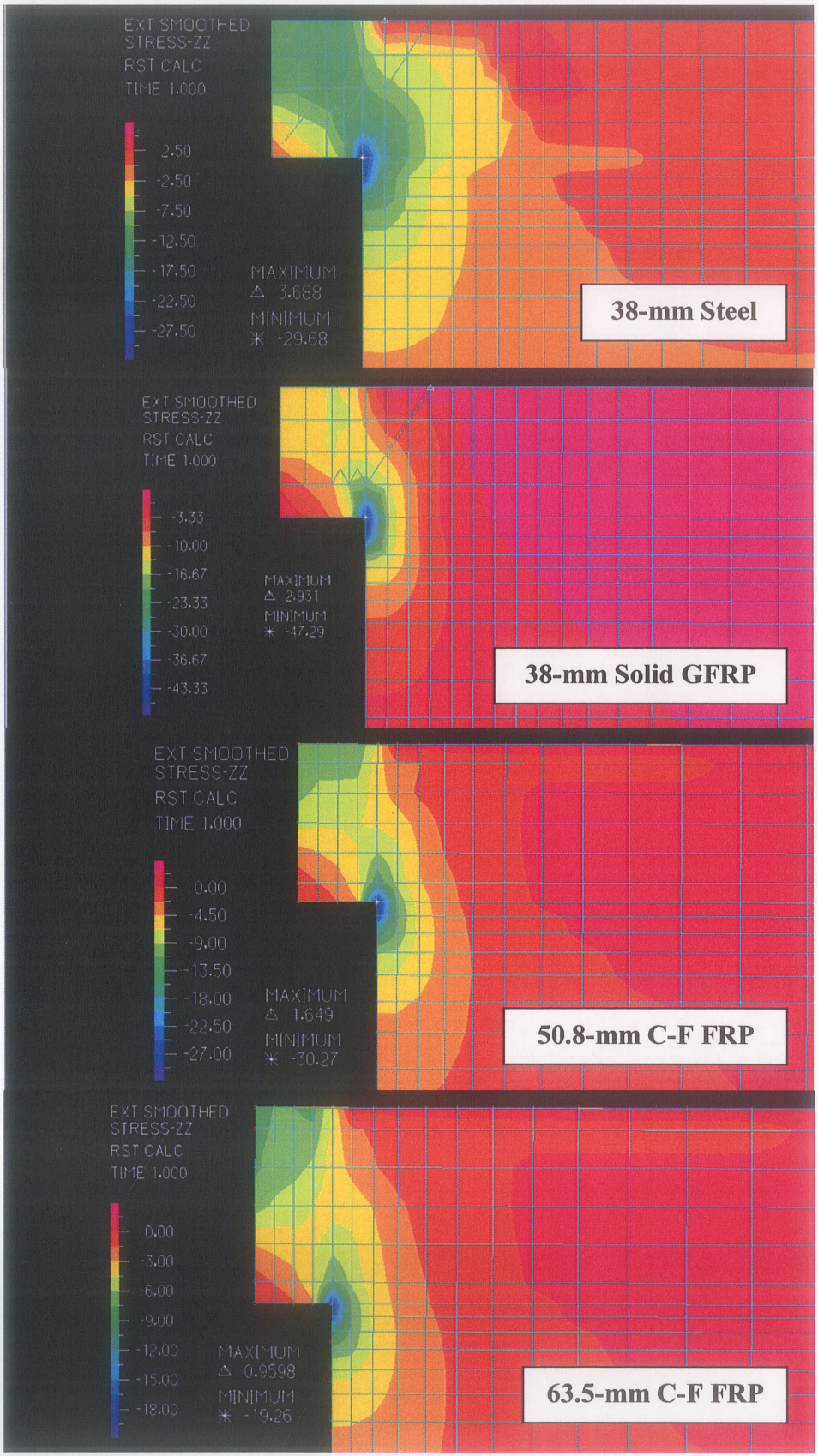

Figure 6.4(b): Snapshots of vertical stress along the length of the dowels (Center)

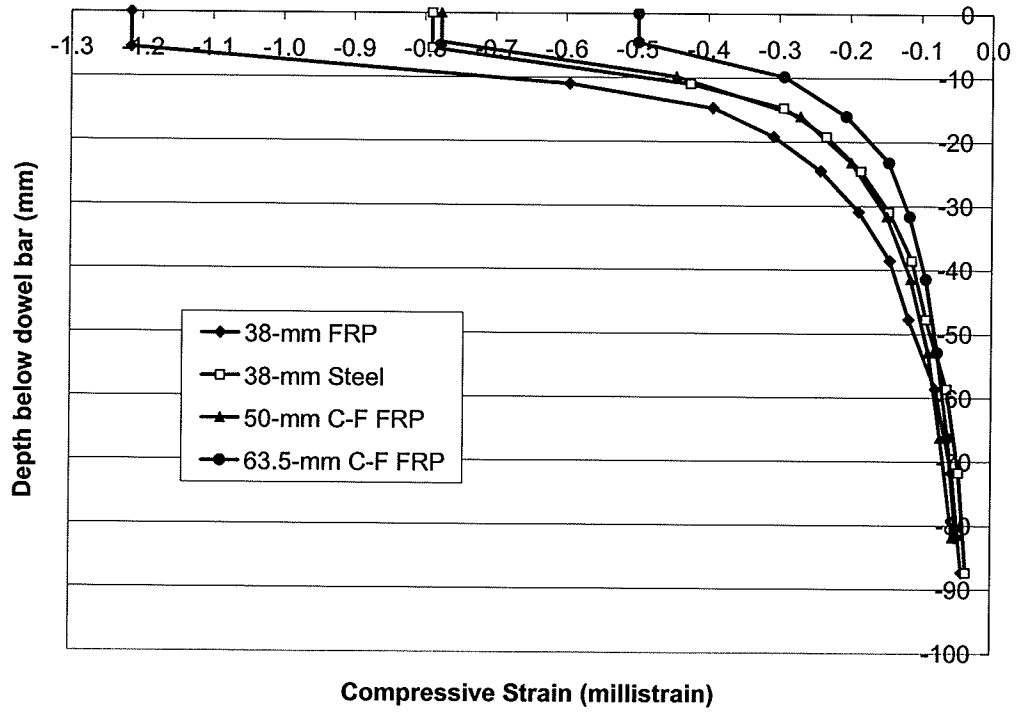

Figure 6.5(a): Vertical Compressive Strain vs Depth of Concrete Slab Below Dowel

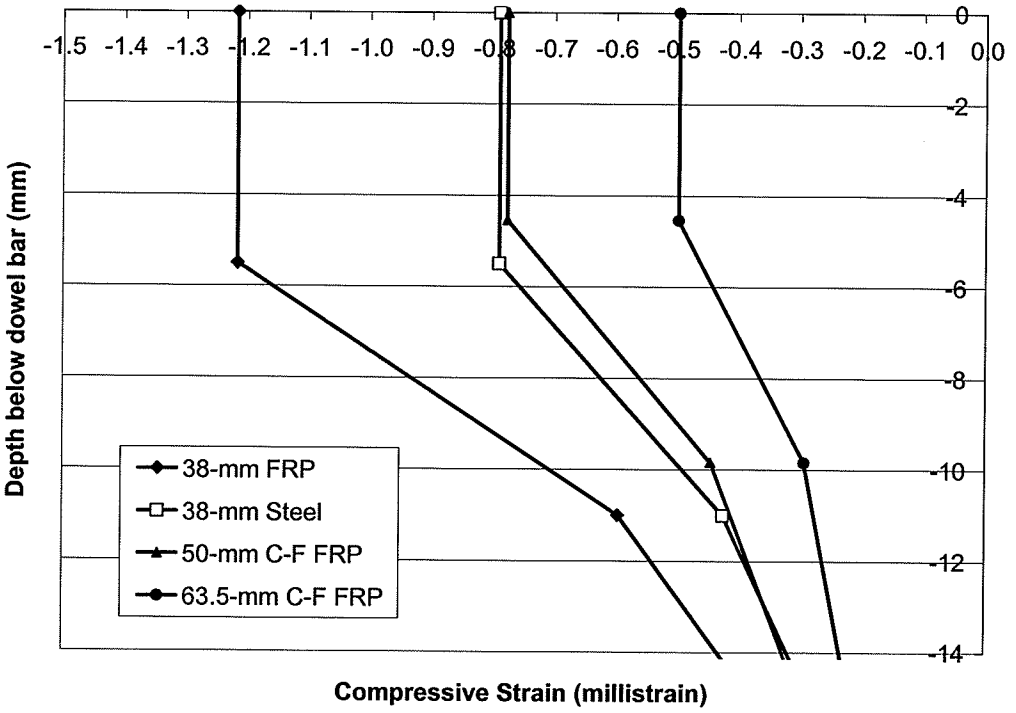

Figure 6.5(b): Vertical Compressive Strain vs Depth Below Dowel – Zoomed-in View

The horizontal tensile strain in the concrete below the dowel bar is plotted in Figure 6.6. The 38-mm dowel exhibits the highest tensile strain in the concrete followed by the 50.8-mm concrete-filled GFRP dowel. The stresses appear to dissipate with depth below the dowel.

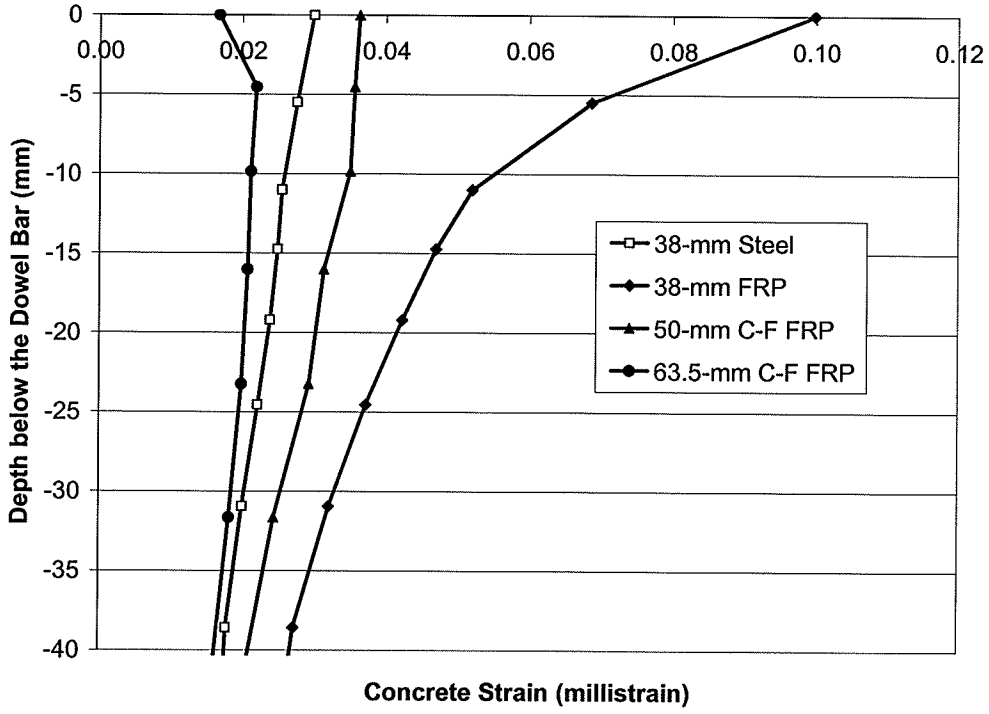

Figure 6.6: Horizontal Tensile Strain in Concrete Below Dowel

When the dowel bar is forced down into the concrete there are both vertical compression and horizontal tensile stresses created in the plane of the pavement slab face. The magnitude of the tensile stress at the joint face of the slab is affected by three major factors. They are the diameter of the bar, the amount of load concentrated near the joint face (affected by flexural stiffness of the dowel), and the stiffness of the bar in the transverse direction. The third factor is one of great importance. A dowel that compresses more easily in the transverse direction will ovalize in shape causing a change in the pressure distribution below it. In fact,

the vertical compressive stress will be lower due to the increased bearing area, and the horizontal bearing stress will be greater due to the widening of the dowel. The increased horizontal forces cause higher tensile stresses in the concrete below the dowel bar. An example of this concept is shown in Figure 6.7.

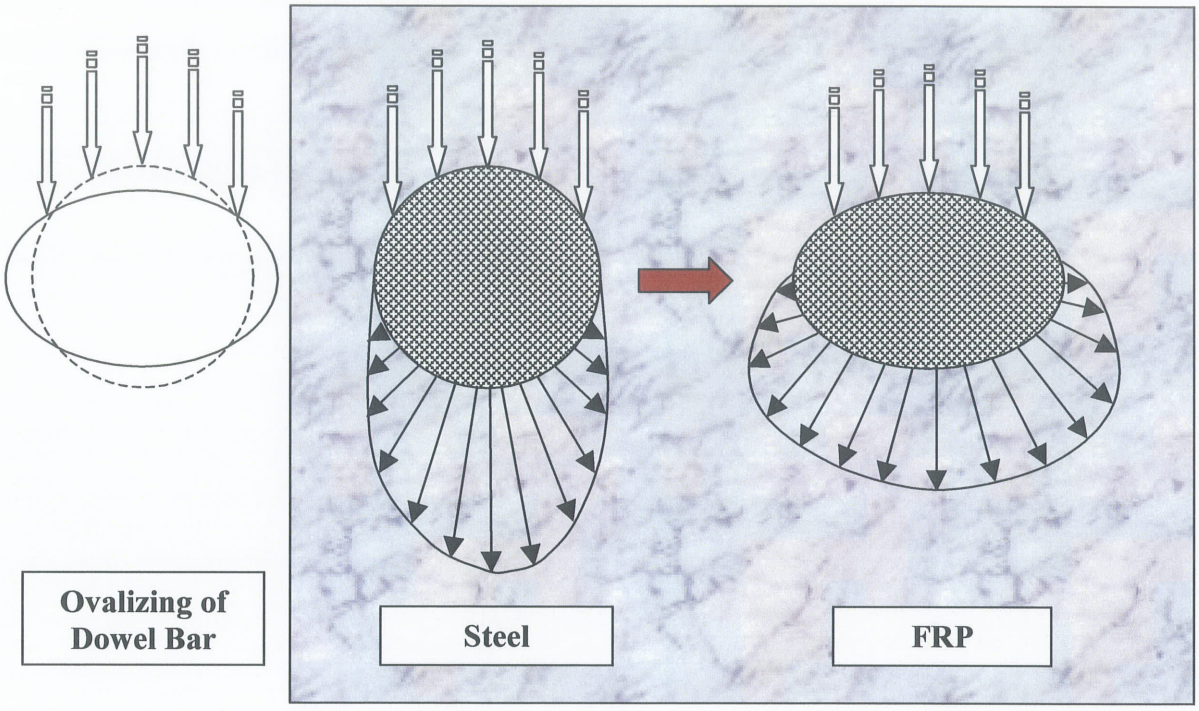

Figure 6.7: Redistribution of Bearing Stresses Due to Ovalizing of Dowel Bar

6.2.3.3 Flexural Strain in the Dowel Bars

The magnitude of the flexural strain in the steel dowel is substantially lower than the strain in the GFRP dowels as expected because of the lower stiffness of GFRP. As seen in Figure 6.8, the distribution of strain (x-direction) due to bending in each dowel bar is also quite different. One clear difference between the steel and GFRP bars is the distribution of the compressive strain at the bottom of the dowel bars. The distribution of tensile and compressive stress in

the steel bar is relatively the same indicating normal bending behaviour of the bar where the neutral axis is located near mid-depth of the dowel. For all of the GFRP dowels, however, the compressive strains are concentrated over a very small region near the joint face. The strains drop substantially just inside of the joint face which indicates that the protruded portion of the dowel bends like a 'hinge' about the edge of the concrete face. Therefore there is a high, unevenly distributed concentration of stress in the GFRP dowels near the joint face. The magnitudes are not extremely high though, and there is no sign that the dowels are over-stressed in any way.

One important point to note is that the FE analysis incorporates a simplistic model where the dowel is fully bonded to the concrete. In Figure 6.8 it is clear that the bending strains in the dowels are transferred directly to the concrete below the dowel. This brings the accuracy of having a fully-bonded dowel into question. It is probable that the dowel is not fully-bonded which can affect the bending behaviour of the dowels. For example, the fully-bonded dowel will exhibit a greater degree of flexural stiffness resulting in lower bending stresses and lower deflections. This issue is discussed in the next section.

Figure 6.9 shows the plots of flexural strain in each of the four dowel types obtained from the FE model. The higher magnitudes of strain in the GFRP dowels, especially the 38-mm GFRP dowel, indicate that there is a high rotation of the dowel occurring at the joint face of the slab. Also, the large increase in compressive strain at the bottom of the solid and concrete-filled GFRP dowels near the joint face indicates a hinge type of bending. The vertical dotted lines in the graph represent the locations on the dowels where strain gauges

were used to measure flexural strain in the laboratory tests. Further comparisons are provided later in this chapter.

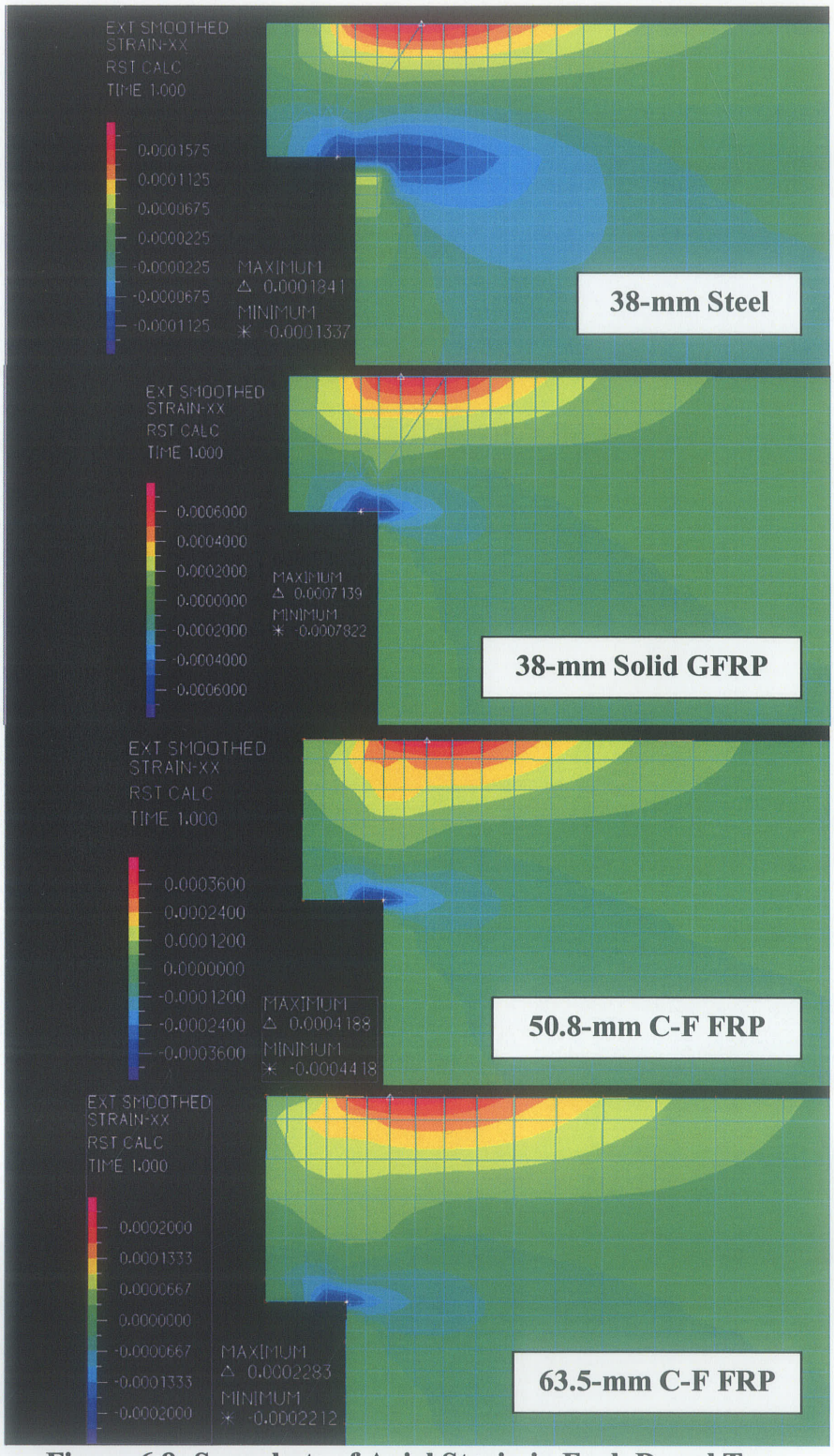

Figure 6.8: Snapshots of Axial Strain in Each Dowel Type

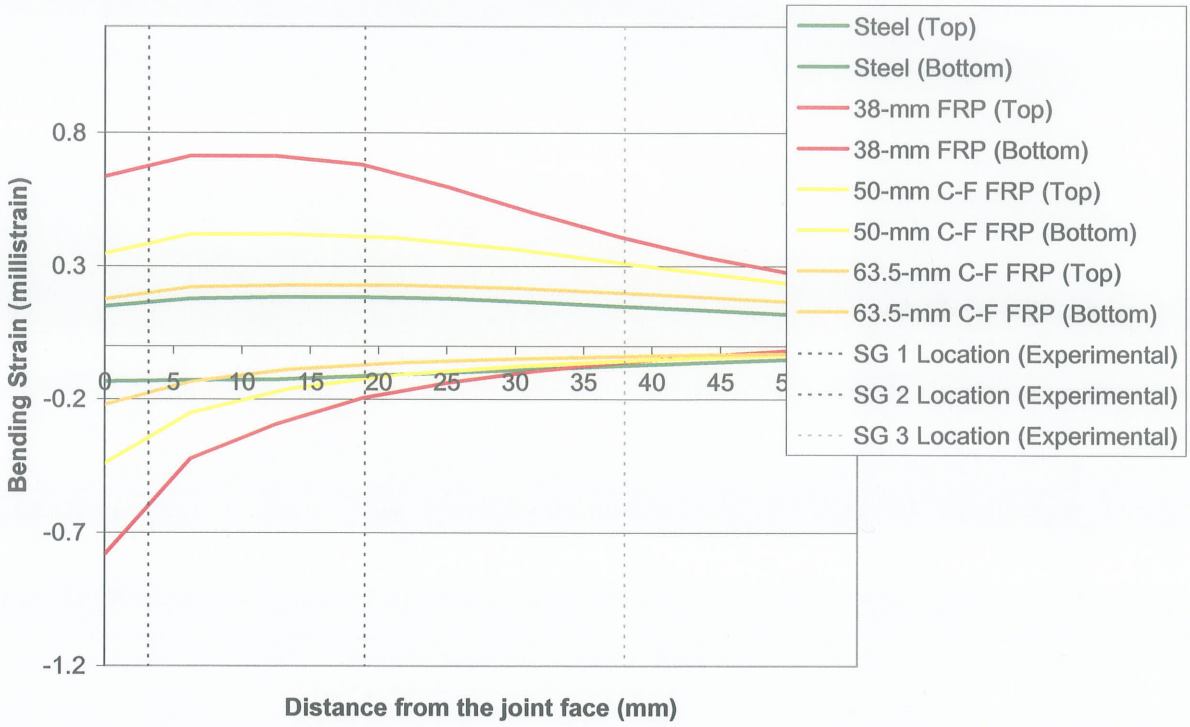

Figure 6.9: Axial strain in dowels due to bending at service load (FEM Results)

6.3 Experimental Results

6.3.1 Dowel Deflections

The deflection of a dowel bar into the concrete surrounding it is an indirect measure of the bearing stresses on the concrete. In theory, bearing stress is computed directly from the displacement of a dowel, as seen in the analytical solutions by Friberg [Friberg 1938]. Therefore, dowels that exhibit greater displacements into the surrounding concrete produce higher bearing stresses.

The plots of the deflected shapes of the four dowel bar types given in Chapter 5 depict the amount of displacement of the dowel bar as measured from the top surface. The LVDTs were used to measure the displacements on the top surface of the dowel, as it would have been impossible to measure the displacement of the bottom surface without affecting the bearing area under the dowel bar. The top surface displacements were used as a reference to compare the deflected shapes of each dowel type after each set of load cycles and to compare results between both phases of testing. Increased displacements over the course of the cyclic loading would indicate possible damage to the concrete surrounding the dowel or damage to the dowel itself. It is known that the downward displacement of the bar into the concrete, or the bottom dowel-surface displacement, is most critical because it affects the intensity of bearing stress. When the dowel bar is subjected to transverse traffic loads, it displaces and deforms the concrete below, however, the dowel experiences some deformation of its own. The amount of deformation the bar experiences depends on the material properties of the dowel and the concrete. In this case, the GFRP dowels have a lower stiffness in the transverse direction than the steel dowels and therefore deform a greater amount. In other words, the GFRP dowels will ovalize, or 'squish', more than the steel. For this reason, the displacements measured at the top of the bar by the LVDTs will be larger than the displacements at the bottom of the bar. The difference is greater for the GFRP bars as they compress more under transverse load than the steel bars do. The results of the finite element analysis were used to estimate the 'true' displacements at the bottom surface of each dowel bar using the measured top displacements as a reference. This is discussed in the next section.

6.3.2 Use of FEM Results to Adjust Experimental Displacement Measurements

It is clear that, of the total dowel displacements measured by the LVDTs, a portion of that amount is displacement of the dowel into the concrete and the remaining amount accounts for deformation or 'squishing' of the dowel bar. The difficulty in measuring the magnitude of transverse dowel deformation due to ovalization through laboratory tests let to the idea of using the finite element model to obtain an estimated value. Using the FEM results for each of the four dowel types, displacement values for the top surface and bottom surface of each dowel were obtained. The difference between the two represented the amount of dowel deformation due to ovalizing of the bar. A ratio of the bottom dowel surface displacement to the total top-of-dowel displacement was computed for each dowel. This ratio was then multiplied by the experimental dowel displacement values to provide an approximation of the deformation of the dowel into the surrounding concrete slab.

The idea is similar to looking at the ratios of the elastic moduli of each material. For example, the elastic modulus of the steel dowel is much greater than the elastic modulus of the concrete slab therefore, of the total displacement measured at the top of the dowel, the majority of the deformation occurs in the concrete and a small portion of the displacement is due to transverse deformation of the dowel. For a block of steel (Es = 200,000 MPa) being pressed against a block of concrete (Ec = 35,000 MPa), the proportion of concrete deformation to the total deformation of the two materials would be 0.85 or 85%. The remaining 15% of the total deformation accounts for deformation of the steel block. The elastic modulus of GFRP is much lower than steel so the deformations of a GFRP dowel would be greater. For two blocks of the same material being pressed together, the

deformation in each would be the same. The transverse deformation ratios calculated using the FEM results were used to determine the proportion of the total displacements measured by the LVDTs that represented concrete deformation and the proportion that represented dowel deformation.

For example, from the FE analysis results, it was determined that the total displacement at the top of the steel dowel is 0.0166 mm. The bottom of the dowel displaced 0.0149 mm into the concrete slab representing the total concrete deformation. The difference of 0.0017 mm represents the amount of dowel deformation and in this case it was very small as expected because of the high strength and stiffness of the material. The ratio of the concrete deformation to the total top-of-dowel displacement is 0.90. Therefore, of the total displacement measured at the top of the dowel, 90% was due to deformation of the concrete below the dowel and 10% was transverse deformation or ovalizing of the dowel. The ratios, obtained for each of the four dowel types in the FE model, were simply multiplied by the total displacements that were measured in the experiments. The ratios calculated for each dowel type using the FEM displacement results are provided in Table 6.1.

Table 6.1: Deformation ratios computed from FEM results

Dowel Type	**FEM Computed Dowel Displacements**			**Deformation Ratio**
	Top of Dowel (Total Displacement) **(1)**	Bottom of Dowel (Concrete Deformation) **(2)**	Difference (Dowel Deformation) **(1) – (2)**	**(2)/(1)**
38-mm Steel	0.0166 mm	0.0149 mm	0.0017 mm	**0.90**
38-mm Solid FRP	0.0317 mm	0.0203 mm	0.0114 mm	**0.64**
50.8-mm C-F FRP	0.0151 mm	0.0252 mm	0.0101 mm	**0.60**
63.5-mm C-F FRP	0.0105 mm	0.0188 mm	0.0082 mm	**0.56**

The revised dowel bar deflected shape plots for the Phase I results, showing the estimated bottom dowel-surface deflections combined with the measured top surface deflections, are shown in Figure 6.10.

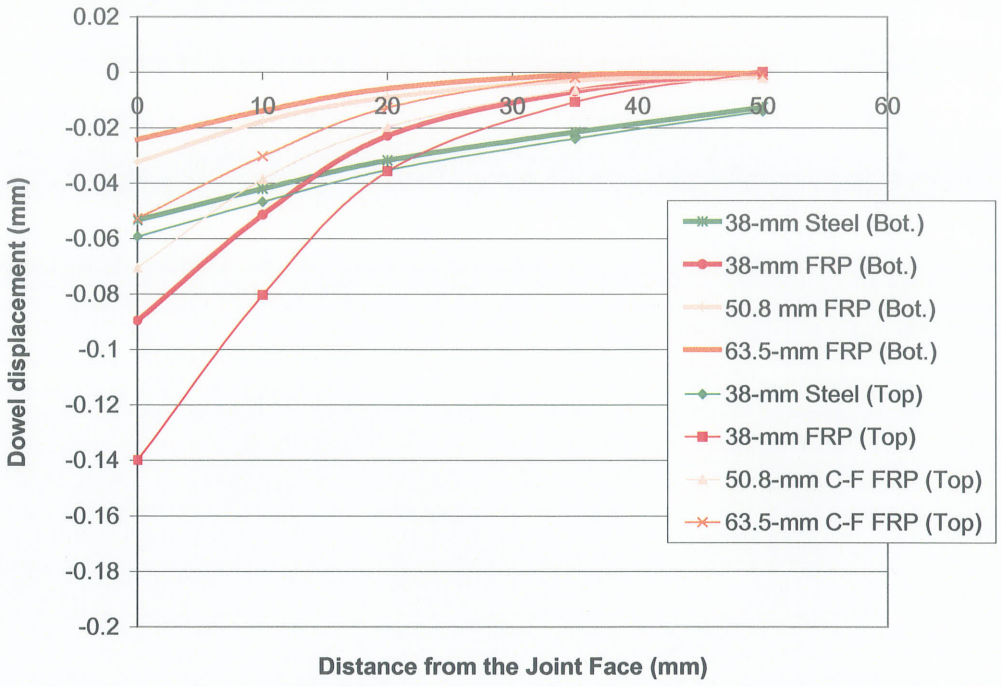

Figure 6.10: Estimated top and bottom dowel bar surface deflections combined

The difference between the top and bottom deflected shapes represents the estimated amount of deformation of each dowel type. For the 38-mm steel dowel, there is only a small difference between the measured (top surface) and 'revised' (bottom surface) displacement curves. This is expected due to the fact that steel is much stiffer than concrete and would exhibit little deformation in the transverse direction. Steel will deform slightly whereas, the GFRP dowels which have a much lower stiffness in the transverse direction, will experience

significantly higher deformations. The concrete-filled GFRP tube dowels have a lower transverse stiffness than the 38-mm solid GFRP dowel and exhibit even greater transverse deformation. From these results, the curves plotted in Figure 6.10 appear logical and can be used for comparing performance between the four dowel types.

6.3.3 Comparing Experimental Dowel Deflections with FEM Results

The purpose of the finite element analysis was to provide a simplistic computer-generated model of a dowel embedded in a pavement slab for which comparisons could be made with the laboratory test specimens. The properties of the FE model were ideal in many ways. For one thing, the mechanical properties of the GFRP materials were modeled as linear-elastic-isotropic. This can have several implications. The shear strength of the GFRP dowels and tubes will be greater than actual to some degree, and there may be inaccuracies in the estimations of the dowel deformations in the transverse direction (perpendicular to axis of dowel). This is because the transverse compressive strength and elastic modulus may be greater than actual. This linear-elastic-isotropic assumption was used because it provided a good approximation of the behaviour of a dowel bar by revealing the internal stresses that the dowel and the concrete slab experience. These internal stresses are extremely difficult, if not impossible, to measure in laboratory tests.

It should be noted that the FE models were run using a non-linear analysis to compare with the linear analysis results and only a very slight difference was observed. This revealed that the non-linearity of the concrete material modeled had little effect on the magnitude of deflection of the dowels in the FE analysis, however, it is understood that the actual

laboratory test specimens could very likely have been affected by this property of the concrete.

Figure 6.11 shows the deflected shapes of the four dowel types for both the FEM and experimental results. The curves for the experimental results represent the 'revised' bottom dowel-surface displacements.

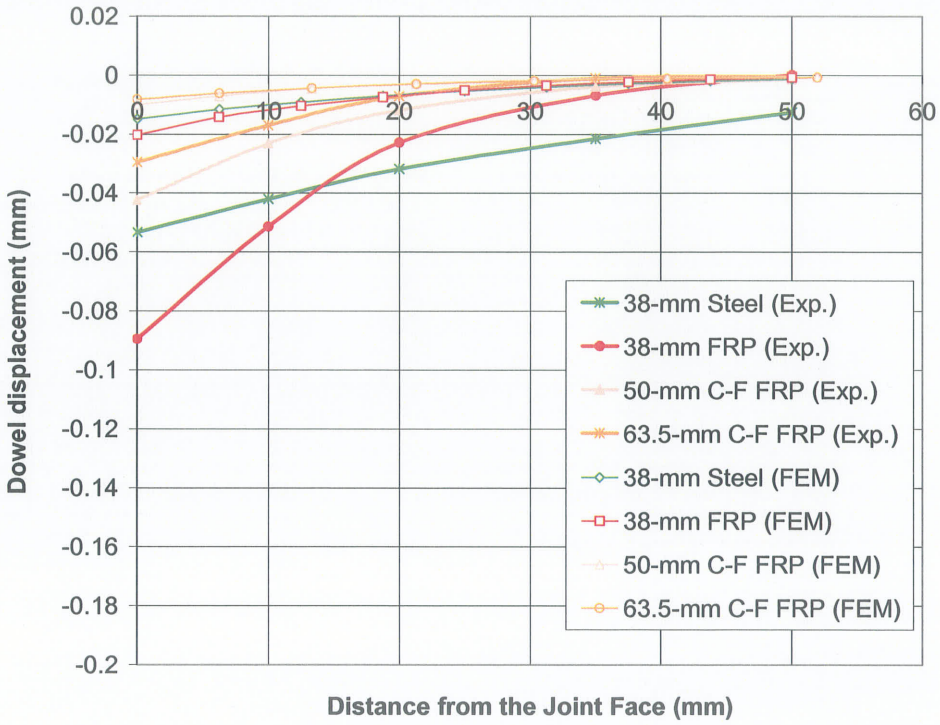

Figure 6.11: Deflected Shapes of Dowel Bars – FEM and Experimental Results

Clearly the finite element dowel deflection values are lower than the experimental values. In fact, the difference ranges between a factor of 3 and 5 which is substantial. There are several reasons why the values differ by such a great amount:

- **Idealization of the material properties** – It is likely that the material properties of the concrete slab in the finite element model differ significantly with the test specimens. The strength and tangent modulus assigned to of the concrete in the FE model could have been higher than the actual values which would have caused the model to exhibit a greater stiffness resulting in less displacement of the dowels. The mathematical idealization of the material can also be responsible. As well, the GFRP dowels would have a slightly higher shear strength in the FE model which would result in less shear deflections and therefore lower dowel displacement. These factors are important, however, when values for the material properties were altered, the change was very small. Therefore, inaccuracies of material properties account for only a small part of the difference in dowel deflections.

- **Contact Elements** – The major reason for the difference in dowel deflection values between the FE model and the experimental results, is the degree of bond between the dowel and the surrounding concrete. In the finite element model, it was assumed that the dowel was fully-bonded to the concrete encasing it. This situation was correct at first, however, the strength of the bond is low and under relatively small loads the bond brakes and the dowel is free to move within the concrete. The level of friction that exists at the dowel-concrete interface greatly affects the stiffness of the system and ultimately the rotation and deflection of the dowel bar. To some degree, the dowel and concrete slab behave like a concrete slab on a steel beam. If the slab is attached to the beam with steel shear studs, the 'composite' section will act as a stiffer system. If there are no shear studs, the beam will be less stiff and will deflect more.

The use of contact elements in the FE model would have allowed the dowel to move relative to the concrete and would have significantly increased the deflection.

- **Boundary conditions and loads** – Small changes to the placement of the load on the dowel in the FE model made very little difference. Similarly, changes to the boundary conditions on the pavement slab had little or no effect. Any differences in how the load was applied to the dowel had a small effect, however, they are still important.

- **Laboratory Measurements** – It is possible that inaccuracies exist in the measurement of dowel displacement in the laboratory. For example, the calibration of the LVDTs could have had a slight error in the range of 1/100 of a millimeter. This is a very small value, however, it is significant in this case because the maximum deflections are measured in 1/100s of a millimeter. It is certain, however, that the experimental measurements are consistent and correlate well with earlier work [Mannava et al. 1999].

The FEM and experimental dowel deflection magnitudes differ by a substantial margin due to the various reasons discussed, however, the FEM results do provide a great amount of data that is valid and of great importance. The internal stresses in the concrete below the dowel as provided in section 6.2 are still relevant. It is important to note that the bearing stress in the

concrete at the joint face of the slab would likely be higher in the test specimens than in the finite element result because the dowel deflections were higher.

When comparing the different dowel bar types, it can be seen that the FEM results exhibit characteristics of dowel behaviour similar to the laboratory results. The relative differences in deflection magnitude for each dowel type are similar and the curved shape of each deflected dowel is comparable as well. For example, the solid GFRP dowels exhibit greater curvature and deflection than the stiffer steel dowels. The larger-diameter concrete-filled GFRP tube dowels deflect less than the solid pultruded GFRP dowel and produce less bearing stress in the concrete. In both the finite element and experimental results, the peak deflections of the 38-mm steel and 50.8-mm concrete-filled GFRP dowels are similar and showing comparable performance.

6.3.4 Comparing Deflected Shapes of the Dowel Bars (Experimental Results)

Figure 6.12 shows the approximate displacements of the bottom surfaces of the four dowel types. There are clear differences in how the dowels deflect into the concrete at the joint face of the slab. The 38-mm (1.5") GFRP dowel exhibits the greatest displacement and the 63.5-mm (2.5") concrete-filled GFRP dowel exhibits the lowest as expected. The GFRP dowels, which have a significantly lower stiffness than steel, exhibit a greater curvature than the steel dowel. Because the GFRP dowels have a lower stiffness, they bend easier and do not distribute the load applied to them further along their embedded lengths. This results in a greater concentration of force near the joint face causing the dowel to apply greater pressure

to the concrete and deflect further. The steel on the other hand, transfers the load deeper along its embedded length spreading the load and applying a more evenly distributed pressure to the concrete below. This is indicated by the higher dowel displacements measured by LVDTs 3, 4, and 5 at 20, 35, and 50 mm inward from the joint face of the slab.

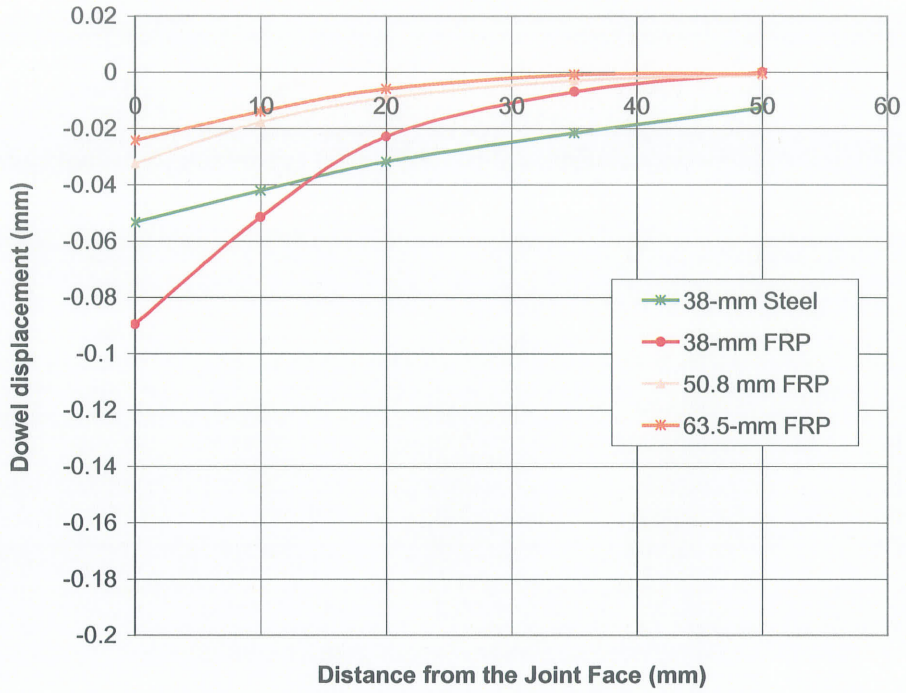

Figure 6.12: Estimated bottom dowel-surface deflections

The concrete-filled GFRP tube dowels experience much lower displacements due to their larger size. The modulus of elasticity of the Extren Series 625 tubes was less than half that of the FiberDowel pultruded GFRP bars as shown in Table 6.2, however, the increased size provided equal or greater stiffness depending on the size of the tube. The 50.8-mm (2") concrete-filled GFRP dowel had almost the same flexural stiffness as the 38-mm solid GFRP dowel, yet exhibited substantially lower displacements. This indicates the effect of dowel

size in spreading the load and reducing bearing pressure to the concrete. The increased size of the concrete-filled GFRP tube dowels proved to have a significant effect on reducing deflections. The displacement of the 63.5-mm concrete-filled dowel was less than half that of the epoxy-coated steel dowel.

Table 6.2: Material Properties of the Dowels

Dowel Type	Elastic Modulus, E (MPa)	Moment of Inertia, I* ($*10^6$ mm^4)	Flexural Stiffness (EI)** ($*10^6$ N-mm^2)	Yield / Rupture Strain (Strain)
38-mm Epoxy-Coated Steel	200,000	0.1034	20,687.1	0.002
38-mm Pultruded FRP	40,000	0.1034	4,136.0	0.016
50.8-mm Concrete-filled FRP Tube	19,300	0.2250	4,027.5	0.011
63.5-mm Concrete-filled FRP Tube	19,300	0.4700	8,413.0	0.011

*** Excluding concrete core**
**** Flexural strength provided by concrete is excluded**

The performance of the different dowel types compares well with the predictions of the finite element analysis. The magnitudes of the displacements were significantly higher in the experimental program, however, the differences between the dowel types are quite similar to those predicted in the FE analysis. The transverse stiffness of the concrete-filled dowels was substantially lower than the solid, pultruded GFRP dowel as evidenced by the high deformation of the dowel under load in the finite element analysis. It appears that this type of dowel experiences a higher degree of ovalization than the other types of dowels due to the low transverse stiffness and the result is a greater reduction in vertical bearing stress. The low transverse stiffness along with the large diameter of the concrete-filled GFRP dowels appears to be a superior combination for reducing deflections.

6.3.5 Cyclic Loading

As was seen in Figures 5.1(a) and 5.1(b) in Chapter 5, the graphs of the deflected dowel shapes before and after 1 Million load repetitions, there was no real increase in displacement to indicate any damage to the concrete slab or the dowels. There are a number of reasons for this to be the case. For one thing, the concrete compressive strength is over 50 MPa and the capacity of the concrete did not appear to be exceeded. In addition to this, the conditions of the testing and the properties of the test specimen are all ideal. In the field, the dowel-slab pavement joint system is subjected to freeze-thaw cycles, frictional stresses due to shrinkage and expansion of the slabs, stresses due to curling and warping of the slabs, loss of foundation support, as well as other environmental effects. Discussion on the condition of the concrete slab is provided later in this chapter.

6.4 Load-Deflection Behaviour

The load-deflection / load-stroke behaviour exhibited by each dowel type was affected by three major factors – the flexural stiffness of the dowel bar, the transverse stiffness of the dowel, and the stiffness of the concrete slab supporting the dowel. In Phase II, the concrete strengths were greater resulting in steeper slopes of the load-deflection plots where the deflection was measured at the joint face of the slab. Dowels with lower flexural stiffness will experience greater rotation under load. This causes greater negative displacements near the joint face as well as upward displacements further in from the joint face along the embedded length of the bar. The load-deflection graphs plotted with the five small LVDTs above the dowels show this effect. The graphs for the four dowel types are shown again in Figures 6.13(a) to 6.13(d) up to a load of 40 kN for comparison. It can be seen in the graph

for the GFRP dowel that there are upward displacements measured by the fifth LVDT (LV 5) at a load as low as 10 kN. The peak downward displacements measured at the joint face are more than twice those of the steel dowel bar at this load. This clearly shows that there is a large rotation of the bar occurring near the joint face.

The flexural stiffness of the dowel bar greatly affects the displacement of the cross-head which applies the load to the dowel at a distance away from the joint face. Obviously, the greater the distance or the larger the joint opening, the greater the bending moment, therefore the result will be higher displacements. In the field, the load is applied to the dowel by an adjacent pavement slab. When that adjacent pavement slab is loaded, it will deflect downward transferring load across the dowel which causes the unloaded slab to deflect downward. It is important to note that dowels with lower flexural stiffness will cause higher differential displacements and these differences will increase with greater joint openings. The expected result would be lower load transfer efficiencies (LTEs). As mentioned in Chapter 2, Falling Weight Deflectometer (FWD) tests on the Bishop Grandin Boulevard field application, containing 38-mm GFRP dowels, have shown excellent load transfer efficiencies to date. By the time of the most recent FWD testing, the field application was subjected to only two years of traffic. More time will be required in order to assess the performance of these GFRP dowels.

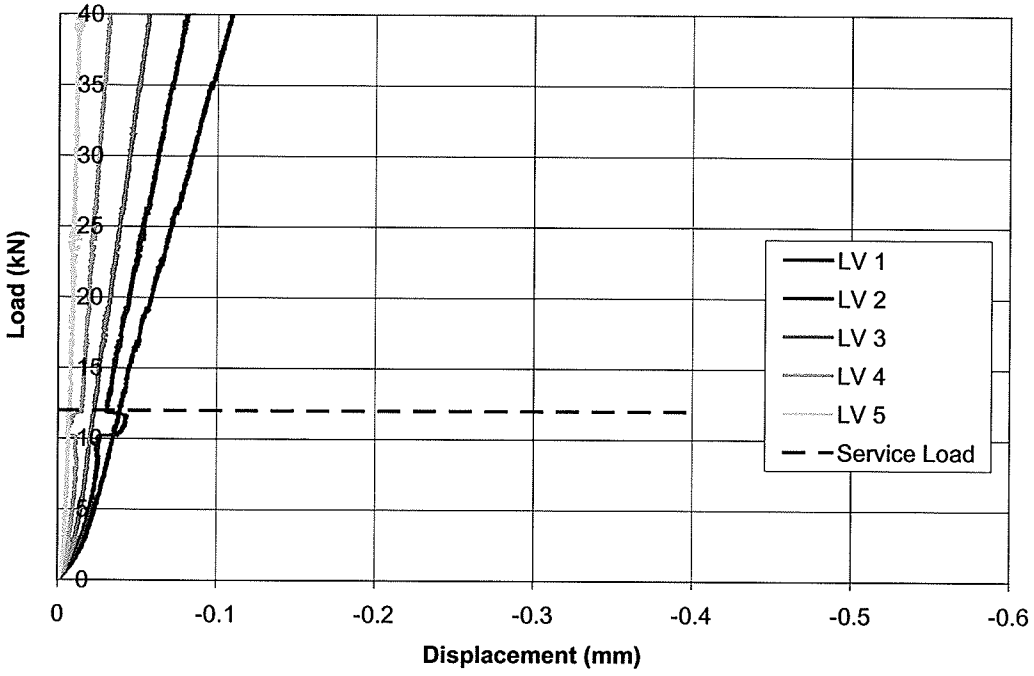

Figure 6.13 (a): Load-deflection behaviour of 38-mm epoxy-coated steel dowel

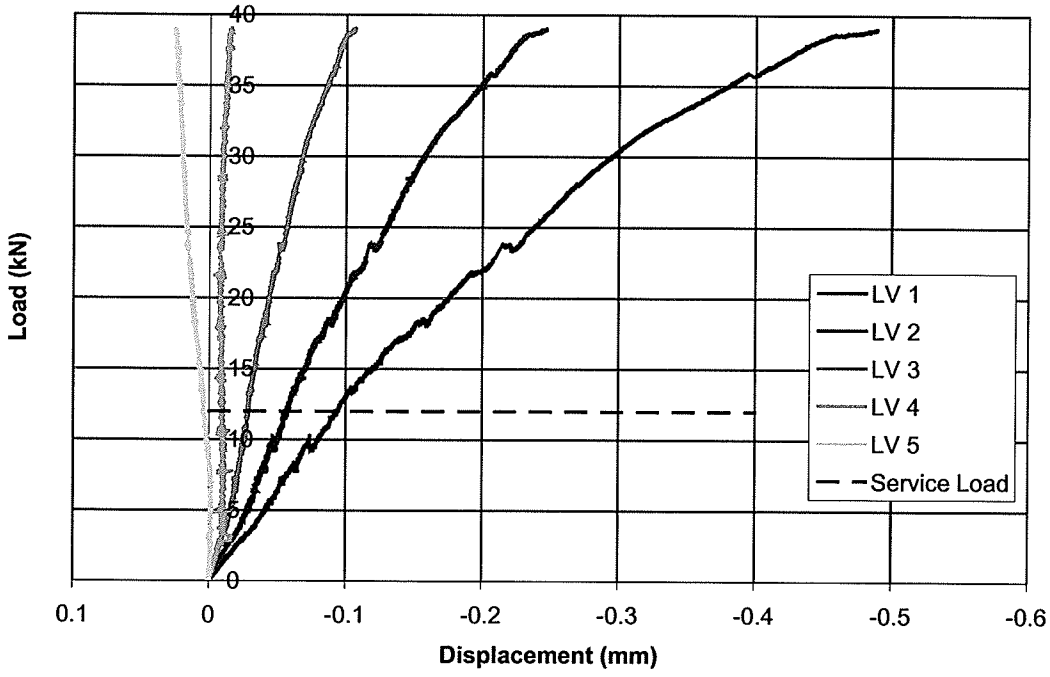

Figure 6.13 (b): Load-deflection behaviour of 38-mm pultruded GFRP dowel

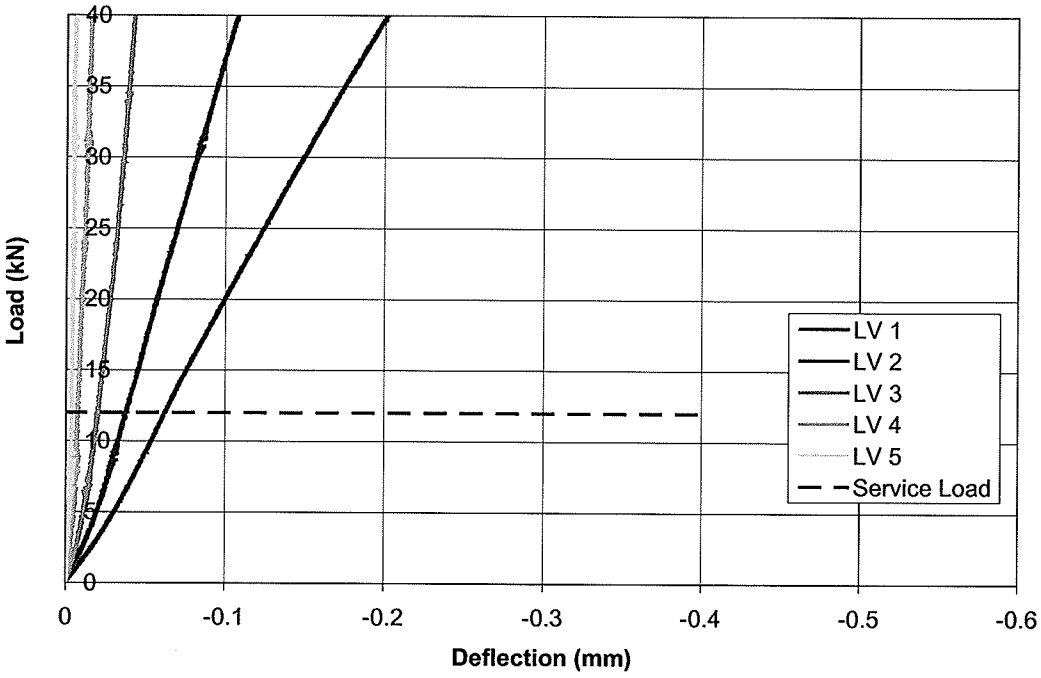

Figure 6.13 (c): Load-deflection behaviour of 50.8-mm concrete-filled GFRP dowel

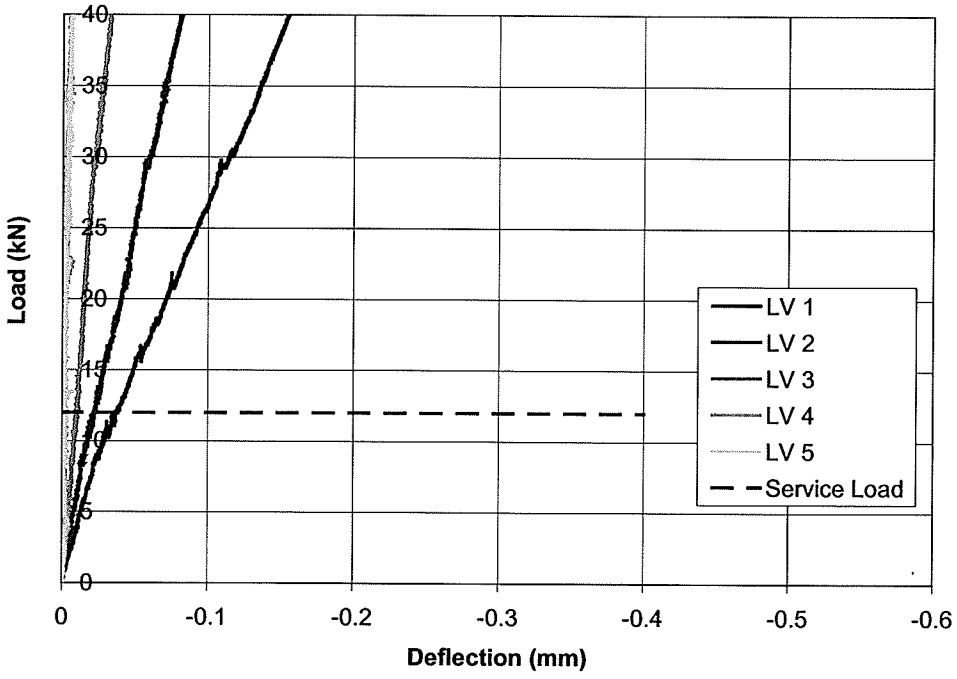

Figure 6.13 (d): Load-deflection behaviour of 63.5-mm concrete-filled GFRP dowel

6.5 Dowel Bar Flexural Strain

6.5.1 Dowel Strain at Service Load –Phase I and II

The lower flexural stiffness of the GFRP bars was quite evident from the high bending strains measured at service load. The strain magnitudes for the 38-mm GFRP dowel were high, however, they were only approximately 10% of rupture strain (f_{rup} = 0.016 strain). The rupture strain for the Extren Series 625 GFRP tubes was lower (f_{rup} = 0.011 strain) and the strains measured in the GFRP tubes were far lower than rupture. The increased size of the concrete-filled GFRP dowels provided a greater stiffness resulting in lower bending strains compared to the 38-mm solid GFRP. Since the strain levels were well below the rupture limit, there appeared to be no concern about fatigue of the GFRP dowels. The bottom strain gauge on the 38-mm GFRP dowel most near to the joint face showed increases in compressive strain over the course of the cyclic loading. The increase in strain between the initial test and the test after 1 Million cycles was approximately 0.5 millistrain. This equals a 27% increase in compressive strain. Pultruded GFRP exhibits lower strength in compression than in tension and due to the hinge type of bending of the bar, the 38-mm GFRP dowel may have experienced a small amount of wear, but it did not appear to be significant over all. There was no visible wear on the dowel after one million load cycles.

The distribution of bending strains revealed differences in how the steel and GFRP dowel bars behave under load. The steel dowels exhibited a fairly even distribution of strain along the length of bar monitored as seen in Figure 6.14. The magnitudes of the tension and compression gauges were approximately equal indicating that the bar behaved in a linear-

elastic fashion and that the neutral axis was located near mid-depth of the dowel as expected. This type of bending behaviour was similar to that predicted by the analytical solution provided in Chapter 2.

The 38-mm GFRP dowels experienced very high bending stains near the joint face. The distribution of strains along the length of bar monitored indicated that the dowel bends in a 'hinge' type of fashion. The curvature of the bar increases substantially where the dowel protrudes from the face of the concrete slab. The bending behaviour does not appear linear-elastic on the compression side of the dowel due to the bar bending about the edge of the concrete slab.

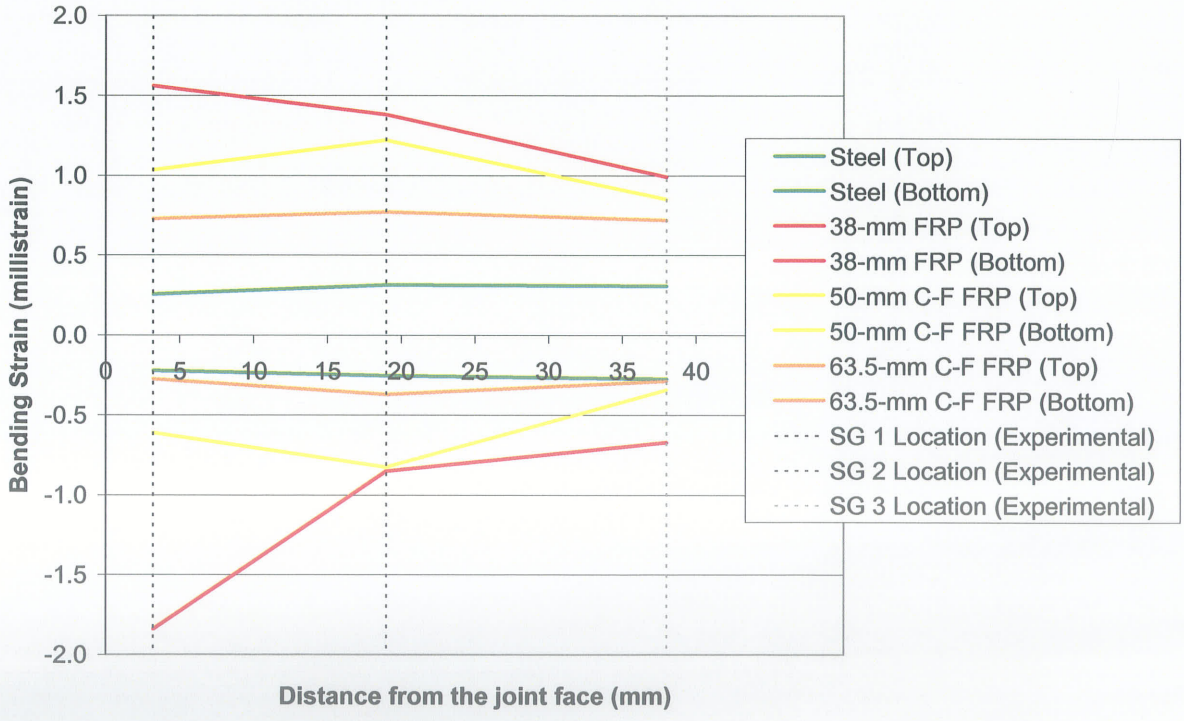

Figure 6.14: Axial strain in dowels due to bending at service load (Experimental Results – Phase I)

The behaviour of the concrete-filled GFRP dowels was similar to the smaller pultruded GFRP dowel, however, the strain distributions were slightly different. These dowels had a greater stiffness resulting in a maximum strain location at the center gauges (19 mm location). The high strains on the top of the dowel combined with low compressive strains on the bottom indicated that the dowel had a hinge-type of bending as well. In other words, the protruded portion of the dowel appeared to bend about the edge of the concrete face, therefore much of the compressive strains were transferred into the concrete below. This resulted in less stress being transferred along the length of the dowel bar. There would be higher compressive strains in the dowel just outside of the joint face that would account for the low strains recorded by the bottom strain gauges in the laboratory tests.

The bending strain profiles measured in Phase II of the experimental program are very similar to those in Phase I. The strain magnitudes were lower as the dowels experienced less vertical displacement due to higher concrete compressive strengths. The strains in the 50.8-mm (2") concrete-filled GFRP tube dowel exhibited higher bending strains in Phase II however. There was a greater concentration of compressive strain in the bottom gauge closest to the joint face indicating a type of bending similar to the 38-mm GFRP dowel. The strain was transferred more along the bottom of the dowel instead of into the concrete edge. This difference in behaviour is probably due to a different crack pattern or crack location in the core of the dowel. This may also explain the fact that this dowel did not exhibit smaller displacements in Phase II as expected. A slight difference in the bending behaviour of the dowel can affect the concentration of force near the joint face and therefore affect the vertical deformation of the dowel. Therefore, the Phase II results for the 50.8-mm concrete-filled

GFRP dowel appear to provide a worst-case type of bending behaviour. The expected deformation of the concrete below this dowel would still be substantially lower than that expected for the 38-mm epoxy-coated steel dowel.

Comparing the strain profiles measured with the strain gauges to the results of the finite element analysis, it is clear that the findings are similar. The magnitudes of the bending strains were lower in the finite element analysis because the vertical displacements of the dowels were lower than experimentally measured. This was due to the fact that the dowel was fully bonded to the concrete slab. The strain profiles for the GFRP dowels, as shown earlier in Figure 6.9, reveal that there are high compressive stress concentrations near the concrete joint face due to the hinge type of bending behaviour just as seen in the experimental results. The strain was not excessive though, as already mentioned and did not appear to be a problem for the dowel in any way.

6.5.2 Load-Strain Behaviour

The slopes of the load-strain curves plotted for the epoxy-coated steel dowels were far steeper than for any of the GFRP dowels due to the significantly higher flexural stiffness. When loaded up to failure in Phase II, the steel dowel exhibited perfectly linear behaviour up until the point when the outer surfaces began to yield. This occurred at a load level just above 80 kN or 80% of peak load. The loading was ceased when all six of the strain gauges, top and bottom, began to yield in tension and compression respectively. Strains in the GFRP dowels increased linearly to a degree up to service load, however, as loads increased the

linearity of the curves diminished. The compressive strain in the GFRP dowels increased rapidly near the joint face indicating that the GFRP is weaker in compression.

The experimental results indicated that the 38-mm GFRP dowel, which had the lowest failure load of all the dowel types, began to experience accelerated failure at approximately double the service load or 24 kN. The peak bending strains in the dowel reached approximately 60% of the rupture strain at peak load. The concrete-filled GFRP dowels did not really show signs of accelerated failure during the application of load. The lower strength of the GFRP tubes and high tendency to ovalize caused the concrete-filled dowels to fail in a combination of ways. They failure mechanism included the dowel shearing off at the concrete joint face at approximately the same time the steel loading device sheared through the top surface of the tube. The peak load for both dowel types was reached soon after this type of failure began to occur. The load capacities of the two sizes of concrete-filled dowels were greater than that of the 38-mm GFRP dowel even though their shear strengths and elastic moduli were lower than that of the solid GFRP dowel. The 38-mm GFRP dowel failed due to inter-laminar shear stresses caused by bending of the dowel. It should be pointed out that the lower strength of the GFRP dowels compared to steel does not make them any less effective as far as load capacity is concerned. The service load was substantially lower than the peak load applied to the dowels, therefore the dowels would not be expected to fail in the field. The real problem exists in the concrete below the dowel bar.

6.6 Strain in the Concrete Slab

Higher vertical displacements of the dowel bar in the concrete lead to higher compressive strains. High strains or stresses can lead to damage of the concrete surrounding and supporting the dowel bar. Therefore, dowels that produce the lowest concrete compressive strain will produce the least amount of damage. One of the objectives of the study was to measure the compressive strain below each dowel bar type to compare and determine which dowel type could be expected to produce the least amount damage, if any, in the field.

6.6.1 Compressive Strain Profiles Below the Dowel Bars at Service Load

In this study, the strain in the concrete was assessed using both a finite element analysis and experimental measurements. In theory, the highest vertical bearing stress in the concrete would exist directly beneath the surface of the dowel bar at the joint face of the pavement slab. The stress and strain in the concrete that was plotted in the finite element analysis showed this to be true and it showed that the strains dissipate with depth below the dowel. The stresses below the dowel resembled stress bulbs similar to those that would exist in the soil beneath a footing. The plotting of the vertical compressive and horizontal tensile strains below the dowel bar obtained from the FE model showed clear differences between the effects that each dowel bar type has on the concrete support surrounding it.

It was clearly seen that the 38-mm GFRP dowel, with a lower stiffness, caused higher strain in the concrete than the steel dowel. This was due to the higher concentration of load near the joint face caused by the inability of the GFRP dowel to transfer the load further along its

length. It was noticed, however, that the GFRP dowel had a lower transverse stiffness resulting in the load being spread out over a wider area perpendicular to the length of the dowel. In other words, the load was spread out more around the diameter of the bar. The change in shape, or ovalizing, of the GFRP dowel reduced vertical strains in the concrete slightly and increased horizontal tensile strains at the same time. This type of deformation of the GFRP dowel is a benefit to the concrete, however, the flexural stiffness was so low that the concentration of force at the joint caused such high strains that the benefit was negligible. Therefore the 38-mm GFRP dowel exhibited higher vertical compressive strain than the 38-mm steel.

The 63.5-mm concrete-filled GFRP dowel that was modeled had a low stiffness similar to the 38-mm GFRP dowel, but the stresses and strains in the concrete slab were much lower. This was clearly due to the fact that the larger diameter spread the load out more substantially. This was also due to the fact that the concrete-filled GFRP dowel deformed in the transverse direction (ovalized) similar to the 38-mm GFRP bar causing the load to be spread out even further. In fact, the transverse stiffness of the concrete-filled dowel was lower than the 38-mm solid pultruded dowel resulting in a greater reduction in strain.

Similar results were expected in the experiment program. The five small electrical resistance strain gradient gauges were expected to capture the different levels of strain existing below the bar at the various depths. It was unfortunate that it was impossible to measure the strain directly beneath the dowel with this method, however, the strains at lower depths were expected to provide data that could be used to compare the different dowel types. As was

clearly seen in the compressive strain profiles provided in Figures 5.8 and 5.19 in Chapter 5, the strain values appeared quite erratic. Now, the concrete itself is not homogeneous and it is not surprising to see some degree of irregularity, however, the irregularities are substantial. Some of the gauges showed higher strains near the bottom and others lower at the top where they were expected to be highest.

The results for Phase I showed that the 38-mm GFRP dowel produced the lowest strain at the top gauge location of all the four dowel types. It was expected that the strain produced by this dowel would be the greatest at the top gauge as predicted by the FE model. Of all the five gauges, the strain was highest for the 38-mm GFRP dowel, but at the location of the fourth gauge from the top which was 8.5 mm below the dowel. These results may show that this method of strain measurement on the face of the concrete slab is not the most effective. It may be possible that the concrete at the surface of the slab strains in a less predictable fashion.

Repeated tests after various cycles of load repetitions in Phase I, shown in Figures 5.9(a) to (d) in Chapter 5, indicated that the strain magnitudes reduced with the number of cycles. This indicated the possibility that the properties of the concrete were changing slightly due to micro-cracking. It appeared as if the strain gauges were 'floating' on a small flake of concrete just below the dowel. With each repeated load, there was a slight softening of the supporting concrete. It may be possible the stresses are redistributed in the concrete due to micro-cracking. They may be redistributed just inside of the joint face or below the region that the gauges are attached to. The load-concrete strain curves, given in Figures 5.10(a) to

(d) for Phase I and Figures 5.21(a) to (d) for Phase II, did not show any sudden drops in strain when loaded up to service and did not indicate any damage at this load level.

It is possible that errors exist due to the way in which the strain gauges were attached, especially with the use of an epoxy to fill in all the air pockets formed on the exterior surface of the concrete in order to provide a better bonding surface. The use of small (2-mm) strain gradient gauges to measure concrete strain may have reduced the accuracy, but it was known that larger gauges would just average the strain over the region which was not acceptable in this case.

Because of the difficulties with the measured concrete strain profiles, it did not appear that they would be a reliable source for making comparisons between the four dowel types tested. The strain profiles showed that the behaviour of the concrete below the dowel bar is more complex than expected. It is clear, however, that dowels which produce greater deflections in the concrete, cause higher bearing pressures on the concrete and will therefore cause greater compressive strains in the slab. Therefore, the dowel deflections can be used as an indirect measure of the bearing stresses produced by a dowel.

6.6.2 Load-Strain Behaviour – Loaded to Failure

In Phase II of the experimental program, the pavement slabs were loaded until the dowels failed or yielded. The strain gauges attached to the concrete joint face were used to measure the strain magnitudes and capture the moment at which the concrete begins to experience severe damage. The steel dowel was loaded until the extreme surfaces began to yield. The

peak load at which the yield strain of 0.002 (2 millistrain) was first reached in at least one of the six strain gauges was just over 80 kN. The load was ceased when all six gauges surpassed the yield strain. There was only a small amount of damage to the concrete observed at the completion of the test which consisted mainly of small concrete flakes or chips near the bottom surface of the dowel. The strain gauges on the concrete indicated some abrupt changes in the load-strain behaviour at different load levels depending on the gauge location. The first sign of change occurred in the second gauge from the top (the top gauge had debonded early in the test) at a load level of just under 40 kN but, this did not indicate the occurrence of damage.

The 38-mm GFRP dowel caused serious damage at a low level of 24 kN, at which point a large flake of concrete began to spall away below the dowel, causing the strain gauges to no-longer function. The concrete surrounding the concrete-filled GFRP dowels showed absolutely no signs of damage at the completion of each test. The strain in the gauges on the concrete below the 50.8-mm concrete-filled GFRP dowel showed massive increases and abrupt changes at around 40 kN, however, inspection of the gauges showed that those gauges had debonded. The bottom gauge was intact and did not show any abrupt changes throughout the course of the test. Due to the fact that the concrete-filled GFRP dowels did not show any signs of damage to the concrete slab above and beyond 50 kN, it appears clear that they produce the least amount of stress compared to the other dowel types.

6.7 Analytical Solution

6.7.1 General

The analytical solution currently used in the design of doweled joints is discussed in Chapter 2. The solution is based on linear-elastic theory and is used to compute the peak deflections of a dowel and subsequently, the peak bearing stress at the dowel-concrete interface. The design is deemed acceptable if the computed peak bearing stress is lower than the Allowable Bearing Stress which is computed by the empirical formula given below.

[8] $$f_a = \left(\frac{4}{3} - \frac{d}{75}\right) f_c'$$

where, f_a = the allowable bearing stress between dowel and concrete (MPa)

d = the diameter of the dowel (mm)

f_c' = the ultimate compressive strength of the concrete slab (MPa)

For example, the maximum allowable bearing stress for a 38-mm steel dowel with a concrete slab having a compressive strength of 53 MPa would be:

$$f_a = \left(\frac{4}{3} - \frac{38}{75}\right) * 53 = (0.8267) * 53 = \mathbf{43.8\ MPa}.$$

Therefore, a computed bearing stress lower than 43.8 MPa will be deemed acceptable for the designed dowel layout at the pavement joint.

The magnitude of dowel displacement is dependant upon the elastic parameter known as the modulus of dowel support or K-value. This value represents the pressure required to cause a unit displacement of a dowel in the concrete. The bearing stress at the dowel-concrete interface is obtained by multiplying the dowel displacement by the same K-value. It was

discussed in Chapter 3 that the selection of a proper K-value is difficult in design. The K-value is dependant upon several factors including concrete strength, dowel size, joint opening and the load applied to the dowel and is almost impossible to predict.

In Chapter 3, the K-values were adjusted to match peak dowel displacements determined by the finite element and theoretical models. The selected K-values were compared and it was found that they varied depending on the type of dowel modeled. In this section, the analytical solutions are compared with the experimental results.

6.7.2 Comparing Analytical Solutions with Experimental Results

Figure 6.15(a) shows the deflected shapes of the four dowel types tested in the experimental program along with the analytical solutions for each dowel. In this graph, the K-value for the 38-mm steel dowel, determined to be 280 GN/m^3, was back-calculated by matching the peak deflections for both steel dowel curves. The same K-value was applied to the other three dowels for comparison. It can be seen that the peak displacements of the 38-mm GFRP dowel curves are fairly close which would indicate that the analytical solution may work well for the solid pultruded dowel as it does for the steel dowel. The analytical solutions for the concrete-filled GFRP tube dowels, however, are not close to the experimental values. Obviously, the K-values would need to be adjusted for the increased diameters, and therefore the deflections would be lower as expected, but the amount of adjustment required appears to be excessive.

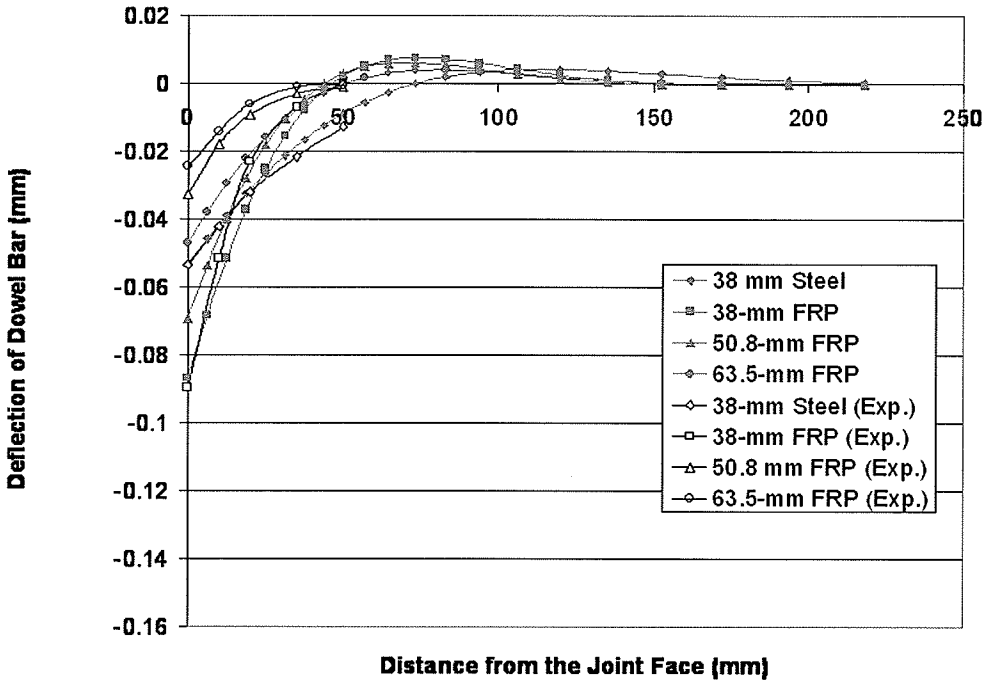

Figure 6.15 (a): Deflected shapes of the dowels – Analytical and experimental results (Peak displacement of steel dowel matched for both results - K = 280 GN/m^3)

The bearing stresses corresponding to these displacements as calculated by the analytical solution are shown in Figure 6.15(b). As expected, the dowels that produce higher displacements produce higher bearing stresses. Again, the differences between the 38-mm dowels appear to be correct, however, the magnitudes of stress appear to be very low. The peak bearing stresses for the 38-mm steel and GFRP dowels, 15 MPa and 24.5 MPa respectively, are approximately half the values predicted by the finite element analysis which were approximately 30 MPa and 49 MPa respectively.

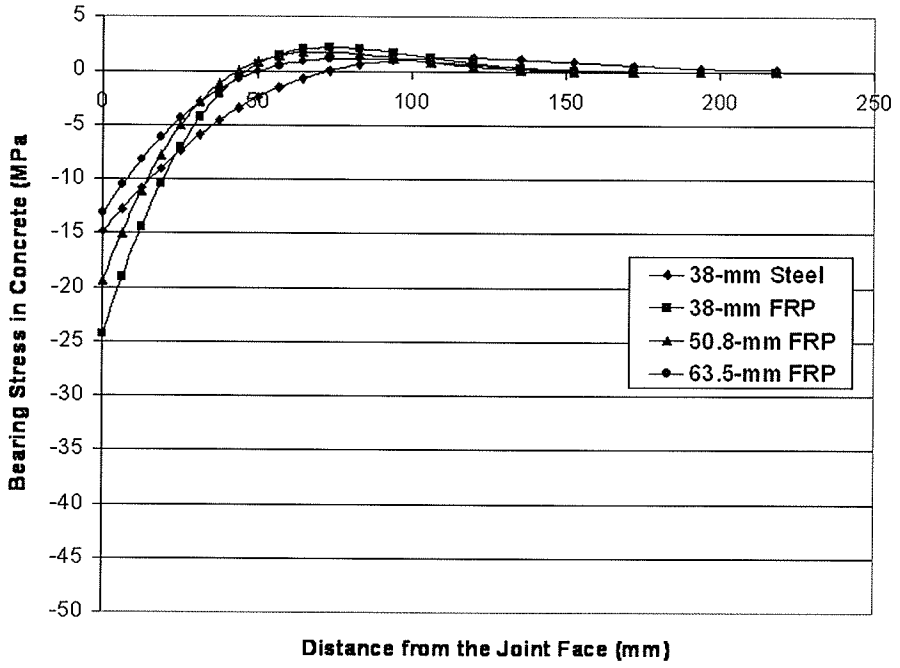

Figure 6.15 (b): Bearing stress below dowels calculated from deflections in the above graph (K = 280 GN/m^3)

In Figures 6.16(a) and 6.16(b) the deflections and bearings stresses are computed using adjusted, back-calculated K-values for each dowel bar type. The curves of the theoretical deflections match the experimental curves fairly well, however, the K-values had to be increased significantly for the concrete-filled dowels as shown in the legend of the graph. When the corresponding bearing stresses are computed, the results indicate a serious problem as seen in Figure 6.16(b). The substantially higher K-values back-calculated to match peak displacements for the concrete-filled GFRP dowels have resulted in excessive bearing stresses. The bearing stresses computed for the concrete-filled dowels are greater than the 38-mm steel dowel. It has been shown in the finite element analysis, that the steel clearly produces higher stress than the concrete-filled dowels indicating that there is a large error in

the analytical result. This discrepancy can be attributed partially to the fact that the properties of the concrete-filled dowels are complex and difficult to model. For instance, the flexural strength provided by the concrete core has been neglected in the analysis, however, the effect will not be substantial.

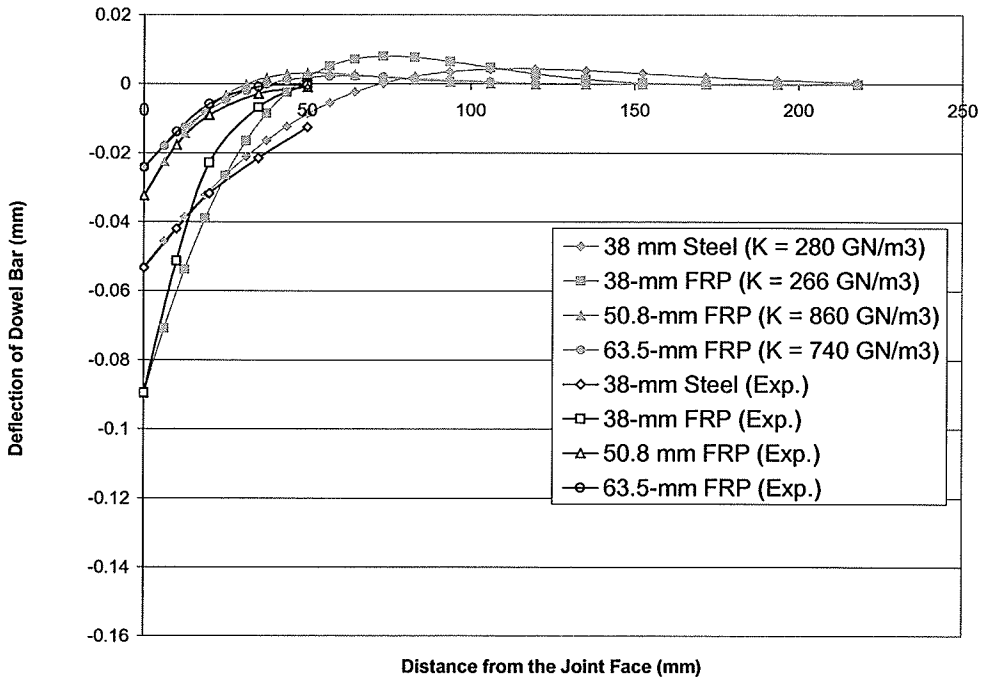

Figure 6.16 (a): Deflected shapes of dowels – Analytical and experimental Results K-values adjusted to match peak displacements for all four dowel types.

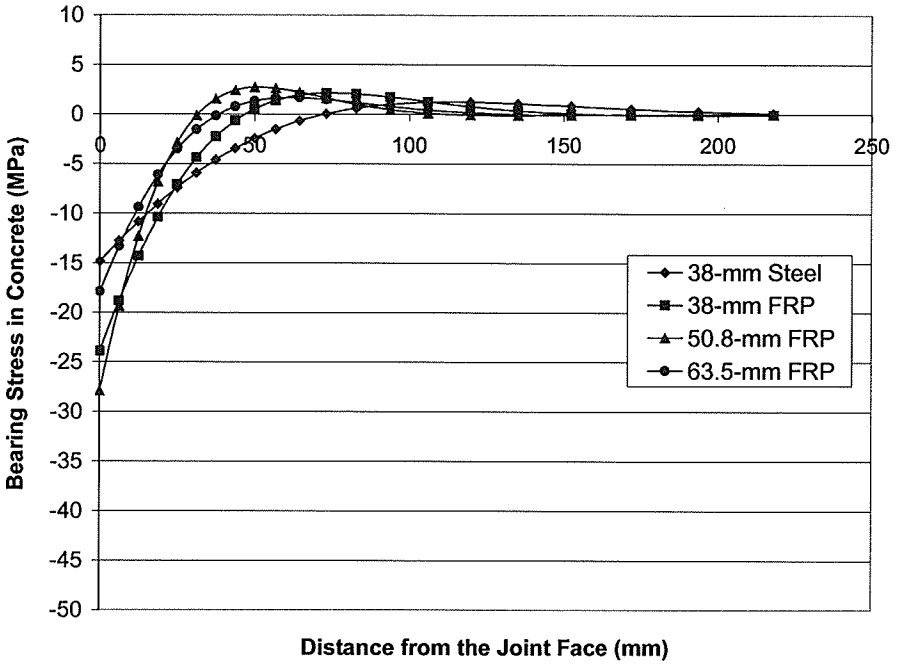

Figure 6.16 (b): Bearing stress below dowels calculated from deflections and K-values shown in the graph above.

6.7.3 Design Implications

The analytical solution appears to predict the deflected shapes of the 38-mm steel and GFRP dowels fairly well, however, the result is highly dependant on the selection of a proper K-value. The K-values back-calculated for these dowels were within the range presented earlier by B.F. Friberg (82-409 GN/m^3). The magnitude of the bearing stresses is clearly too low however. The analytical results appear to be 50% of the value obtained from the FE analysis. In addition, the FE result may be lower than actual because the model was more 'stiff' and had lower dowel displacements which would result in lower compressive strains in the concrete. No matter what the analytically determined bearing stresses are, they clearly under-predict the true stresses for all dowel types. This indicates a serious problem for the design of doweled concrete pavement joints.

The greatest bearing stress computed for the 38-mm steel dowel with 53 MPa concrete was obtained from the finite element analysis and the value was approximately 30 MPa. This is double the analytical result, however, it is lower than the maximum allowable limit of 43.8 MPa computed earlier. The design would still appear to be acceptable in this case. The problem is that, in the field, damage occurs to the concrete surrounding the 38-mm epoxy-coated steel dowels. Therefore, it would appear that the allowable stress is too high, or that the stresses experienced by the dowel and concrete in the field are much higher than predicted. These results indicate that the analytical solution should be either altered or replaced in order to provide a set of design formulas that account for these issues.

6.8 Summary

In this chapter, results of the finite element analysis and experimental program were discussed and compared. Characteristics that describe the behaviour of each dowel type were presented and discussed including dowel deflection, strain, load-deflection, and concrete pavement slab stresses and strains. The performance of each dowel type was compared through finite element, experimental, and analytical methods.

It was found that the simplified finite element analysis that was conducted for this study predicted lower dowel deflection magnitudes than were measured experimentally. The major reason for this was the fact that the dowel was fully bonded to the surrounding concrete which created a stiffer composite system. The use of contact elements with a prescribed friction coefficient that has yet to be determined, would allow the dowel to slide relative to

the concrete and therefore, deflect more. Other than for the difference in deflection magnitude, the finite element model and laboratory specimens exhibited similar behaviours. Both methods predicted similar differences between the four dowel types as follows:

- The solid pultruded and concrete-filled GFRP dowels had a lower stiffness than the steel dowel which prevented the transfer of load along the length of the bar and caused the dowels to deflect a greater amount.
- The peak deflections of the 38-mm (1.5") epoxy-coated steel and 50.8-mm (2") concrete-filled GFRP tube dowel were very similar. The concrete-filled tube had a lower stiffness than the steel, however, its larger diameter countered the inability to spread load along its length by spreading the load around its greater circumference.
- The lower strength of the GFRP dowels, both in shear and flexure, caused them to bend or kink about the edge of the concrete slab face when loaded. This caused a concentration of compressive stress in the dowel near the joint face of the slab whereas, for the steel dowel, the flexural stresses were spread out more uniformly along the length of the bar. The strains measured in the GFRP bars were high, however, they were not near the peak value for the material.

The finite element model was very helpful in understanding the internal stress states of the dowel and concrete slab which are nearly impossible to measure in the laboratory. The effects of a dowel changing shape under load, or 'ovalizing' were seen in the stress plots for bearing and tensile stresses in the concrete below the slab. GFRP, having a lower strength,

'squishes' or ovalizes under load and reduces vertical bearing stress below the bar while increasing horizontal bearing stress at the sides of the dowel.

The dynamic loading up to one millions cycles for each dowel type in the experimental program showed all four dowels to withstand the load without any significant signs of damage. Similarly, the concrete around each dowel showed no visual signs of damage, however, the strain gauges on the concrete surface indicated the possibility of increase micro-cracking over time. The ideal conditions of the laboratory tests do not take into account the effects of environmental factors such as freeze-thaw and expansion and contraction at the joints. Combined with traffic loads, the stresses on the dowels can be very high. Therefore, it is important to minimize stresses due to traffic loads.

The concrete-filled GFRP tube dowels, especially the larger 63.5-mm (2.5") tube, were found to perform the best in this study. The deflections and resulting bearing stresses were the least for the four dowel types and the performance over the set of one million load pulses was excellent.

In the analytical section of this study, it was found that the linear-elastic design formulas do not apply well to the GFRP dowels. The kinking at the joint and the transverse deformation of the dowel and all resulting effects are not accounted for in the linear solution. It appears clear that design methodologies for GFRP or similarly low-stiffness materials will be needed.

Chapter 7

Conclusions and Recommendations

7.1 Summary

In this study, the performance of concrete-filled GFRP dowels in concrete pavement joints was investigated and compared with the performance of 38-mm epoxy-coated steel and solid pultruded GFRP dowels. Analytical, finite element, and experimental investigations were conducted. The study showed that the concrete-filled GFRP tube dowels are a feasible alternative to steel dowels for use in jointed concrete pavements. The non-corrosive properties of GFRP can prevent damage due to joint locking and the smoothness of the outer dowel surface eliminates the need to apply de-bonding agents prior to paving. This study shows the significance in using larger diameter dowel bars to reduce bearing stresses in the concrete. The need for larger-diameter dowels is greater when using GFRP dowels because of the low flexural stiffness.

The analytical study involved a finite element analysis of a dowel bar embedded in a pavement slab. Solutions of the finite element model were compared with theoretical solutions that are currently used in design. The analytical study was used to predict the behavioural differences between steel and GFRP dowels of different sizes. The study showed that GFRP dowels cause greater deflections and bearing stresses in concrete than steel dowels of the same diameter. It also showed that using larger diameter dowels reduces bearing stresses substantially. In addition, the analytical study showed that the design

formulas developed from theory tend to under-predict the magnitude of the maximum bearing stress in the concrete slab in the vicinity of the joint face.

An experimental program comprising two phases was carried out. In Phase I, four pavement slabs were tested under static and cyclic loading at service load. Four dowel types were tested including 38-mm epoxy-coated steel dowels, 38-mm solid pultruded GFRP dowels, and 50.8-mm and 63.5-mm concrete-filled GFRP tube dowels comprising 6.35-mm thick FRP tubes filled with 50 MPa compressive strength concrete. The dowels were cast in full-scale depth concrete slabs having compressive strengths of 53 MPa at the time of testing. Phase II, involved the testing of four additional slabs where the dowels were loaded up to failure.

7.2 Conclusions

The main objective of this study was to examine and compare the performance of concrete-filled GFRP tube dowels with two dowel products currently used in the field, 38-mm epoxy-coated steel dowels and 38-mm pultruded GFRP dowels. The concrete-filled GFRP tube dowels clearly exhibited better performance than the 38-mm solid steel and GFRP dowels. The 63.5-mm concrete filled dowels produced the lowest deflections and therefore, lowest bearing stresses in the concrete. The concrete-filled GFRP dowels exhibited lower deflections than the 38-mm dowel as expected because of the larger diameter. The 50.8-mm concrete-filled dowel and 38-mm epoxy-coated steel dowel exhibited similar peak displacements and bearing stresses at the joint face of the slab, however, the displacements and stresses dissipated with distance away from the joint face more rapidly for the concrete-

filled dowel. The concrete-filled dowels proved to have ample strength and durability for use in concrete pavement joints and are capable of withstanding the millions of repeated traffic loads.

Benefits of the concrete-filled GFRP dowels include:

- GFRP tubes are non-corrosive which prevents locking of pavement joints.
- The synthetic veil surrounding the GFRP tube along with a vinyl-ester resin, provide protection against the alkali environment of the concrete.
- The large diameter reduces bearing stress significantly compared with 38-mm epoxy-coated steel and 38-mm pultruded GFRP dowels.
- The high strength and durability provide excellent resistance to repeated traffic loads.
- They are a lower cost alternative to using stainless steel (approx. 1/3 the cost of 38-mm solid stainless steel dowel)
- The smooth outer surface of GFRP tube eliminates the need to apply de-bonding agents prior to paving to prevent the dowel from locking in the joint.
- Although not part of this study, it is expected that the low stiffness and large diameter will require a shorter dowel length which is preferable for dowel retrofitting.

There will be limitations on the thickness of the pavement slab when using concrete-filled GFRP dowels. They are not recommended for use in pavement slabs that are less than four

times the diameter of the dowel. Further work will need to be conducted to determine the minimum pavement slab thickness for each concrete-filled dowel size.

The 38-mm pultruded GFRP dowels produced the greatest deflections and bearing stresses in the concrete compared to the other dowel types. This was due to the small diameter and low flexural stiffness. The GFRP dowel exhibited ample strength and durability for use in concrete pavement joints, however, the concrete bearing stress is most critical in design. In order to reduce the bearing stress, the pavement joint will require either shorter dowel spacing (more dowels to share the load) or larger dowels or a combination of both. Both of these options will increase costs, however, the cost of using stainless steel will be even greater.

The 38-mm epoxy-coated steel dowels performed better than the 38-mm GFRP dowels in this study, however, the effects of corrosion and other environmental factors were not incorporated. There is no question that the problem of dowel corrosion must be eliminated and one of the most economical ways to eliminate the problem is to use GFRP.

The design equations developed from theory have been shown to under-predict the bearing stress in the concrete produced by a dowel under load. Results of the finite element analysis discussed in Chapter 6 showed bearing stresses to be almost twice the values computed by theory. This study indicates that there is a need to re-evaluate the validity of the design equations.

It is understood that the finite element results for dowel displacements did not match the experimental results. This was mainly because the dowel was fully-bonded to the concrete slab which created a stiffer system. The bearing stresses at the dowel-concrete interface in the FE model were quite high indicating that the actual bearing stress could be even greater, because the dowel deflections for the laboratory test specimens were greater than those in the FE model. The analytical, finite element, and experimental methods all showed that bearing stress increases with dowel deflection.

7.3 Recommendations

This study has examined the interaction between a dowel and the surrounding concrete. Dowel deflections, concrete bearing stresses, and dowel bar flexural strains have been analyzed and compared. The results of this study clearly show the differences in how the various dowel types behave under simulated traffic loads. It has also been shown that design practices need to be re-assessed in order to insure that doweled joints perform as expected. It is recommended that further work be conducted on examining the validity of the design equations. Part of this work should involve a set of laboratory tests that incorporate a method of measuring accurate bearing stress at the dowel-concrete interface either directly or indirectly. In addition, a more detailed finite element model that incorporates contact elements between the dowel and concrete will be required to investigate the internal stresses in the pavement slab. The FE model should consider the orthotropic material properties of GFRP dowels. This will be a major requirement in determining the validity of any set of design equations. A valid set of equations will allow a designer to properly choose the best dowel configuration in a pavement joint especially when using GFRP dowels.

REFERENCES

1. Ambroz, J., Seiler, W.J., and Darter, M.I. "A state of the art report: Load Transfer Design and Benefits for Portland Cement Concrete Pavements." ERES Consultants Incorporated, Report #96-128-E1,1998.

2. Bhattacharya, Kamal. "Nonlinear Response of Transverse Joints of Airfield Pavements", Journal of Transportation Engineering, Vol. 126, No. 2, March-April 2000.

3. Brown, V.L., and Bartholomew, C.L., "FRP Dowel Bars in Reinforced Concrete Pavements", Proceedings of the International Symposium on Fiber-Reinforced-Plastic Reinforcement for Concrete Structures, FRPRCS-1, Vancouver, Canada; Ed. by A. Nanni and C.W. Dolan; American Concrete Institute, Detroit, MI, ACI SP 138, p. 813-829, 1993.

4. Buck, N., and Zollinger, D.G. "Development of dowel looseness Prediction model for Jointed Concrete Pavements." Transp. Res. Rec. 1525, Transportation Research Board, Washington, D.C., 21-27, 1996.

5. Davids, W.G., Mahoney, J.P., "Experimental Verification of Rigid Pavement Joint Load Transfer Modeling with EverFE", Transportation Research Record No. 1684, TRB, National Research Council, Washington, D.C., pp. 81-89, 1999.

6. Davids, W. G., Turkiyyah, G.M. "Development of Embedded Bending Member to Model Dowel Action." Journa of Structural Engineering-ASCE, Vol. 123, No. 10, p. 1312-1320, October 1997.

7. Dei Poli, S., Di Prisco, M., and Gambarova, P.G. "Shear Response, Deformations and Subgrade Stiffness of a Dowel Bar Embedded in Concrete." American Concrete Institute Structural Journal, 89 -S-63, p. 665-675, 1992.

8. Dulacska, Helen. "Dowel Action of Reinforcing Crossing Cracks in Concrete." ACI Journal, Vol. 69, No. 12, p. 754 – 757, 1972.

9. Eddie, Darren. "FRP Dowels for Concrete Pavements." Masters thesis at the University of Manitoba, 1999.

10. Eddie, D., Shalaby, A., Rizkalla, S., "Glass Fiber-Reinforced Polymer Dowels for Concrete Pavements", American Concrete Institute Structural Journal, vol. 98, no. 2, March-April, 2001.

11. Friberg, B.F. "Design of Dowels in Transverse Joints of Concrete Pavements." ASCE, Vol. 64, pt. 2, p. 1809-1828, 1938.

References

12. Huang, Y.H., "Pavement Analysis and Design", Prentice Hall, Englewood Cliffs, New Jersey, 1993.

13. Ioannides, A.M., and Korovesis, G.T., "Analysis and Design of Doweled Slab-on-Grade Pavement Systems", Journal of Transportation Engineering, Vol. 118, No. 6, p. 745-768, 1992.

14. Ioannides, A.M., Lee, Y.H., and Darter, M. "Control of faulting through joint load transfer design." Transportation Research Record 1286, Transportation Research Board, Washington, D.C., 49-56, 1990.

15. Mannava, S.S, Bush, T.D. Jr., Kukreti, A.R. "Load-Deflection Behavior of Smooth Dowels", ACI Structural Journal, V.96, No. 6, November-December 1999.

16. Marcus, Henri. "Load Carrying Capacity of Dowels at Transverse Pavement Joints." ACI Journal, Proceedings, v. 48, no. 2, pp. 169-184, October 1951.

17. Shalaby, A, Murison, W.S., "Using Fiber-Reinforced Polymer Load Transfer Devices in Jointed Concrete Pavements", Proceedings, 7th International Conference on Concrete Pavements, Vol. 2, Orlando, FL, pp. 607-621, September 2001.

18. Soroushian, P., Obaseki, K., Rojas, M.C. "Bearing Strength and Stiffness of Concrete under Reinforcing Bars." ACI Materials Journal, v. 84, no. 3, pp. 179 – 184, May-June 1987.

19. Tabatabaie, A.M., Barenberg, E.J., "Finite Element Analysis of Jointed or Cracked Concrete Pavements", Transportation Research Record No. 671, TRB, National Research Council, Washington, D.C., 1978.

20. Teller, L.W., Cashell, H.D., "Performance of Dowels under Repetitive Loading", Public Roads, Vol.30, No. 1, pp. 1-24, 1958.

21. Timoshenko, S., Lessels, J.M. "Applied Elasticity", Westinghouse Technical Night School Press, East Pittsburg, Pensylvania, 1925.

22. Westergaard, H.M., "Computation of Stresses in Concrete Roads," Proceedings, Fifth Annual Meeting, Highway Research Board, 1925.